Spring 2017

Imaging a fly ash landfill using non-invasive technologies (ERT and MASW)

Atiat Shaban Qasim Alsaaideh

Department: Geosciences and Geological and Petroleum Engineering

IMAGING A FLY ASH LANDFILL

USING NON-INVASIVE TECHNOLOGIES (ERT AND MASW)

by

ATIAT SHABAN QASIM ALSAAIDEH

A DISSERTATION

Presented to the Faculty of the Graduate School of the

MISSOURI UNIVERSITY OF SCIENCE AND TECHNOLOGY

In Partial Fulfillment of the Requirements for the Degree

DOCTOR OF PHILOSOPHY

in

GEOLOGICAL ENGINEERING

2017

Approved by:

Neil L. Anderson, Advisor
J. David Rogers
Stephen Gao
Kelly Liu
Lesley Sneed

ABSTRACT

Electrical resistivity tomography (ERT) data were acquired across a segment of an existing fly ash landfill in southwestern Missouri. The objective was to map potential karst features and identify probable groundwater seepage through and beneath the landfill.

Variations in the moisture content were mapped below and above the two liners (clay and synthetic) systems, the soil and bedrock. Seepage pathways were mapped through the fly ash and the underlying soil and rock. No visual evidence was found on any of the 3D ERT profiles of the presence of either pre-existing air-filled voids or pre-existing or newly infilled clay-filled voids. There was also no evidence that moisture was seeping into the subsurface through the basal clay liner.

Imaging beneath the geosynthetic liner system using the ERT technique was achieved due to the moisture resulted from permeability in the geosynthetic liner, which enabled the conduction of current through the geosynthetic liner.

Multichannel analysis of surface waves (MASW) data were acquired to constrain and verify the accuracy of the ERT interpretations. The interpretations of ERT data were consistent with MASW and borehole control.

Based on the investigation, it is concluded that the study site is devoid of karst features that could affect the landfill. The interpretation revealed no evidence of groundwater seepage pathways through the basal clay liner and, hence no potential hazard of groundwater contamination.

ACKNOWLEDGEMENTS

To the soul of my beloved father Shaban Qasim Alsaaideh, who passed away on Thursday, March 2nd, 2017. May Allah bless him in the eternity, save his soul and reward his patience on sickness with heaven. No love after his love, no care after his care, and life is vague after he left.

To me, Dr. Neil Anderson has been more than an advisor. His help and support extended to all aspects of my life. His guidance hastened my understanding of theoretical, fieldwork and research methods in geophysics. His mentoring will guide the rest of my life. Thank you for being my advisor.

It is a difficult for me to acknowledge Dr. J. David Rogers, because I will find no words that expresses the humane side of him, his advising and guidance. He unlimitedly supported me and he will remain in my life.

I very much appreciate the support, help and advices of my committee members, Dr. Stephen Gao, Dr. Kelly Liu and Dr. Lesley Sneed. I bear to them, respect, love and appreciation for every support and help they gave me.

My beloved kids…Mosbah ……. Fairouz ……. Tala ……and Adam. My success would have never been without you. You equally suffered with me to make this achievement and together we aspire for a better life ……. I love you. To my lovely mom, Fatima and to my sisters and brothers.

To the many friends and colleagues who surrounded me, supported and helped me … Thank you.

TABLE OF CONTENTS

LIST OF ILLUSTRATIONS

LIST OF TABLES

1. INTRODUCTION

The Ozarks region is underlain by Paleozoic age carbonate rocks that were subjected to karstification in the Mississippian time, and more recently in the late Quaternary, where such units lie within proximity (~ 152 m; 500 ft.) to the present-day ground surface. This situation portends likely hazards associated with the local gradual to catastrophic collapses associated with karst features, when improvements are constructed over such features without the knowledge of their precise natural geometry. The study area in southwestern Missouri is underlain by thick carbonate rocks (~ 59 %) that host a wide variety of karst features such as sinkholes, limestone ridges, caves and extensive underground and/or exposed streams and drainage systems that were created by the dissolution process of limestone and dolomite rocks by the seepage of surface and underground acidic water (Figure 1.1).

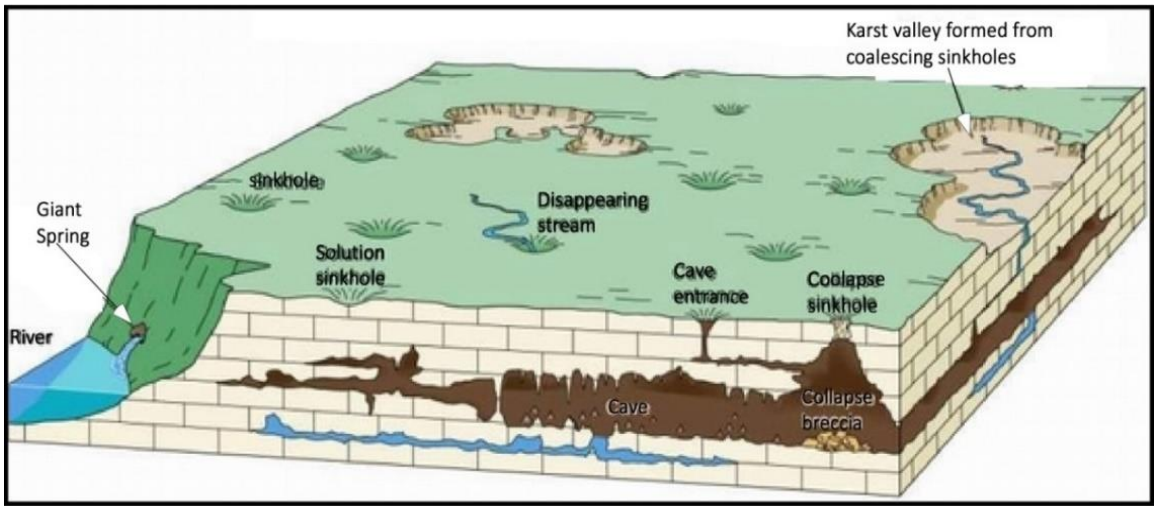

Figure 1.1: Block diagram shows some karst features (Source: http://www.ocean.odu.edu/ ~spars001/common/graphics/Figures/plummer).

The significance of this research is to map potential karst features, if any, beneath an existing fly ash landfill, using the electrical resistivity tomography (ERT) and multichannel analysis of surface waves (MASW) techniques, and to image any possible seepage patterns and flow pathways through and beneath the fly ash landfill, and to map the variations in moisture content beneath and above the liners systems, and to assess the condition of the landfill liners. The research will implement those integrated geophysical techniques to characterize the karst terrain beneath the landfill that developed within 30 meter (100 feet) of the original ground surface. In order to achieve optimum results, we utilized ERT and MASW methods, which have shown themselves to be cost effective techniques for characterizing large tracts of land (e.g. > 100 acres) (Anderson, personal communication).

The research will hopefully show the wisdom of employing more than one non-invasive geophysical imaging technique to more accurately study existing landfills and mapping the variations in the depth to the top-of-rock at low cost.

This research is essential in helping fly ash landfills owners to assess the structural stability of these landfills, and should help in preventing karst-related settlements that could impair the long-term integrity of the fly ash landfills, or impune groundwater quality by damage of the liner/containment systems through localized sinkholes collapses beneath landfills, or the migration of potentially hazardous leachate into the subsurface soils and groundwater table.

The research and utilization of these techniques will hopefully assist in avoiding the potentially high cost of mitigating the impacts of such foundation movements beneath or immediately adjacent to the existing landfill.

Missouri is ranked the 16th state in the production of fly ash in the United States that is disposed in man-made landfills (Figure 1.2). The weight of the fly ash landfill embankments and/or preferentially-directed/concentrated runoff can hasten the collapse of sinkholes, or water-filled voids and cause possible contamination of groundwater (Evans, et al, 2011).

Figure 1.2: An aerial view of a fly ash landfill at Dominion's Chesapeake Energy Center (Source: Bill Tirenan file photo, the Virginian Pilot, http://pilotonline.com/news/local/environment/tennessee-spill-brings-fly-ash-dangers-to-forefront/article, Jan. 24, 2017).

Fly ash which is generated in the burning process of coal in power generation plants contains many toxic elements, and poses serious challenges of surface and subsurface environmental contamination that directly and indirectly affect the living organisms (Openshaw, 1992). The massive produce of fly ash requires a well-engineered disposing systems and well-designed landfills.

Electrical resistivity tomography (ERT) is one of the most proficient methods for subsurface studies in karst terrains to a depth of about 30 m (100 feet), because it can measure the spatial variations of electrical resistivity of natural subsurface materials such

as rocks and soils and man-made materials, including the fly ash. The 2-D and 3-D ERT imaging is not capable of exploring the natural subsurface features only, but also capable of imaging man-made structures such as fly ash landfills.

The multichannel analysis of surface waves (MASW), is a highly efficient geophysical technique that can adequately be used in mapping the variations in the rigidity of soils, rocks and man-made materials, including fly ash, and as well, the variations in the elevation of top of rock. The MASW technique is often used as complementary method that constrains and verifies the interpretation of the ERT data (Torgashov, personal communication).

1.1 RESEARCH OBJECTIVES

- map any karst features beneath the fly ash landfill (if any);
- identify possible pathways of seepage or water flow through and beneath the fly ash landfill;
- image the fly ash beneath and above the landfill geosynthetic liner;
- map the variations in moisture content in fly ash, and rocks and soils; and
- map the variations in the elevation of top-of-rock.

1.2 DESCRIPTION OF THE RESEARCH

This research intended to accurately survey and image an existing fly ash landfill in Southwestern Missouri, with the objectives of determining the subsurface conditions beneath the landfill, noting any karst features, and to detect the seepage pathways and

to image the fly ash below and above the geosynthetic liner of the landfill and to determine the variation in the moisture content in fly ash, and rocks and soils and to determine the elevation of the top-of-rock.

3-D electrical resistivity tomography (ERT) data were acquired along traverse profiles, varying in length between 150 m (500 feet) to more than 300 m (1000 feet), in a west to east orientation. The data acquired using an automated multi-channel resistivity meter SuperSting system connected to dipole-dipole electrode array of 168 electrodes, spaced by 1.5 m (5 feet) apart and separated by 6 m (20 feet) distance. The Res2dinvx64 software was employed for the ERT data processing.

The proposed orientation was selected normal to the general direction of the underlying geologic structure, and the spacing between adjacent profiles (6 m) is intended to enhance data resolution and to produce 3-D image for the shallow subsurface. The resistivity contrast was employed as a reliable factor for the identification of the various stratigraphic units.

The multichannel analyses of surface waves (MASW) data were acquired at separate locations across the fly ash landfill using a 24-channel Seistronix engineering seismograph and 24 geophones, spaced at 1.5 m (5 feet) or at 0.76 m (2.5 feet) intervals (depending on the regularity of the depth to top-of-rock along the array line of the geophones). The acquired MASW data were used to determine the engineering properties of the subsurface to depth varies between 9 m (30 feet) to 30 m (100 feet)

The broader impact of this research is that it safeguards communities from the possible inadvertent migration of fly ash pollutants into subsurface soils and groundwater.

2. LITERATURE REVIEW

Yeheyis et al. (2009) defined fly ash as a by-product of coal combustion in thermal power generating stations. It is composed mainly of silt-sized spherical amorphous ferro-aluminosilicate minerals (Fisher et al., 1976) and is generally characterized by low permeability, low bulk density, and high specific surface area (Roy et al. 1981).

Fly ash contains many elements that include SiO2, Al2O3, and Fe2O3 and trace elements such as As, Ba, Cu, Cr, Mn, Pb, Sr, V and Zn. Fly ash produced by burning coal in power generation plants introduced many challenges, on top of which, is the surface and subsurface environmental contamination that directly and indirectly affect the living organisms. (Openshaw, 1992).

Fly ashes produced from coal combustion in power generating plants require careful treatment and safe disposal in landfills. The efforts directed to the reduction of the highly visible surface contamination problems, such as the blowing of or the burning debris. The possibility of ground-water contamination by fly ash landfills is of importance because of the composition of the fly ash. Douglas S. Cherkauer,1980 has mentioned that fly ash contains considerable concentration and types of trace elements such as Ti, Mn, K, Cu,Zn, Cr, Mo.,Ni and Pb. Jones et al. (1978) and Duvell et al. (1979), on the other hand, recognized that composition of fly ash is highly variable depending on the coal used, but has been shown to be generally high in Si, Al, Fe, Ca, Mg and S, among the major constituents. Tao et al., (2015) found that the dielectric constant of fly ash is dependent on the size of the grains of fly ash, such that the electrical

conductivity decreases with the decrease of the grain size, which means that the grain size plays an important role in the electrical conductivity of fly ash.

The major concern of the Environmental Protection Agency (EPA) related to groundwater pollution by leachate from coal combustion by-products, is the high concentration of their constituents of soluble salts and toxic trace elements and heavy inorganic components that include boron, sulfate, Arsenic, Barium, Cadmium, Chromium, Lead and Selenium (USEPA, 1988). Carlson and Adriano, 1993, found that the chemical and physical characteristics, climate and the hydrological conditions at the disposal site largely determine the groundwater contamination extent and concentration attenuation, and that major impacts of coal combustion residues are generally associated with changes in water chemistry, including changes in the pH and the concentrations of potentially toxic elements. Using fly ash as a soil amendment can improve soil texture and water-holding capacity, and increase the soil pH, and enhance soil fertility. However, it may also result in excessive soluble salt concentrations, excess Boron, and increased concentrations of other potentially toxic trace elements.

Mathematical solution techniques and modeling of contaminants transport are largely used in evaluating the impact of contaminants on groundwater. Most approaches to describing and predicting the movement of contaminants treat groundwater as a two-phase system in which contaminates partition between immobile solid constituents and the mobile aqueous phase. Contaminants that are sparingly soluble in water and that have a strong tendency to bind to aquifer media are assumed to move much more slowly than the rate at which groundwater flows (Figure 2.1).

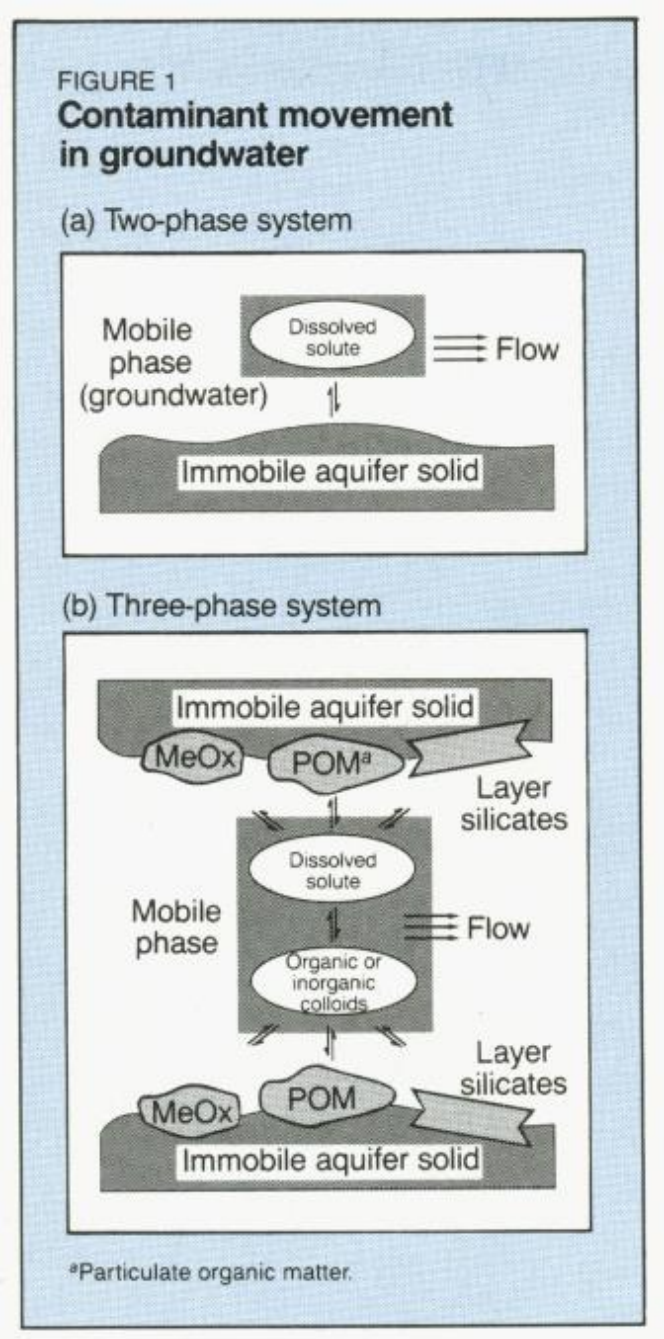

Figure 2.1: The two and three-phase systems of contaminant transport in groundwater (Source: McCarthy and Zachara, 1989).

Many contaminants readily absorb to immobile aquifer media and therefore are considered, to be virtually irremovable in the subsurface and to present little danger to groundwater supplies. For example, in soil and aquifer material, many metals and

radicals bind strongly to mineral components; therefore, many nonpolar organic contaminants tend to bind to particulate or link-matter and colloids in the solid phase, however, also may be mobile in subsurface environments. Because the composition of colloids is expected to be chemically like that of the surfaces of immobile aquifer material, these particles also could absorb organic and inorganic contaminants and stabilize them in the mobile phase (John F. McCarthy et al., 1999).

Landfill failures are evident in many parts of the United States. On December 22, 2008, a dike ruptured at an 84-acre ash fill operated by the Tennessee Valley Authority's Kingston Fossil Plant in Roane County, TN. 1.1 billion gallons of fly ash slurry were released, and covered over 300 acres with up to 1.8 m (6 feet) of sludge. The spill was larger than the Exxon Valdez, damaging neighboring properties and contaminating nearby waterways.

Electrical resistivity tomography is often used in conjunction with other non-invasive geophysical techniques in detecting and characterizing landfills in general, while for fly ash landfills the (ERT) technology supported by multichannel analysis of surface waves (MASW), has proved to be of importance in assessing the conditions of fly ash landfills. Muchingami, (2013) selected the (ERT) as the appropriate tool for the elucidation of potential flow paths and brine dispersion in ash dump. Thus, he could utilize (ERT) in monitoring and evaluating the impact of ash dump on the hydrological system at Tutuka, South Africa. The researcher was further able to estimate the flow rate of brine and to apply the (ERT) to understand and extract knowledge of the underlying hydrogeology and the geology of the study area without the application of intrusive methods.

Similar study by Muchingami et al. (2013) in Mpumalanga, South Africa utilized Electrical resistivity for monitoring infiltration of salt fluxes in dry fly ash dumps, based on the changes in moisture and salt concentration.

Sinkholes are considered by some to be difficult to study. Electrical resistivity tomography was found as an appropriate method to map sinkholes because of its capability of detecting resistive features and discriminate subtle resistivity variations. Schoor, (2002) used (ERT) in detecting two sinkholes in the dolomites of the Lyttelton Formation near Pretoria, South Africa.

ERT has gained a universal acceptance in the detection and imaging of sinkholes and underground karst features, especially when these features are buried under the sand. In Algeria, Fahdi et al. (2011) conducted 2-D electrical resistivity imaging in the Cheria Basin and was able to differentiate between the developing and mature sinkhole based on the detection of the resistive air-filled cavities. Youssef et al. (2012) detected sinkholes in Saudi Arabia that were successfully confirmed by field observation, using different electrode spacing with the dipole-dipole method. Shishay et al. (2016) found that electrical resistivity tomography is routinely used in Missouri to image the shallow subsurface in karst terrain because of the presence of the undisturbed soil, carbonate rock, clay in-fill, and air-filled cavities, which are characterized by very high resistivity contrast.

Combined ERT and GPR were used by Kruse et al. (2006) to resolve the structure of the clay-rich semi confining layer that floors sinkholes in many karst terrains and to image individual fractures or conduits below a main depression in the northeastern part of Tampa Florida. The study results confirmed that the combined geophysical methods were

able to image the target depression in the clay-rich semi confining layer, and that the 3-D GPR could further be used to detect the subtle vertical undulations.

Information from borehole log together with 2-D electrical resistivity data are used by Shishay et al. (2016) to generate geologic models depicting the subsurface structure and the formation mechanism of the karst features beneath the subsurface, therefore, with the help of borehole and MASW control and previous knowledge of the author in the study area, ERT contour values for the different geophysical unites in specific area can be determined.

3D electrical resistivity tomography (ERT) was used by Ogilvy et al. (2002) to map the 3D spatial distribution of waste and leachate concentrations within a closed and unconfined landfill as the 2D (ERT) and borehole sampling failed to detect the pollution plume. The 3D survey determined the pattern of leachate drainage within the waste and presented as 3D volumetric tomograms that showed the waste distribution and leachate flow-paths. In a study by Ahmed et al. (2001), the researchers were intending to evaluate the groundwater and soil pollution near Seri Petaling landfill in the State of Selangor, Malaysia. The results from (ERT) agreed with the geochemical analysis and investigation, revealing a general down-stream trend of pollutants.

Electrical resistivity imaging was employed in surveying the leachate content and to evaluate the boundary of a waste disposal site in Northern Israel. The research was challenged by the highly water saturated fat nonconsolidated clay, but was able to determine that the landfill body bottom was intensively saturated with leachates (Frid et al. 2008).

A recent research study by Shishay et al. (2016) in southwestern Missouri showed that the increase of clay content with depth is a reliable indicator of vertical water flow and piping and washing down of fine soil material into subsurface, and that the higher the moisture and piped clay, an anomalously low resistivity values is produced.

3. STUDY AREA

3.1. LOCATION

The study site is in Springfield Plateau, part of the Ozark natural division in southwestern Missouri. The natural divisions of Missouri are described by Richard et al., (2004) as a hybridized regionalization scheme that divides the state into six major divisions, namely, the Glaciated Plains, the Big Rivers, the Ozark Border, the Ozark, the Osage Plains, and the Mississippi Lowlands; that by integrating the geologic history, soils, bedrock geology, topography, plant and animal distribution, the pre-settlement, vegetation and other natural factors (Figure 3.1).

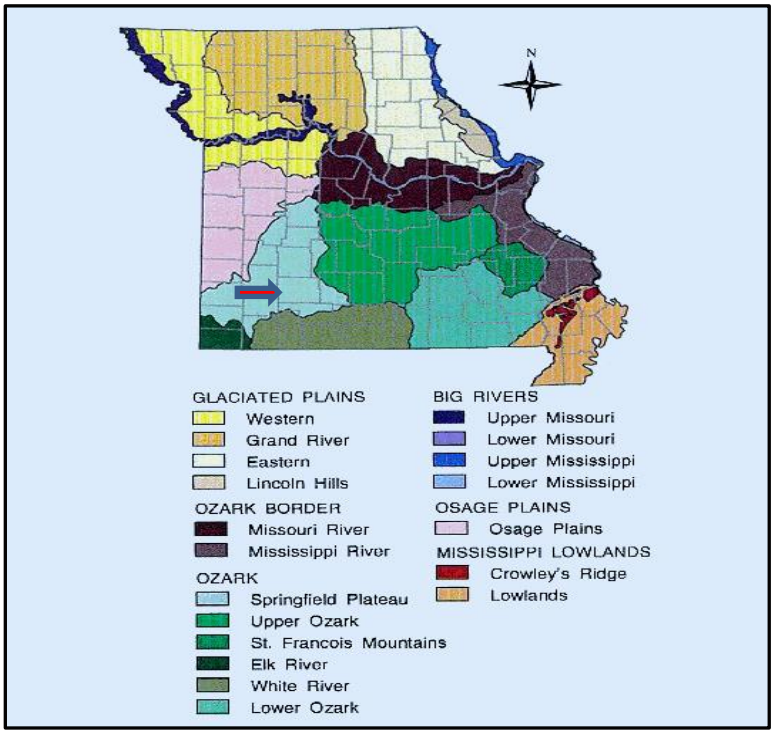

Figure 3.1: The location of study area in the Springfield Plateau in the Ozark Natural Division (red arrow) (Source: http://web.archive.org/web/20030930114729/ www.mdc.state.mo.us/ nathis/natcom/natdiv/).

The Springfield Plateau in south-central Missouri and northernmost Arkansas, being part of the Ozark Plateaus Province, falls within the general elevation of the Ozark natural division between 122 m (400 feet) to 548 m (1,800 feet) (a.s.l.), where elevations of 1800 feet reported in Springfield Plateau, and steep hillsides at elevations in the order of 304 m (1,000 feet) to 426 m (1,400 feet) occupy the hilly southeastern parts of the plateau (Figure 3.2).

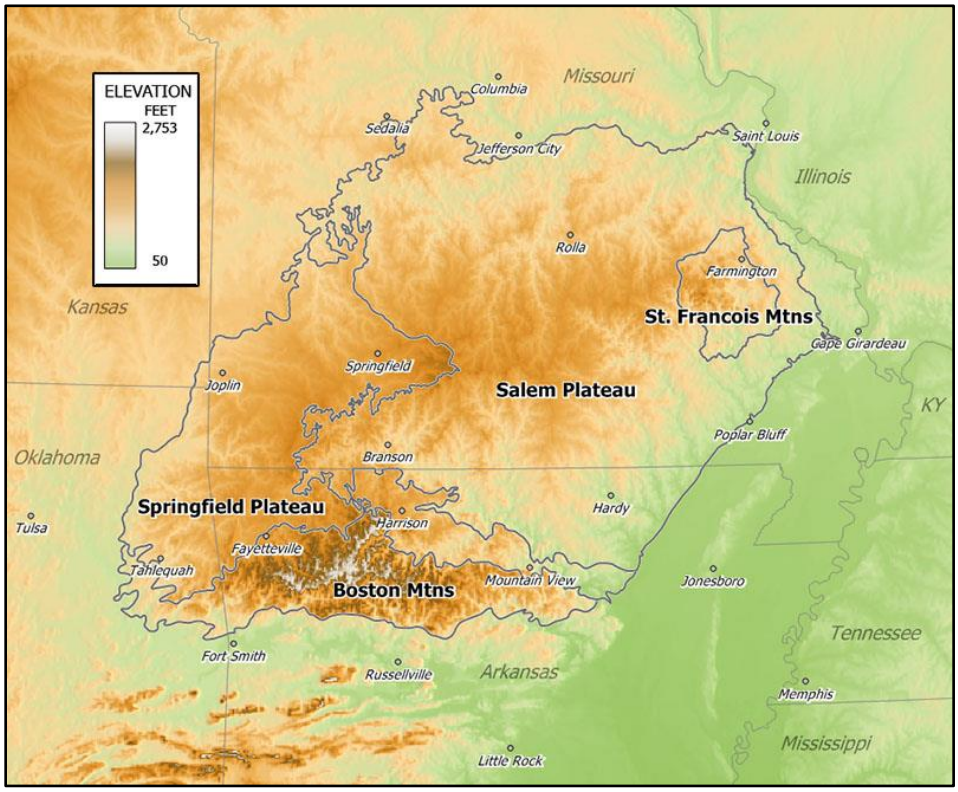

Figure 3.2: Elevations of the Springfield Plateau study area within the Ozark Region (Source: https://en.wikipedia.org/wiki/Ozarks#/media/File:OzarkRelief.jpg; By Tosborn at English Wikipedia - Transferred from en.wikipedia to Commons. Public Domain, https://commons.wikimedia.org/w/index.php?curid=4346100).

This research conducted at the northern section of a larger study area in southwestern Missouri (Figure 3.3). 3-D ERT data were acquired along west-east traverses for the purpose of imaging a fly ash landfill and map the underneath subsurface

to an approximate depth of 30.48 m (100 feet), using AGI SuperSting unit coupled to 168 electrodes, spaced at 1.5 m (5 feet) intervals.

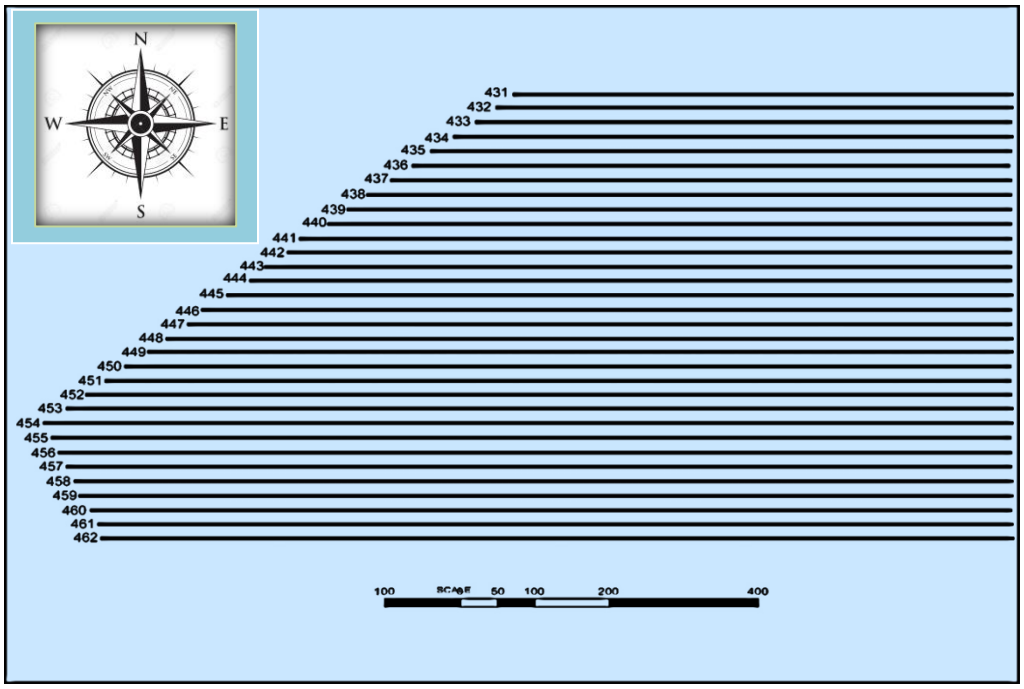

Figure 3.3: Traverses configuration where the ERT data acquired in the study area in southwestern Missouri, USA.

3.2. GEOLOGICAL SETTING

A characteristic feature of the Ozark Plateau, which encompasses Springfield Plateau, Salem Plateaus and the Boston Mountains, is the gentle southward dipping of its sedimentary rock formation, which were laid as shallow marine deposits and reached a thickness of more than 1524 m (5,000 feet), during the Ordovician- Pennsylvanian Period (http://www.geology.ar.gov/education/geo_ozark_plateaus.htm). As shown in Figure (3.4), the major rock formation of Springfield Plateau is the limestone dolomite, sandstone, and limestone with minor amounts of shale; rocks of Mississippian age, which are mostly cherty limestones; rocks of Pennsylvanian age, which consist mostly of shale,

sandstone, and limestone; and Post-Paleozoic sediments, which consist of sands, gravels, and clays. The Springfield plateau is recognized for its marvels of extensive cave systems and prominent sinkholes that have developed in the Mississippian limestone of the Burlington-Keokuk Formation that forms most of the extensive surface bedrock (Ismail and Anderson, 2012).

The Precambrian age igneous rocks underlying the Ozark Plateau province of the granite, rhyolite and diabase and the sedimentary rocks, are extensively fractured and faulted, and exposed only in the St. Francois Mountains of south-central Missouri and where rivers incision was deep through the overlying sedimentary formation.

Structures in the Ozark, in general and in the Springfield Plateau, such as faults and major river systems are vertical to steeply dipping, have strike-slip displacement, and trending northeasterly and northwesterly. Joints in the rocks are generally vertical too and are trending north-south and east-northeast (James C. et al., 2016).

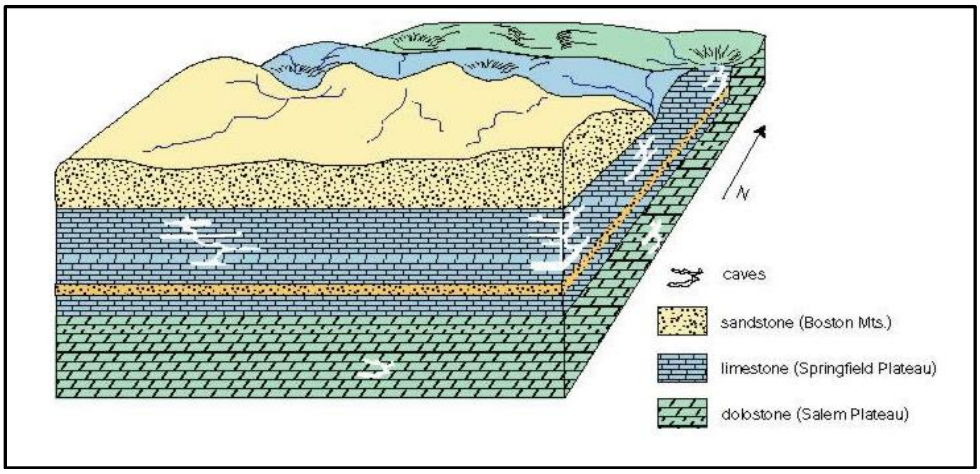

Figure 3.4: The principle rock formation and stratigraphic setting of Springfield, Salem and Boston Mountains of the Ozark Plateau (Source: http:// www.geology.ar.gov/ education/geo_ozark_plateaus.html).

3.3. TOPOGRAPHIC SETTING

The surface of Springfield Plateau is characterized by an undulating topography and is dominated by gently rolling hills. The plateau is less highly dissected compared to the other Plateaus of the Ozark, but in some of its parts, the plateau consists of steep hillsides associated with the deeply entrenched stream valleys.

Except at St. Francis Mountains, the study area is characterized by karst features in the entire Ozark region, which include sinkholes, caves, bluffs and large springs, calcareous wet meadows, losing streams, and streams with entrenched meanders. Streams are generally clear and meander in a northerly direction, such as Gasconade, Niangua, Lower Osage, Bourbeuse, and Meramec Rivers (Figure 3.5).

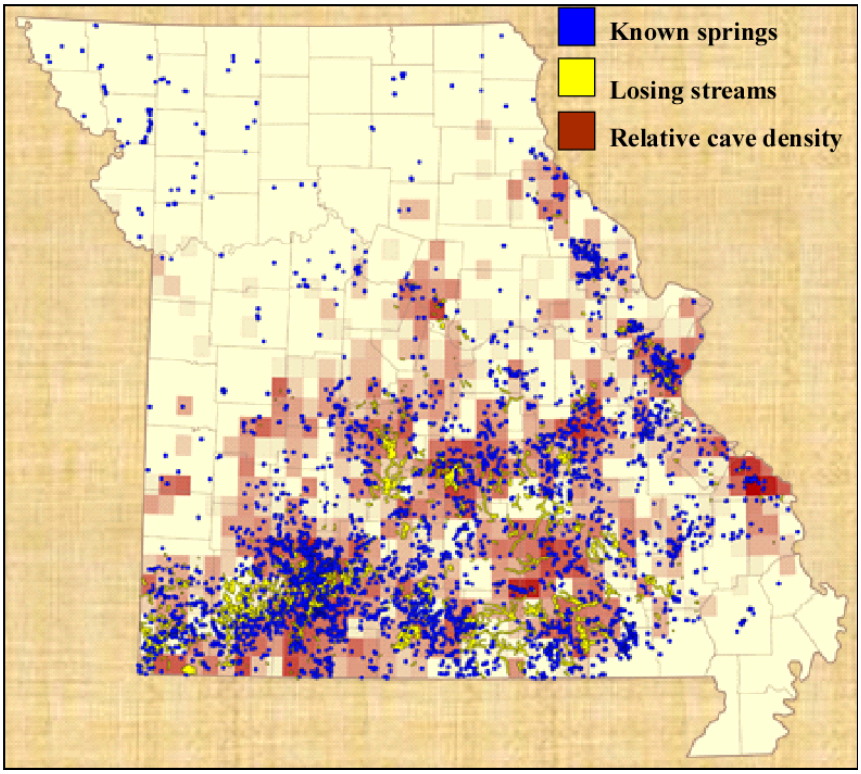

Figure 3.5: Karst features distribution in Missouri (Source: https://www.nature.nps.gov/Geology/parks/ozar/index.cfm).

3.4. SOILS

The soil in the study area is part of the Ozark Division; it is characterized by thin, often stony residual soils and scanty thin loess. Soils are highly weathered and contain high iron and aluminum. Soils of the study area can be extremely gravelly and have high permeability with short retention time.

Alfisol and ultisol soil types underlie most of the study unit. These soils are moderately to deeply weathered and have a wide range of hydraulic properties. The fertile alfisols are commonly found in both Salem and Springfield Plateaus. They are fairly fertile and good for vegetation growth (USDA, 1981 and Frey et al., 2014).

3.5. CLIMATE AND VEGETATION

Climate and vegetation are two of the elements that are detrimental in the creation and transportation of contaminant. Vegetation cover and type controls the intensity and velocity of water, therefore, landfills that are at the proximity of dense vegetation cover would likely be less affected by input water compared to landfills that are located at areas devoid of vegetation cover. Climate, on the other hand is also controls the amounts of water and the seasonality of possible pollution.

3.5.1. Climate. The climate of Missouri is generally controlled by the cold Canadian air masses and the warm moist air from Gulf of Mexico, thus Missouri has a continental type of climate marked by strong seasonality and is unchallenged by any topographic barriers, but periodically swing south from the northern plains and Canada. Precipitation varies from 0.889 m (35 inches) in the north and northwest to 1.27 m (50 inches) in the extreme southeast, mostly falls during April – June. Missouri receives little

amount of snow during December – February and the State lies in the path of maximum tornadic activity (Rafferty, et al. 2016).

The maximum temperature is experienced during January at about mid 40's degree Fahrenheit, in the southeast and mid 30's in the north and northwest, but summer temperatures may exceed the 100 °F (38 °C) in any part of the state.

The weather conditions between March and June brings about approximately 1.21 m/year (48 in/year) of rainfall to southwestern Missouri, while in the cold season extending between October and March, the average seasonal precipitation during is approximately 0.30 m/year (12 in/year), and it is important to know that precipitation is generally acidic in nature with pH values between 4.6 and 5.0, thus, would greatly impact the carbonate rocks in the region and the enhancement of karst development process.

3.5.2. Vegetation. Most of Missouri lands are covered by forests and prairie grasses. Bottomland deciduous forest is common due to the large number and size of the streams. Studies of pre- settlement vegetation (palynology) in the Ozarks revealed that a mixture of pine and oak forests were common under pre-settlement conditions. Vegetation was described as a mosaic of grassland, savannah, oak forest with open grass undergrowth and densely wooded valley bottoms. The Niangua darter (Etheostoma nianguae Gilbert and Meek) and bluestripe darter (Percina cymatotaenia) are Ozark endemics species, together with Wild pink (Silene caroliniana). Early settlers of the Ozarks during the 1800's cleared considerable forests areas for grazing and crop production (Foreman, A. T., 2014).

4. FLY ASH

4.1. WHAT IS FLY ASH?

Fly ash is the lightweight by-product particles that produced from coal combustion process in electric utility or industrial boilers, and it is carried off with the flue gases in electric generating plants by a mechanical collector or an electrostatic precipitator as they flow down from the boilers. Fly ash is composed mainly of silt-sized spherical amorphous ferro-aluminosilicate minerals (Fisher et al., 1976) and is generally characterized by low permeability, low bulk density, and high specific surface area, and is considered as waste and disposed in landfills (Roy et al., 1981).

4.2. PHYSICAL AND CHEMICAL PROPERTIES

Fly ash is mainly composed of silt sized glassy spheres typically ranging in size between 2 µm -50 µm (Martin et al., 1990) (Figure 4.1).

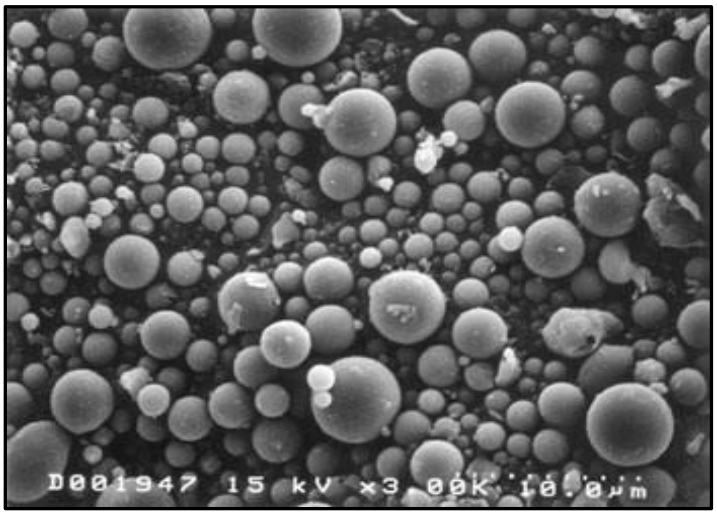

Figure 4.1: Fly ash particles at 2,000x magnification (Source: https://www.fhwa.dot.gov/pavement/recycling/fach01.cfm).

Some of the spheres are hollow, termed cenospheres, or spheres filled with smaller spheres termed plerospheres. The fly ash properties are dependent on the composition of the parent coal, conditions during combustion, efficiency of emission control devices, storage and handling of the byproducts, and climate (Adriano et al., 1980).

During the combustion and subsequent cooling process many different metal oxides can precipitate and concentrate on the surfaces on these spheres. These oxides control the chemical properties of the ash, and tend to vary from ash to ash. The oxides may also affect the physico-chemical properties of some fly ashes, especially the pozzalonic (cementious) reactivity (Stewart et al, 1996)

Fly ash is generally considered a ferro-aluminosilicate mineral with aluminum (Al), silicon (Si), calcium (Ca), magnesium (Mg), iron (Fe), potassium (K), sodium (Na), chlorine (Cl_2), and sulphur (S), as the predominant elements. In addition, fly ash contains all naturally occurring elements and generally enriched in the trace elements compared with the parent source coal, like boron (B), arsenic (As), cadmium (Cd), molybdenum (Mo), selenium (Se), and zinc (Zn). Many of these trace elements are concentrated in the smaller ash particles. Ash pH depends on the sulphur content of the parent coal.

Classifying and sorting fly ash into types or groups was governed by the purpose of the ash utilization, such as an input in the cement industry and in soil fertilization, but the environmental protection agency (EPA), is considering the risk of mobilization of ash and other slid wastes as a classification approach based on the toxicity of some particular mobilized waste. Other than Griffin (1982) classification, which is based on the chemical composition, hydration pH and particle size distribution, the American Society for

Testing and Materials (ASTM), is the main classification method used. The method is based on the source of coal and the major element oxide content of the fly ash. Accordingly, fly ash in the U.S. is classifies into type (F) and type (C), where type (F) contains at least 70% of SiO_2 + Al_2O_3 + Fe_2O_3, and type (C) must have a minimum of 50% SiO_2 + Al_2O_3 + Fe_2O_3 , and higher calcium content (Openshaw, 1992).

The physical, chemical, and mineralogical characteristics of fly ash depend upon several factors including the composition of the parent coal, combustion conditions, the efficiency and type of emissions control devices, and the method of ash disposal (Carlson and Adriano, 1993). Ash varies from acidic to alkaline because of the chemical make-up of the source coal. Physical appearance varies depending on coal type and furnace. All fly ash samples are mainly composed of glass-like porous beads that vary in chemical composition with respect to Al/Si/Fe ratio and pH, from extremely low pH (near 3) to extremely high pH (near 12). Alkaline fly ash is often associated with high boron levels and exhibits extremely low pH buffering (V.P. Evangelou, 1996).

4.2.1. Physical Properties. The physical properties of fly ash depend upon several factors, including the type of coal burned, the boiler conditions, the type and efficiency of the emission controls, and the disposal method (Adriano et al., 1980). Certain characteristics tend to be similar in most ashes. Fly ash is mainly composed of silt-sized materials having a diameter of less than 10 microns (Chang et al., 1977, Terman, 1978 and references therein). The grain size of fly ash affects its electrical resistivity, such that the electrical resistivity increases with the decrease of the grain size (Tao et al., 2015). When compared with mineral soils, fly ash has lower values for bulk density, hydraulic conductivity, and specific gravity. Both crystalline (mullite) and

amorphous (glass) phases have been identified by X-ray diffraction in fly ash (Mattigod et al., 1990).

4.2.2. Chemical Properties. Fly ash consists primarily of oxides of silicon, aluminum iron and calcium. Magnesium, potassium, sodium, titanium, and sulfur are also present to a lesser degree. The chemical properties of fly ash will largely be determined by the metal oxides that were surface adsorbed during particle formation. In the U. S., fly ash from eastern coals, which usually are higher sulfur coals, tend to be higher in Fe, Al, and S and lower in Ca and Mg when compared to western coals. The ranges of chemical analyses of U.S. fly ashes from different types of coal are shown in Table 4.1 and 4.2.

Table 4.1: Partial elemental composition of various fly ash sources (Terman, 1978).

Power Plant	Location	Electrical composition							Neutralizing value meq.H_3O^+/g
		K	Ca	Mg	P	B	Zn	Mo	
Big Sandy	Louisa, KY	3.10	0.72	0.53	0.04	319	51	7.4	0.12
Clinch River	Cleveland, VA	2.69	2.52	0.74	0.08	342	55	9.2	1.23
Glen Lynn	Glen Lynn, VA	2.41	0.58	0.23	0.05	307	36	6.8	0.09
Kanawha River	Glasgow, WV	3.19	0.67	0.27	0.03	391	46	5.6	0.09
Muskingum River (1)	Beverly, OH	2.33	0.45	0.84	0.06	301	115	11.8	acidic
Muskingum River (2)	Beverly, OH	1.97	0.82	0.49	-	340	-	9.3	-
Phillip Sporn	New Haven, WV	2.51	0.65	0.09	0.05	340	88	11.1	0.05
Mont Storm	Mont Storm, WV	2.29	0.90	0.11	0.07	278	378	16.9	Acidic
Albright	Albright, WV	2.50	0.31	0.22	0.04	264	30	6.2	0.04
Rivesville	Fairmont, WV	2.45	0.65	0.26	0.07	236	13	7.8	Acidic
Fort Martin	Maidsville, WV	2.25	2.44	0.82	0.17	415	88	15.5	0.58
Crawford Edison	Chicago, IL	2.42	3.27	0.80	0.10	613	363	39.3	1.33
John Sevier	Rogersville, TN	3.14	0.61	0.46	0.05	323	74	9.4	0.01
E.C. Gaston (1)	Wisonville, AL	2.70	0.71	0.82	0.15	428	186	24.4	0.25
E.C. Gaston (2)	Wisonville, AL	2.65	0.97	0.30	-	367	-	24.8	-
Hoot Lake	Fergus Falls, MN	0.65	12.3	5.99	0.21	618	86	5.7	3.05
Lewis and Clark	Sidney,MT	1.07	12.56	6.02	0.28	414	132	7.5	3.73
Kansas Power and Light	Lawrence,KS	-	-	-	0.06	48	353	-	1.87

Table 4.2: Ranges and average chemical composition of fly ash (Roy and Griffin, 1982).

Constituent	Range (%)	No. of data	Avg. (%)
SiO_2	2.19-68.1	58	44
TiO_2	0.5-2.55	39	1.3
Al_2O_3	3.39-39.4	60	23
Fe_2O_3	3.60-29.2	58	11
CaO	0.2-31.0	58	8.2
MgO	0.4-12.8	58	2.7
Na_2O	0.2-8.0	50	1.8
K_2O	0.2-8.1	49	2.0
C	0.1-25.7	21	5.0
SO^2	0.1-7.28	48	1.6

(Table 4.2 data from the literature and unpublished data from Illinois State logical survey files).

The electrical resistivity of the fly ash depends on the physical characteristics, chemical composition and moisture content of fly ash. In a research on the chemical composition and moisture effects on of fly ash electrical resistivity, conducted by Andrabi, et al. (2012), he found that increasing combined calcium and magnesium oxides, increases the resistivity of fly ash due to the low conductivity of these elements when in combination, and also concluded that combining sodium and potassium oxides, decreases resistivity when their percentages increase because sodium is an ion donor and is abundant in fly ash, unlike potassium that has minor effect in decreasing the resistivity.

Fly ashes from eastern coals also tend to be higher in the trace elements As, Cd, Cr, Pb, V and Zn (Roy et al., 1981). Most of these elements can substitute into the iron pyrite structure, and coals higher in pyrite therefore tend to produce fly ashes which contain higher levels of these elements. The element selenium does not seem to be correlated with any coal property. Selenium is known to be a volatile element and its behavior may be highly dependent upon the burning conditions within the boiler. (Stewart et al, 1996).

4.3. FLY ASH PRODUCTION

In coal combustion processes, coal is crushed into small particles, which is then burned at temperatures that exceed 1500°C. 70 to 90% of the raw coal is burned in this process leaving a small fraction of impurities, which is known as fly ash (coal combustion by-product). One fifth of this by-product settles down to the bottom of the furnace, and is known as "bottom ash'', while the remainder is quickly (~ 4 seconds) removed to low temperatures (~200^{o}C), where it is expelled from the furnace with the flue gas in a crystalline or non-crystalline glassy form, known as fly ash.

More recent combustion technologies tends to introduce clean methods by pre-treating raw coal before combustion by removing the mineral particles and reduce the toxic contents of the coal and to eliminate the gaseous materials.

Fly ash is the second largest industrial waste seam in the United States. Approximately 90 million tons of coal combustion byproducts were produced in the USA in 1994 (Stewart, B. et al., 1996), while 114.7 million tons was produced in 2013 (American Coal Ash Association, https://www.acaa-usa.org, August 2016) (Table 4.3).

Table 4.3: Production of coal byproducts in the USA, 2013.

	VOLUME 2013	PROJECTED VOLUME 2033	PROJECTED TOTAL GROWTH	PROJECTED AVERAGE ANNUAL GROWTH RATE
Production				
Fly Ash	53.4	54.6	2.2%	0.1%
FGD Material	35.2	38.8	10.1%	0.5%
Bottom Ash	14.5	14.7	1.2%	0.1%
Boiler Slag	1.4	0.8	-43.2%	-2.8%
FBC Ash	10.3	11.8	14.5%	0.7%

The generated fly ash in Missouri is about 2,679,742 tons annually (http://earthjustice.org/sites/default/files/StateofFailure_2013-04-05.pdf).

Most of the coal combustion byproducts is fly ash with approximately 53.4 million tons in 2013 (https://www.acaa-usa.org, Aug. 2016), and it is projected to be 54.6 million tons in 2033 (Figure 4.2).

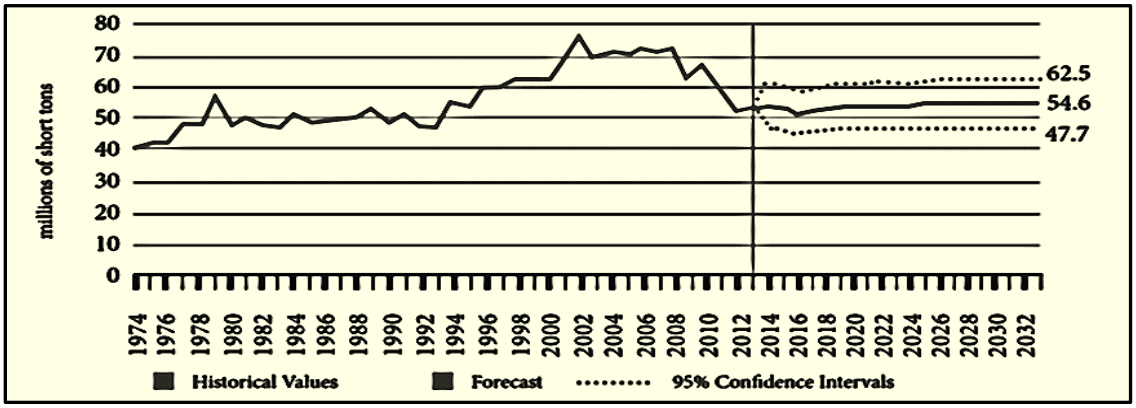

Figure 4.2: Projected production of fly ash in the United States (Source: ACAA, https://www.acaa-usa.org, Aug. 2016).

4.4. UTILIZATION OF FLY ASH

Although fly ash is considered waste by itself, it has become a valuable by-product in numerous environmental and commercial applications due to its pozzolanic, cementitious and alkaline properties. These include its use as raw material in cement production, as an admixture in blended cements and as replacement for cement or as a mineral admixture in concrete; for agriculture to improve soil structure and water-holding capacity, as a liming agent to neutralize acidic soils, and as essential source of micronutrients for agricultural crops. (Muluken B. Yeheyis, Julie Q. Shang and Ernest K. Yanful, 2009).

Utilization of fly ash is increasing and is expected to increase over the next 20 years, by 53 percent, that increase is triggered by the growth of the ready-mixed concrete industry. (Figures 4.3 and 4.4).

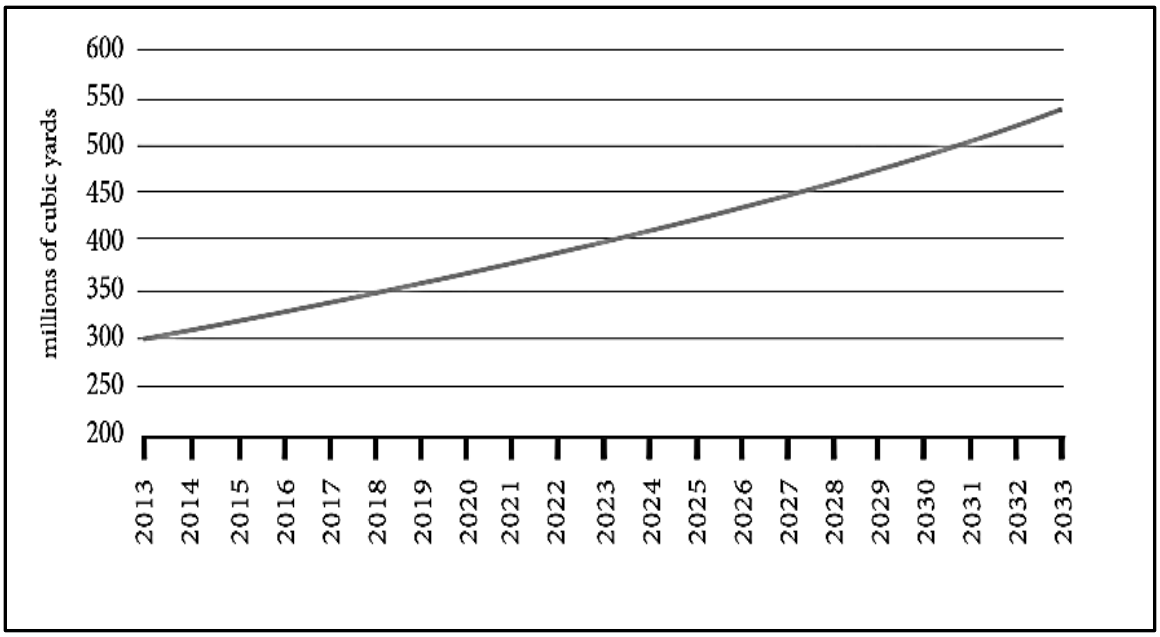

Figure 4.3: Projected demand for ready-mixed concrete (Source: ACAA, https://www.acaa-usa.org, Aug. 2016).

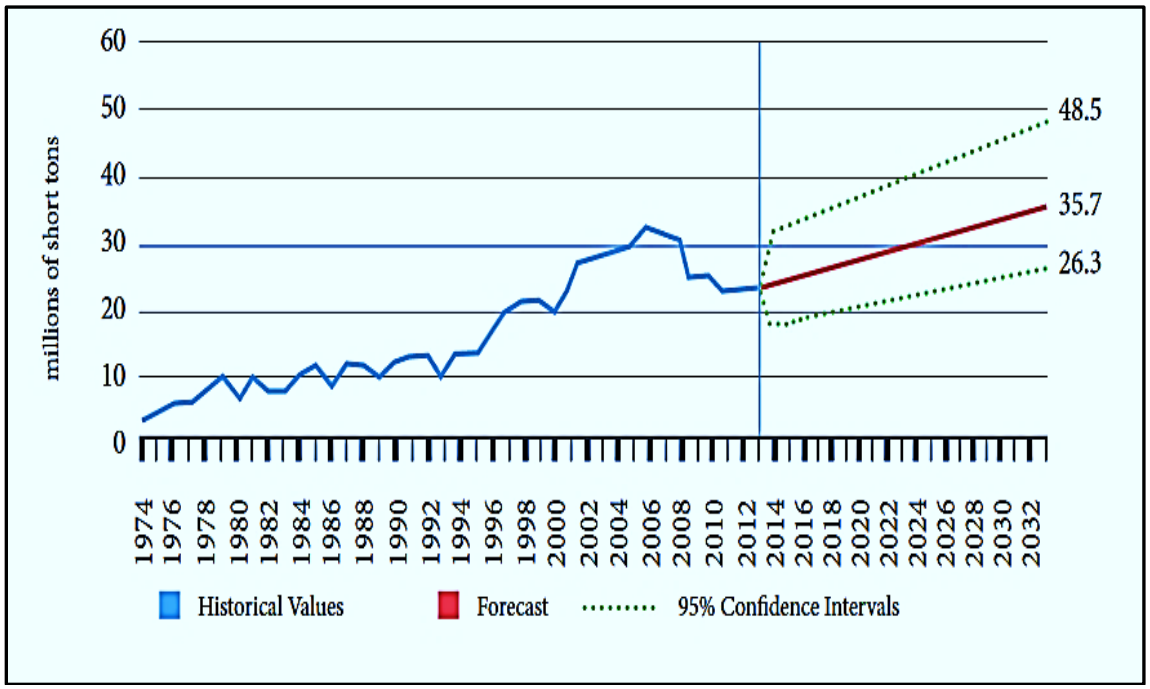

Figure 4.4: Fly ash utilization (Source: ACAA, https://www.acaa-usa.org, Aug. 2016).

5. DESIGN AND CONSTRUCTION OF FLY ASH LANDFILLS

Landfill is the physical construction built (designed) for disposing solid wastes in the earth's surface soil (either in the ground or on the top of the ground) to avoid polluting the surrounding environment and the ground water. Fly ash landfills are a special landfill types that are constructed and designed to accommodate the by-products of coal combustion residues, which contains toxic materials contained in heavy metals, trace elements and soluble oxides of chemical elements that are considered of primary concern by environmental, governmental and community bodies in the contamination of ground water pollution and subsurface soil.

Increasing production of fly ash, from coal based industrial constructions or from power plants, is posing a challenging problem in terms of its safe disposal and proper utilization. Fly ash is enriched in leachable heavy metals such as arsenic and boron, which are considered highly hazardous materials according to the environmental regulations in most of the countries of the world. Fluctuating water table and rain water interacts with fly ash in landfills, causing the leaching of toxic heavy metals and trace elements to the subsurface soil and groundwater, thus, leads to serious environmental issue. As such, it becomes mandatory to characterize fly ash, along with the identification of its leaching characteristics to adopt efficient disposal strategies (Devendra N. Singh et al, 2002).

Fly ash landfills are constructed to eliminate the visual and non-visual environmental threats of trace elements, heavy metal and other element oxides that are generated from the combustion of the different types of coal, and to prevent these toxic

and hazardous materials from migrating to groundwater or be retained by subsurface soils and ultimately reach for the food-chain and impact human life and living organisms.

Landfill designs are all meant to be secured, but for fly ash landfills, the secure landfill construction requires a number of elements to be considered that include (i) a bottom-liner system (compacted clay layer and/or geosynthetic layers) at the base and sides of the landfill, to prevent the scape of the leachate material to subsurface soils and groundwater, (ii) leachate collection pipes to collect the leachate from the landfill base and to prevent the leachate clogging, (iii) geotextile filter layers to filter or become as a pipe drain the leachate to the removal area (iv) final cap cover soil to divert the surface drainage away from the landfill, (v) landfill structural stability, and (vi) a hydrogeological setting and surface water drainage system to minimize the chances of washing the landfill materials into the natural drainage system (Figure 5.1 and Figure 5.2).

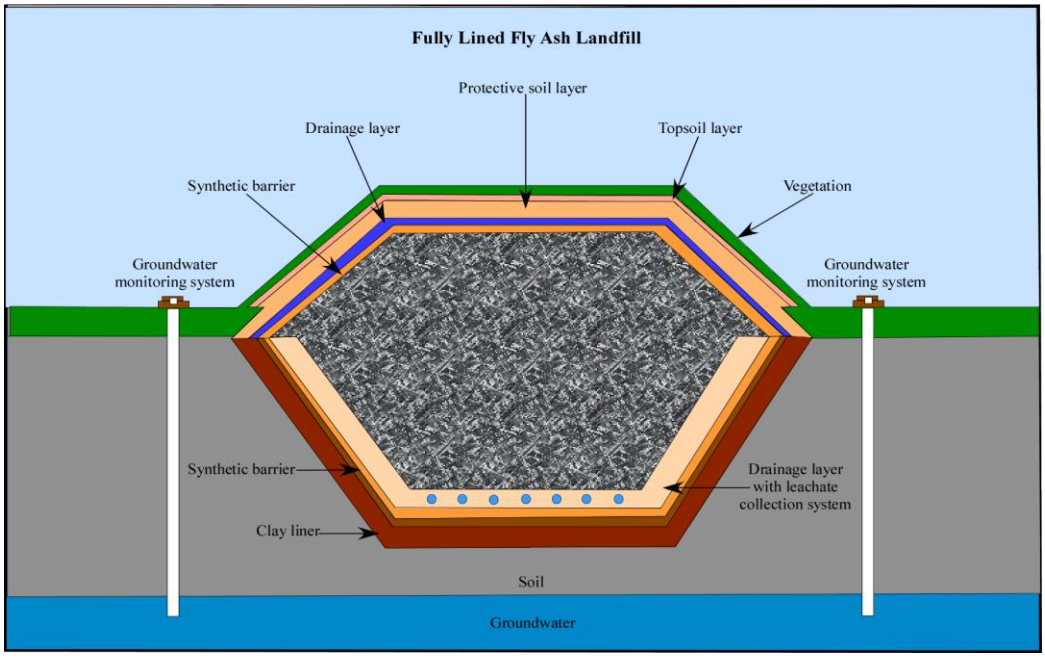

Figure 5.1: Elements of design of fly ash landfill (source: https://www.duke-energy.com/).

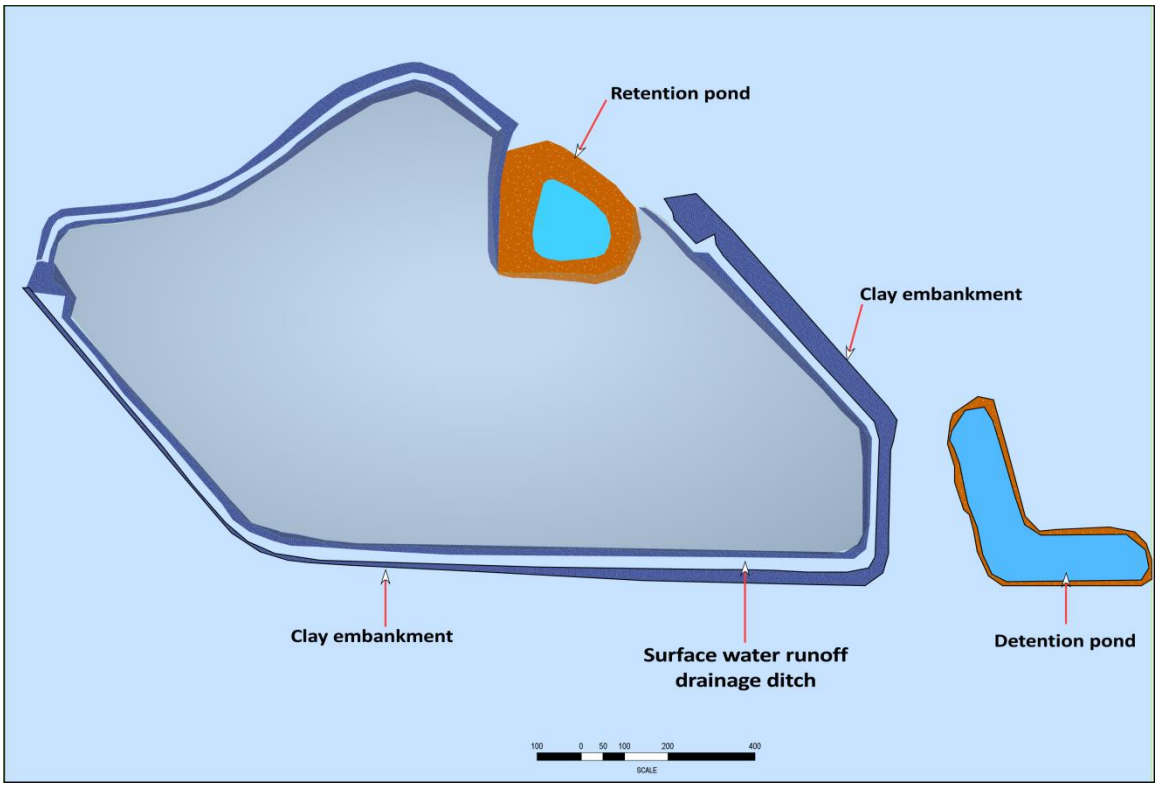

Figure 5.2: Illustrative figure for a fly ash landfill.

5.1. THE LINER SYSTEMS OF FLY ASH LANDFILLS

The liner system in landfills is the principle element in the design, as it secures the leachate and prevents it from reaching for the groundwater and subsurface soils. Many developments occurred in designing, constructing and maintaining liners for variety of purposes. The main types of liners include the clay liners, the geosynthetic liners and the geosynthetic clay liners.

5.1.1. Clay Liners. The compacted clay material is used as classical liner in landfills due to the relatively low hydraulic conductivity (10^{-7} cm/sec) that characterizes compacted clay. In 1984, the Environmental Protection Agency (EPA) enforced a minimum of double liner system design for leachate collection and removal (Figure 5.3).

Prior to the enforcement of double liner systems, single clay liner or single geomembrane liners were commonly used for landfills.

The double liner system is dependent on the properties of the materials used in the design, such as the clay and the synthetic material properties. For clay to be used as liner, compaction is considered as the most challenging task, because of the flocculent structural property of the clay. For the optimum compaction of the clay, the compaction moisture content will reduce the degree of flocculation to its minimum. Exceeding the optimum moisture content will reduce the dry soil unit weight, despite that it leads to clay particle orientation, which is a desired property.

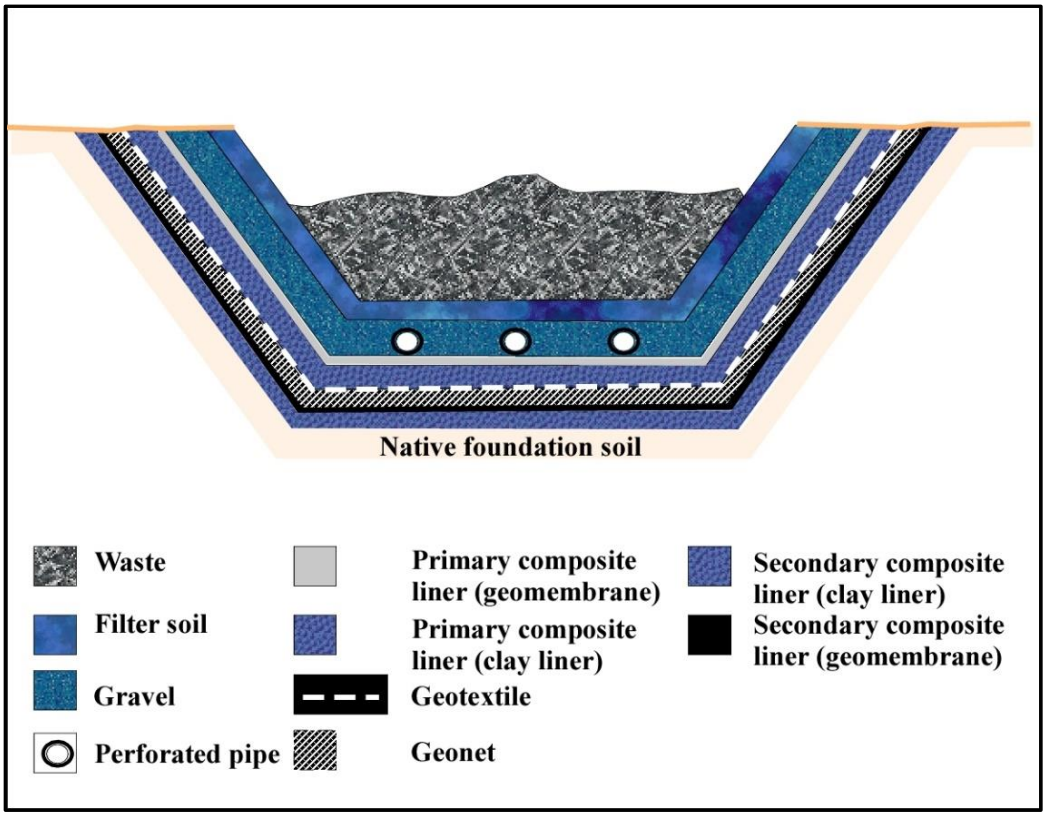

Figure 5.3: Cross section of double-liner system (Source: Das, B. M., 2014, Principles of Geotechnical Engineering).

To achieve optimum compaction results of clay, at least 20% of the soil should be of the fine fraction (i.e. silt and clay), and that the plasticity index (PI) to be greater than 10, and the gravel-size content to be less than or equal to 10%, and the soil should not contain greater than 25 to 50 mm-size chunks of rocks.

The ideal mix of plastic and non-plastic materials needed to produce liners that comply with the requirements for the minimum hydraulic conductivity for clay liners where the mixtures liquid limit is greater than 50%, was introduced from laboratory experiments, and is satisfying the equation:

$$\log K = \frac{e - 0.0535\,(LL) - 5.286}{0.0063(LL) + 0.2516}$$

where,

K = hydraulic conductivity (permeability) of bentonite- non-plastic soil mixture (m/sec)

e = void ratio of compacted mixture

LL = liquid limit of mixture (%)

(Source: Das, 2008).

Permeability and hydraulic conductivity (K) are often interchangeably used terms for the same property. Permeability (K) is defined as a measure of the amount of fluid that will flow through a sample for a given time without causing displacement. Fluids actually flow through the void space, not the particulate matter, and that gives porosity a controlling influence on permeability.

The coefficient of permeability equivalently refers to the hydraulic conductivity and is given by the equation (Openshaw, 1992):

$$K = \underline{k}\gamma/\mu$$

where

γ = specific weight of fluid

μ = dynamic viscosity of fluid and,

$\underline{k}$ = the intrinsic property of the medium.

It is essential for successful compaction of clay layers; the permeability is highly reduced for both, the liners and the clay, and between the compaction lifts, otherwise, leachate could escape through the compaction lefts interfaces (Figure 5.4).

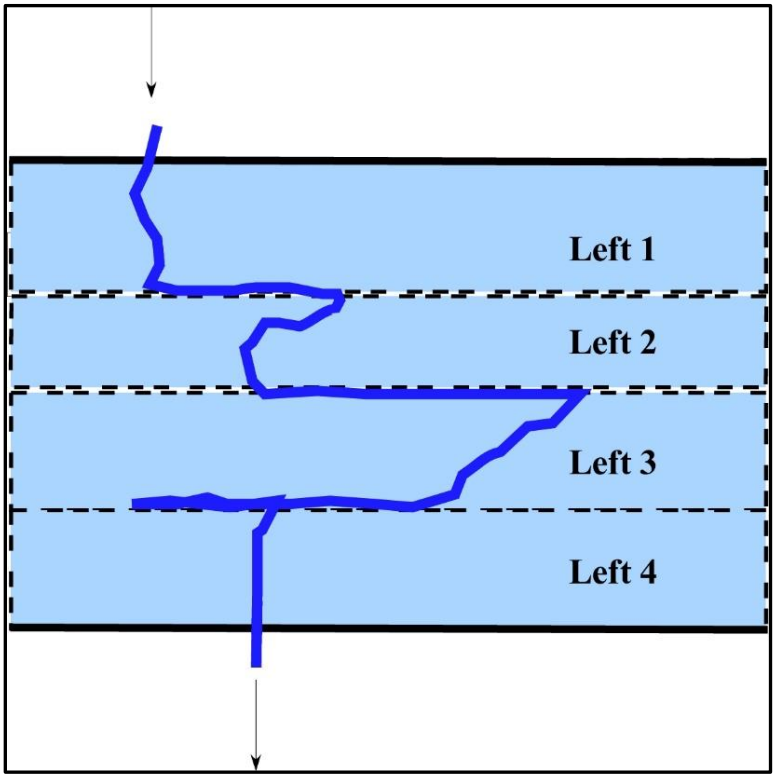

Figure 5.4: Pattern of flow through compacted clay with improper bonding between lifts (After J.5. Environmental Protection Agency, 1989).

5.1.2. Geosynthetic Liners. The Geosynthetics liners are similar to natural textiles, but are manufactured from polymer materials such as polyester, polyethylene, polypropylene, polyvinyl chloride, nylon and chlorinated polyethylene, to be utilized in the separation, reinforcement, filtration and drainage and as a moisture barrier in a variety of applications, including, essentially, the landfill leachate liners. Examples of these Geosynthetic materials and their most common functions in the landfills liners systems are illustrated in Figures 5.5 to 5.7.

5.1.2.1. Geonets. Geonets are formed by the continuous extrusion of polymeric ribs at acute angles to each other and are used basically for drainage, and are made of medium to high density polyethylene (Figure 5.5).

They are available in rolls with widths of 1.8 m to 2.1 m, and their lengths could be 30 m to 90 m. The approximate aperture sizes vary from 30 mm x 30 mm to about 6 mm x 6 mm. The thickness of geonets that is commercially available can vary from 3.8 mm to 7.6 mm.

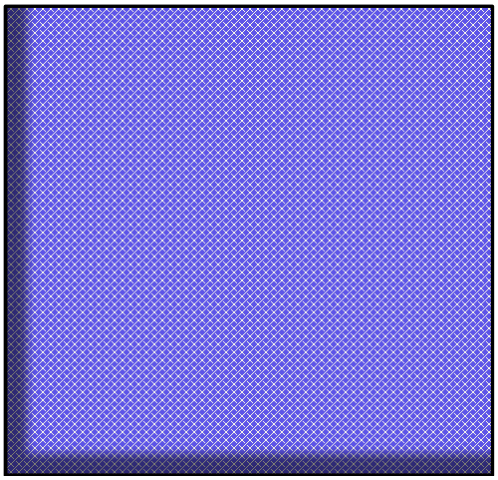

Figure 5.5: Polyethylene geonets as drainage liners (Source: Das, B. M., 2008, Principles of geotechnical engineering, seventh edition).

5.1.2.2. Geomembranes. These are Impermeable liquid or vapor barriers, made of continuous polymeric thermoplastic or thermoset flexible sheets, and the material used for their manufacturing include polyethylene, chlorinated polyethylene, and polyamide. The thermoset polymers include ethylene vinyl acetate, polychloroprene, and isoprene-isobutylene.

The hydraulic conductivity of geomembranes is in the range of 10^{-12} to 10^{-15} m/sec, and their thickness range from 0.25 mm to about 0.4 mm. Types and field configurations of geomembrane seams include, (a) lap seam; (b) lap seam with gum tape; (c) tongue-and-groove splice; (d) extrusion weld lap seam; (e) fillet weld lap seam; (f) double hot air or wedge seam (Figure 5.6).

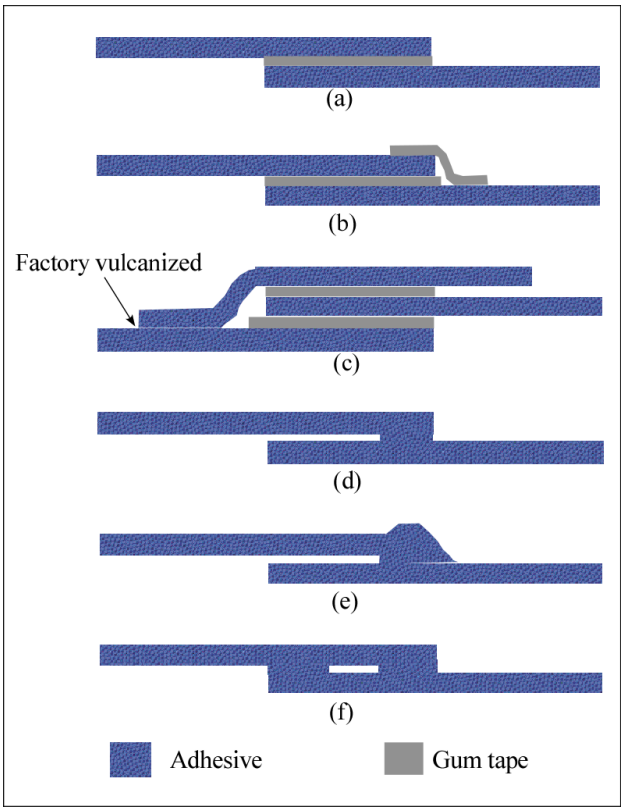

Figure 5.6: Types and field configurations of geomembrane seams (Source: Das, B. M., 2008, Principles of geotechnical engineering, seventh edition).

5.1.2.3. Geotextiles. Geotextiles encompass the woven and nonwoven types and they both require intensive testing's of their properties to approve them to be used as liners in landfills (Figure 5.7).

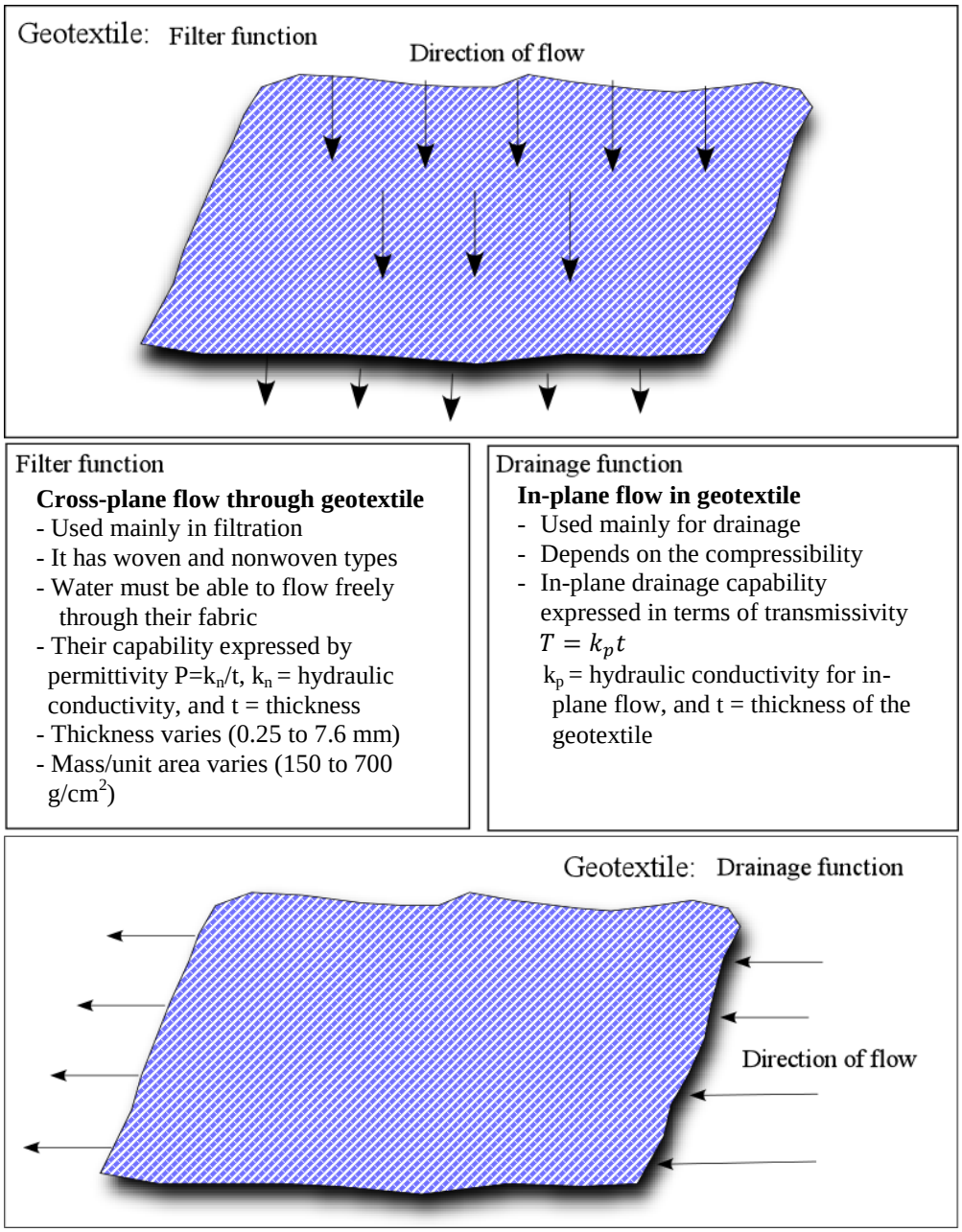

Figure 5.7: The drainage and filter types geotextiles and their properties (Source: Das, B. M., 2008, Principles of geotechnical engineering, seventh edition).

The mass per unit area, the percentage of open area, the equivalent opening size and the thickness of the geotextile are among the general properties, whereas the ultraviolet resistivity, the permittivity, the transmissivity are more concerned with micro properties, while the puncture resistance, resistance to abrasion, compressibility, the tensile strength and elongation are of the physical properties, and the testing and measurement of the chemical resistance.

To use the Geomembranes as liner component, similar measurements and testing is advisable, as in the case of Geotextiles, in addition to measuring and testing density, water vapor transmission capacity, tensile behavior, tear resistance, resistance to impact stress cracking, and the thermal properties and seams behavior.

In practice, geomembrane sheets are assembled and seamed together in larger sheets to avoid their failure when they are used as liquid or vapor barrier (Figures 5.4-5.7).

5.1.3. Geosynthetic Clay Liners. These are mixed geosynthetic-clay components that are designed to provide the maximum protection as a fly ash landfill, in place of the clay liners, due to the low hydraulic conductivity of the bentonite that is used in these liners (Lin and Benson, 200; Egloffstein, 2001, 2001 and Benson et al., 2006).

The bentonite layer is securely and professionally locked between two or more geotextile layers. The calcium and magnesium of the Bentonite are exchanged for the sodium, which has very low hydraulic conductivity in the order of ~10^{-11} m/s (the sodium ion is smaller compared to the calcium and magnesium). Furthermore, the sodium rich bentonite is hydrated to increase its moisture absorbance capability.

5.2. THE LEACHATE REMOVAL SYSTEM

The leachate in landfills is caused by washed-down of the landfill materials by rain water, snow melt and flood water into the subsurface. It represents a major source of pollution to groundwater and subsurface soils. Therefore, proper containment deems necessary to be implemented in constructing and designing landfills that are equipped with double linear systems to avoid the anticipated hazards of fly ash leachate in fly ash landfills.

The leachate removal systems employ pumping or gravity to efficiently remove leachate from the base of the landfill, thus, proper gradation of the landfill floor is a vital design element to drain leachate to the collection and removal point (Figures 5.8 & 5.9).

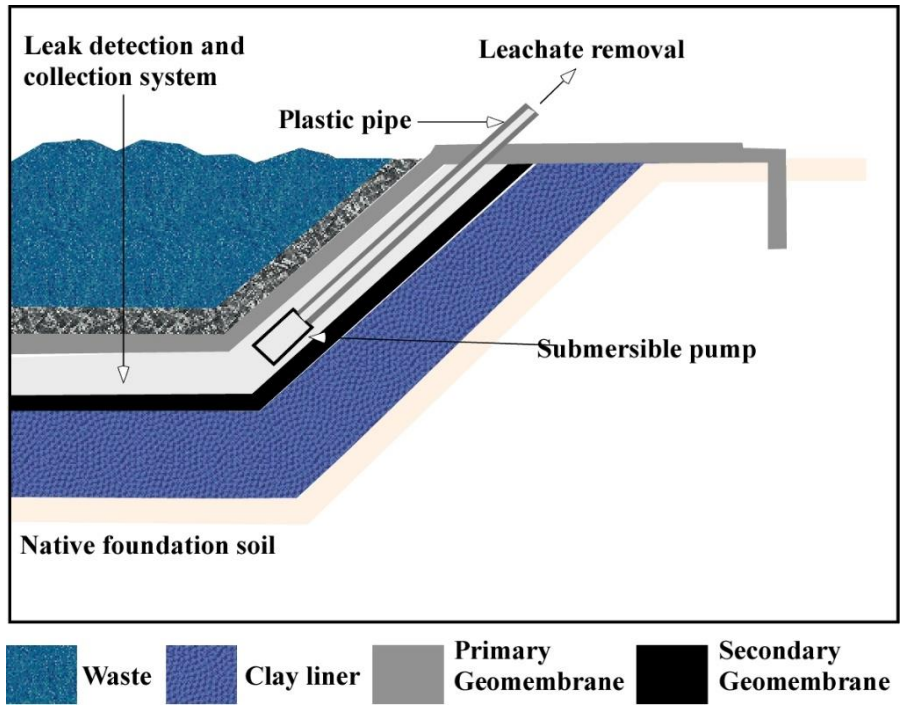

Figure 5.8: Secondary leak detection, collection, and removal (LDCR) system, by means of pumping (Note: The plastic pipe penetrates the primary geomembrane) (Source: Das, B. M., 2014, Principles of Geotechnical Engineering).

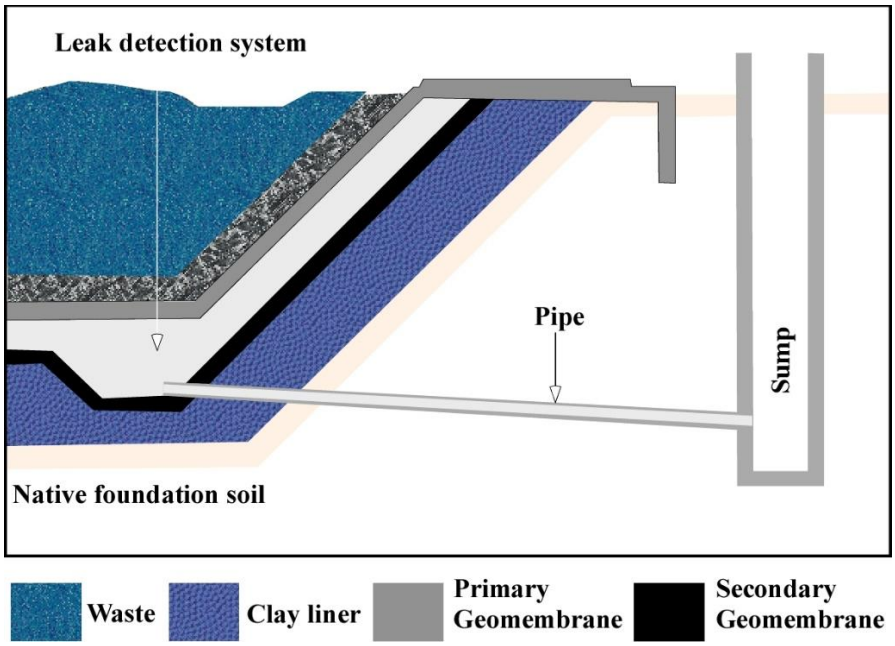

Figure 5.9: Secondary LDCR system, by means of gravity monitoring (Note: The plastic pipe penetrates the secondary geomembrane) (Source: Das, B. M., 2014, Principles of Geotechnical Engineering).

5.3. CLOSURE OF LANDFILLS

At the end of the age of the landfill, a cap cover is implemented for minimizing the production of leachate and minimizing the infiltration, and as a result protecting the groundwater from being contaminated (Figure 5.10). Clay-rich soils used in constructing low-hydraulic-conductivity covers for landfills (Daniel, et al. 1993). The cap cover is constructed of layers of compacted clay, topped by geomembrane and drainage layer and finally, covered by topsoil (Figure 5.11).The upper topsoil allow water to percolate to the protective impermeable layer or geomembrane. The function of this protective layer or geomembrane is to direct the water flow laterally away from the fly ash landfill. The diverted storm water will be collected at the designed drainage system at the toe of the landfill (drainage ditch), and eventually be directed to the natural drainage system and/or the low area of the landfill where the retention pond is located. Storm water that collects

via the drainage ditch will reach to the groundwater, bearing no contaminants, while on the other hand, the protective soil layer or geomembrane will prevent storm water to contact the leachate of the landfill.

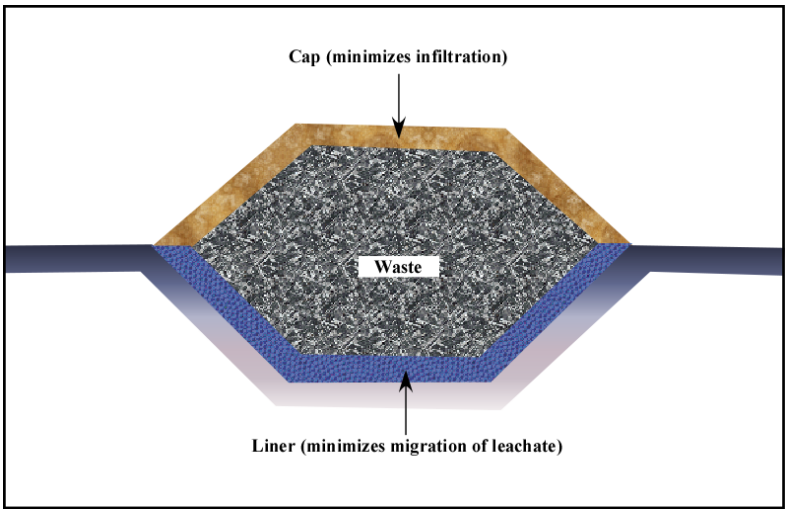

Figure 5.10: Landfill with liner and cap (Source: Das, B. M., 2014, Principles of Geotechnical Engineering).

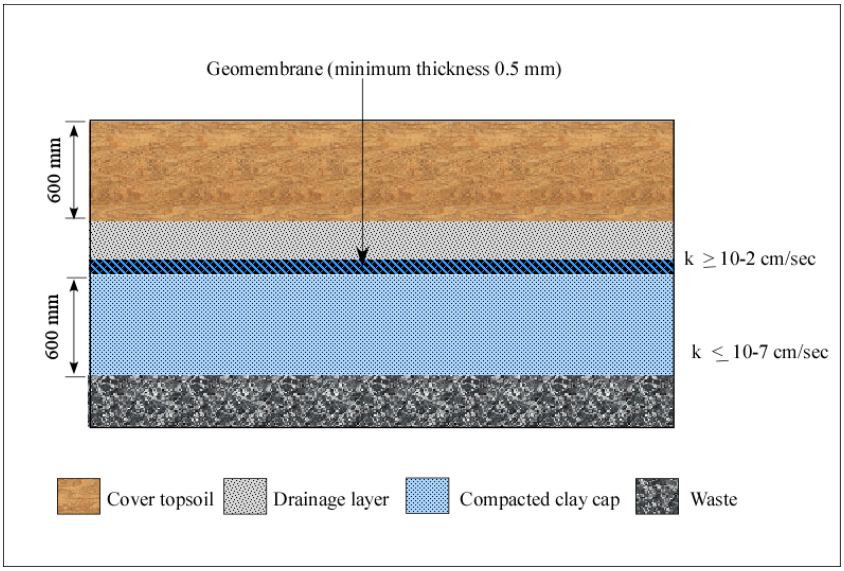

Figure 5.11: Schematic diagram of the layering system for landfill cap (Source: Das, B. M., 2014, Principles of Geotechnical Engineering).

5.4. FLY ASH LANDFILLS STABILITY

Landfills stability is controlled by many factors that individually or combined can lead to failures. These factors include angle of slope, the nature and the properties of the base and liner's side's and the interface material, the height and weight of the material and the change of pore pressure. These factors affect the stability of landfills by changing the shear strength. The stability of the landfill liner system is affected by the interface shear strength between the geosynthetic materials; the interface shear strength between geosynthetis and soil materials; the internal shear strength of geothynthetic clay liners; the internal shear strength of solid waste and on the slope and height.

Stability analysis studies of fly ash landfills showed that the dominant landfill failures occurs at the interfaces between the different liner planes of the base and along the side slopes in a composite liner systems (Bergdo, D. T., et al, 2006, Dixon, N., et al., 2006). Failures of bottom liner landfills induce leachate leakage into subsurface soils and groundwater. Mal functioning and clogging of leachate draining systems can lead to spill over landfill sides and/or change of pore pressure and pressure on the bottom liner and consequently, increase the probability of failure. Leachate can leak in the bottom of the landfill when a failure of the bottom liner happens, or it can fill up the landfill and spill over its sides, if the landfill fills up with a fluid, this fluid weight puts pressure on the bottom liner, which will lead to bottom liner failure. Other reported failures include sudden sinkhole collapses in karst terrains. The existence of either pre-existing air-filled voids or pre-existing or newly infilled clay-filled voids can highly affect the landfill stability and causes failure.

5.5. THE IMPACT OF FLY ASH LANDFILLS ON HYDROLOGIC SYSTEM

Fly ash in most landfills comes eventually in contact with water and generates a leachate, which passes contamination threats to hydrologic systems. Most of the efforts in landfill operations go to reduce the highly visible surface contamination problems, while concerns with the invisible impacts of fly ash on groundwater are growing (G. S. Ghuman et al).

5.5.1. Groundwater Contamination by Fly Ash Constituents. The potential for groundwater contamination due to leachate from coal combustion by-products disposal sites was identified by USEPA (1988) as the primary concern, based on the elevated concentrations of soluble salts and potentially toxic trace elements.

Evangelou, V.P., 1996, stated that coal ash is made of three types of solids (i) chemically water stable solids (SiO, FeO, AIO) (ii) relatively water soluble solids (e.g., metalSO_4, metal-BO_3), and (iii) water reactive metal-oxides (e.g., CaO, MgO, K_2O, Na_2O, etc.). On the other hand, Carlson and Adriano, 1993 showed that the effects of fly ash on groundwater quality depend on the physical and chemical characteristics of the ash, the hydrogeological conditions and the climate at the disposal site, hence safe disposal of fly ash with respect to surface and groundwater protection depends on having the know-how to evaluate the potential of a given fly ash to release its toxic pollutants.

5.5.2. The Leaching Behavior of Fly Ash in Landfills. The leaching behavior of fly ash is a complex process and could be exemplified by the dissolution of lead. Understanding leaching behavior of fly ash and the leaching process is crucial in preventing the anticipated pollution and migration of the liquid that is collected at the bottom of the fly ash landfill (leachate) to groundwater and subsurface soil, and is

important in assessing and guiding the landfill disposal and detoxification of fly ash. (Gong, Y. and Kirk, D.W. 1993).

The constituent of landfill leachate is the water-laden fly ash soluble and heavy material and the rain and surface water percolating through the ground. Different chemical and physicochemical reactions occur to transfer the fly ash constituents to the rain and surface water in a cation exchange process. The capacity and ability of soil to retain heavy metals is determined by the Cation Exchange Capacity (CEC) of the soil, which is defined as the number of milligrams of cations that are absorbed by 100 grams of the soil, and by the amount of minerals and organic colloidal matter present in the soil.

The diminishing of the concentration of the migrating leachate material through the subsurface is determined by the mechanical filtration, the amount of precipitation and surface water and the cation exchange capacity of the soil.

Leachate collection systems are essentially included in the landfill design to prevent the migration of leachate generated inside a landfill from reaching the soil and ground water beneath the landfill, with the aid of liner system, and methods to control and minimize leachate heads within the landfill, and to prevent the damage of the liner system which is composed of compacted clays, geomembranes and geosynthetic clay liner.

5.6. CASE EXAMPLES OF LANDFILL FAILURES

In Harriman, Tennessee on December 22, 2008, a coal ash dam at the Tennessee Valley Authority (TVA) Kingston Fossil Plant broke, releasing 4,16395 billion liters of coal ash into the Emory and Clinch Rivers, destroying three homes and damaging a

dozen others, and destroying three homes and damaging a dozen others. By volume, this spill is the largest environmental disaster in U.S. history that destroyed a highway and railroad line (Figure 5.12), and at around 10 a.m. on Sept. 4, 2013 the owner of the Big Run Municipal Solid Waste Landfill near Ashland, KY., reported a solid waste slide (Figure 5.13). About 800,000 tons of municipal solid waste slid from its disposal location to an area extending some 121.92 m (400 feet) off the landfill plastic liner and clay. The total slide was about 6 m (20 feet) deep and consisted of about 32374,9 m^2 (8 acres). The amount of waste represented about one year's worth of disposal effort. (Kentucky Energy and Environment Cabinet).

Figure 5.12: Aerial images before and after the landfill failure in Tennessee, 2008 (Source: http://www.cnn.com/2009/HEALTH/07/13/ coal.ash.illnesses/ index. html eref=rssus).

The forensic report of the landfill failure revealed that there have been a buildup and increase in pore pressure and a development of wetted spots along the soil cover that contributed to the failure, by inhibiting the draining of the abundant heavy rain water.

The absorption properties of the waste varied according to the waste type, hence, contributed to the failure by creating the soft wetted spots. The net result of the report is that water was trapped at the base and the sideways were the only scape for it, thus it took the garbage along.

Figure 5.13: Aerial view of Big Run, KY landfill slide failure (source: https:// kydep. wordpress.com/ 2014/04/24/what-does-an-8-acre-garbage-slide-look-like-big-run-landfill-slide-cleanup/).

Failure of fly ash landfill caused by the damage occurred in the liner and/or the leachate system, could cause a wide spread of contaminants into groundwater and subsurface soils that requires equipment to trap and collect water back into the leachate tanks. The cost of repairing and reconstructing these systems poses considerable financial and legal burden on companies and landfill owners. Imaging landfills using ERT and MASW geophysical technologies will become an indispensable effort and cost reduction option for such problems.

Fires might erupt following failures of solid waste landfills, due to the gasses that escape the cover layer, allowing waste to contact with air. This situation requires urgent treatment with sealant material to contain the gasses.

6. ELECTRICAL RESISITIVITY TOMOGRAPHY

6.1. THEORITICAL PRINCIPLES

Electrical resistivity tomography (ERT) is a noninvasive geophysical technique that measures the electrical resistivities of subsurface materials, which depend on the lateral variations in subsurface resistivities.

Theoretically the principle of surface electrical resistivity technique is because, the distribution of electrical potential in the ground around a current-carrying electrode depends on the electrical resistivities and the distribution of the surrounding soils and rocks, to estimate the true resistivities of the subsurface materials (W. Ed Wightman et al., 2002-2003).

The basic physical concept of the electrical resistivity technique is derived from Ohm's Law that gives the relationship between the current (I), the change in potential (ΔV), and the resistance (R), in the electrically conductive materials. This relationship is expressed by Ohm's Law equation as:

$$\Delta V = IR$$

where:

ΔV = change in voltage,

I = current,

R = resistance.

Resistivity of a material is a measure of the efficiency of the material in detaining the flow of electrical current.

The electrical resistivity concept is understood in the context of current flow through a subsurface medium consisting of layers of materials with different individual resistivities. Thus, the resistance (R) of a wire of length (L) and across-sectional area (A) is given by the equation:

$$R = \rho L/A \quad (1)$$

where

R = resistance (Ω)

ρ = resistivity of the medium composing the wire (Ωm),

L = length (m),

A = area of the conducting cross section (m^2).

To allow for multi-dimensional calculation of the heterogeneous medium, Ohm's Law can also be expressed in a vector format by the equation:

$$J = \sigma E \quad (2)$$

where:

σ = conductivity of the medium,

J = current density vector

E = electric field intensity vector

The change in the electric potential represents the electric field intensity, represented by the equation:

$$E = - \nabla V \quad (3)$$

where:

∇V = the change in the electric potential.

Substituting for E in equation (2);

$$J = - \sigma \nabla V \quad (4)$$

$$J = - 1/ \rho \nabla V$$

Considering equation (3),

$$J = 1/ \rho E$$

For two current electrodes configuration (Figure 6.1), the two electrodes are considered as point sources. Ohm's law in terms of the total current flow from or toward each electrode across the surface of a half sphere of radius (r) and area ($2\pi r^2$), is given by the equation:

$$J = - 1/ \rho \nabla V$$

$$J = - 1/ \rho \, dV/dr \quad (5)$$

In homogeneous surfaces, (ρ) is constant, and equation (5) is considered a first order differential equation that can be integrated to give the value of the electrical potential at distance (r) from the electrode V(r):

$$V(r) = \rho I/2\pi r \quad (6)$$

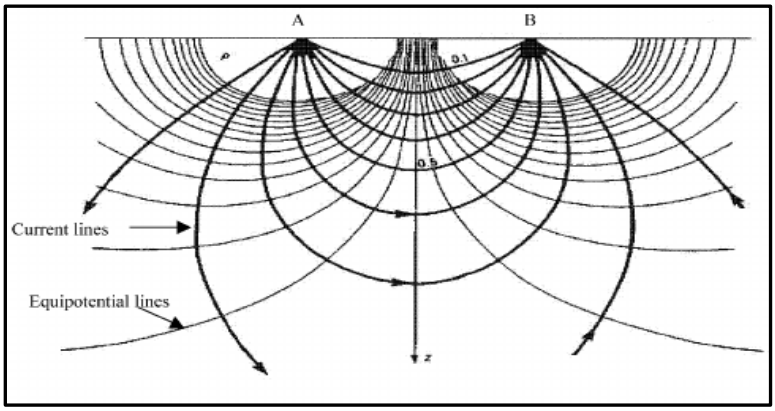

Figure 6.1: Current flow pattern between two electrodes in homogeneous medium (Source: https://www.researchgate.net).

In electrical resistivity techniques, four current electrodes configuration is usually used (Figure 6.2). The current is provided by electrodes A and B, whereas the potential difference between electrodes C and D is given by the equation:

$$\Delta V = V_C - V_D = \rho I/2\pi\{(1/r_A - 1/r_B) - (1/R_A - 1/R_B)\} \quad (7)$$

From equation (7), resistivity (ρ) is given by the equation:

$$\rho_a = 2\pi\, \Delta V /I\{(1/r_A - 1/r_B) - (1/R_A - 1/R_B)\} \quad (8)$$

For homogeneous surface, resistivity (ρ) is constant and is independent of electrode spacing and surface location.

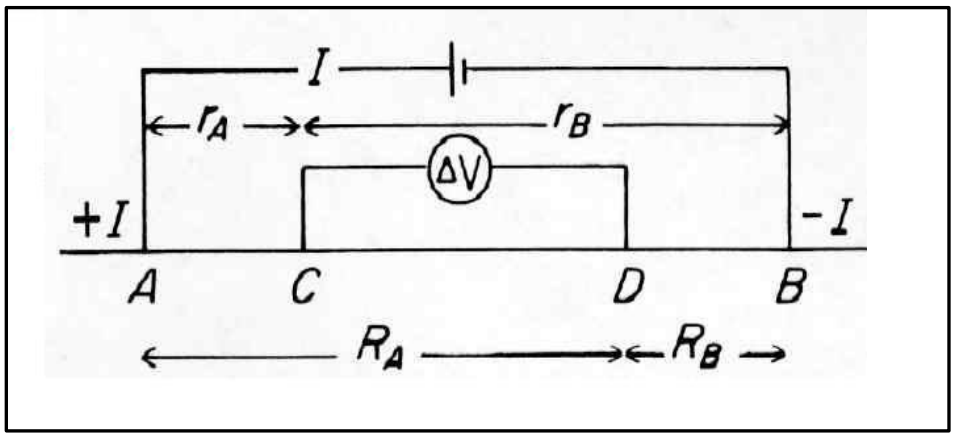

Figure 6.2: General configuration of four current electrodes where current is delivered through the electrodes A and B, and potential difference is measured between electrodes C and D.

For inhomogeneous subsurface, resistivity varies with the relative position of electrodes and surface locations, and is known as the "Apparent Resistivity", which is defined as the resistivity of a homogeneous ground that will give the same resistance value for the same electrode arrangement, but it is not the true resistivity of the subsurface (Loke, 2011).

Apparent resistivity is given by the equation:

$$\rho_a = 2\pi \Delta V / I\{(1/r_A - 1/r_B) - (1/R_A - 1/R_B)\} \quad (9)$$

Apparent resistivity depends on the form of the inhomogeneity.

$$\rho_a = k \Delta V/I \quad (10)$$

where,

$$k = 2\pi/\{(1/r_A - 1/r_B) - (1/R_A - 1/R_B)\}$$

k = array geometric factor that depends on the geometry of the electrode arrangement. (Gibson and George 2003).

$$\rho_a = kR \quad (11)$$

where

$$R = \nabla V/I$$

To obtain the true resistivity, the apparent resistivity of the medium can be found from measured values of V, I, and K (obtained by the instruments), then the apparent resistivity values are acquired from field observations at various locations and various electrode configurations. Finally, the true resistivities for the different earth materials are estimated by applying inversion techniques on the apparent resistivities.

6.2. RESISTIVITY AND CONDUCTIVITY OF EARTH MATERIALS

Electric current is the measure of the rate of flow of electrons in the medium, while electrolytic current is the current generated by the fluids containing dissolved current conductive materials. Current flow in the subsurface is electrolytic, and is carried through the rock by the passage of ions in pore space by water. Thus most rocks conduct

electricity by electrolytic rather than electronic processes where current is generated due to the positive and negative charges in conductive non-aqueous media.

Resistivity is considered an intrinsic property of the material, and it depends on the homogeneity or heterogeneity of the rock or soil under investigation. Table 6.1 displays some of the typical ranges of resistivity values for natural rocks and earth materials.

Table 6.1: Typical electrical resistivities of earth materials.

Material	Resistivity (ohm-m)
Clay	1 – 20
Sand (wet to moist)	20 – 200
Shale	1 – 500
Porous limestone	100 – 1,000
Dense limestone	1,000 – 1,000,000
Metamorphic rocks	50 – 1,000,000
Igneous rocks	100 – 1,000,000

Homogeneous materials theoretically produce identical resistivity values. Whether these values are low or high depends on the properties of these materials, however, in real life homogeneity of earth material does not exist. Resistivity values for heterogeneous materials represent the average resistivity of the different components of the investigated area, which is a function of the average properties of the heterogeneous material. To account for the inherent heterogeneity of the earth, the calculated resistivity value is not the true resistivity of the subsurface, but an “apparent” value that is the resistivity

of a homogeneous ground that will give the same resistance value for the same electrode arrangement. (Loke, M.H., 2016).

Approximate resistivity values were obtained for the common rocks, soil materials and chemicals as shown in (Figure 6.3). The lateral or vertical variation of earth material resistivities is emphasized in variations in the relationship between the applied current and the potential distribution as measured on the surface. These measured variations define subsurface properties such as porosity, water content, and salinity of the pore water, grain size distribution and composition of clay mineral and metal content.

Properties that affect the resistivity of a soil or rock include porosity, water content, composition (clay mineral and metal content), salinity of the pore water, and grain size distribution.

Resistivity of rocks is governed by the degree to which the rock is intact or fractured and jointed. In this situation, igneous and metamorphic rocks are the ideal earth material representatives that possess high resistivities. However, depending on the sedimentary rocks intactness or fracturing and jointing, and the dryness or wetness, these rocks can have a wide range of resistivities (10’s to thousands of ohm-m), since joints and fractures allow water and soft infill materials (i.e. clay and silt particles) to percolate inside the solid rock and produce low resistivity values.

In applied geophysical research, these properties of the igneous and metamorphic rocks is utilized in the detection of groundwater in arid regions and in geotechnical investigation of subsurface in order to construct dams, bridges, large buildings and highways.

Unlike igneous and metamorphic rocks, sedimentary rocks are known for their porosity and storage ability of water and dissolved solids. The resistivity is generally

lower, yet they also possess a range of resistivities, depending on their mode of formation (chemical, mechanical, silicified, or compacted), and the intensity of their fracturing, and they can exhibit resistivity values ranging from 10 to 10000's ohm-m.

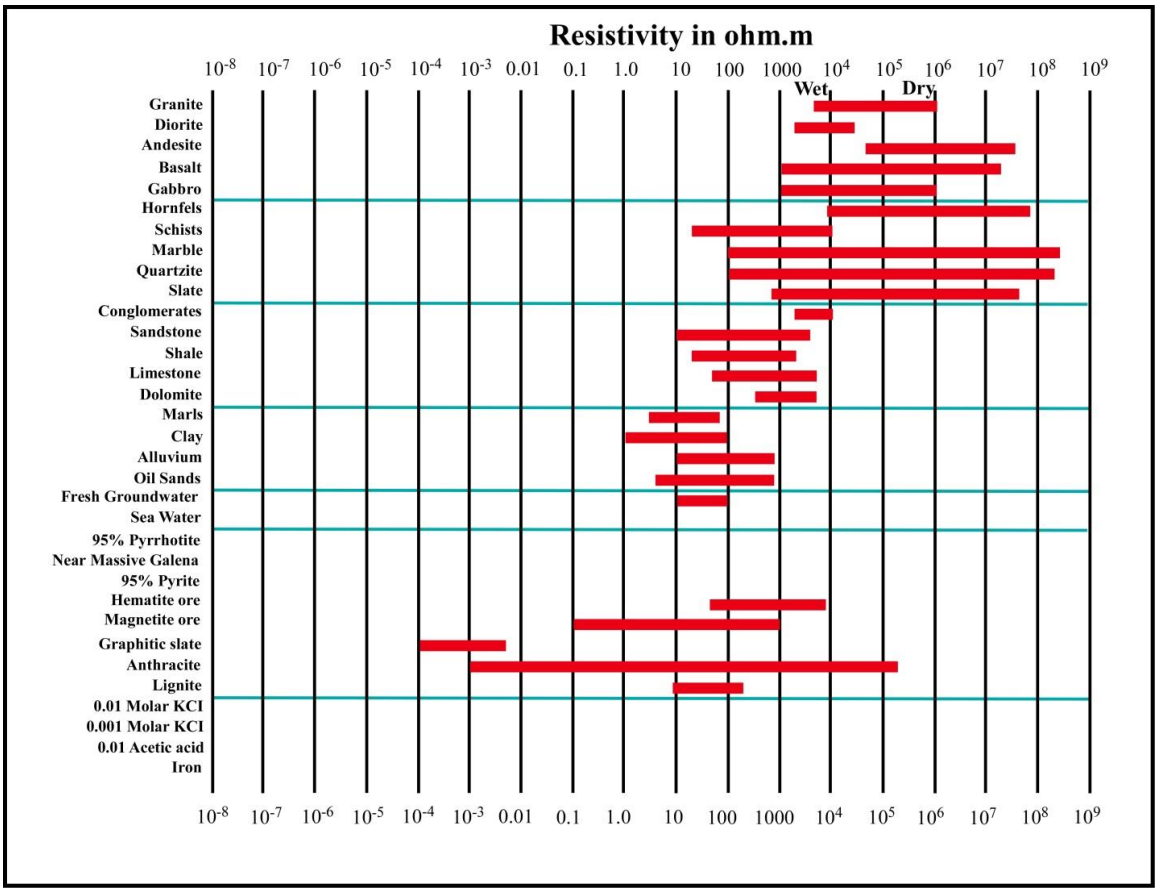

Figure 6.3: Resistivity of common rocks, soils and earth materials (After: Keller and Frischknecht 1966, Daniels and Alberty 1966, Telford et al. 1990).

The least earth material that display very low resistivity is the unconsolidated sediments, which, is an easy media for the interaction of water, soluble and insoluble solids and gaseous and oxygen circulation. These unconsolidated materials possess resistivities less than 10 ohm-m. However, a spectrum of resistivities is also evident and

is controlled by the degree of compactness and the wetness-dryness of these materials. Clayey soil normally has lower resistivity value than sandy soil.

The resistivity of groundwater typically varies from 10 to 100 ohm-m depending on the concentration of dissolved salts. Note the low resistivity (about 0.2 ohm-m) of seawater due to the relatively high salt content. This makes the resistivity method an ideal technique for mapping the saline and fresh water interface in coastal areas. One simple equation that gives the relationship between the resistivity of a porous rock and the fluid saturation factor is Archie's Law. It is only applicable for certain types of rocks and sediments, particularly those that have low clay content. The electrical conduction is assumed to be through the fluids filling the pores of the rock. Archie's Law is given by

$$\rho = a\rho_w\varphi^{-m} \tag{12}$$

where,

ρ = the rock resistivity

ρ_w = fluid resistivity

φ = porosity (the fraction of the rock filled with the fluid)

a and mare two empirical constants (Keller and Frischknecht, 1966) that depend on the geometry of the pores. For most rocks, a is about 1 while m is about 2.

The conductivity (σ) of a material is defined as the ability of that material to conduct electricity, which is given by the reciprocal of the resistivity (ρ) of that material. Resistivity of rocks and soils is affected by many factors, on top of which are the porosity, water saturation, water salinity and clay mineralization (i.e. pure water is non-conductive). Conduction of electrical current through earth material occurs basically in the aqueous media of pore space or in the openings of joints.

The porosity represents the volume of void space (space filled with air or water) in soil or bedrock (Aalpha, T.R., et al). Generally, with low porosity, the density increases, conductivity decreases, and the resistivity increases in well sorted rocks/soil, where the pore-space becomes tiny and occupied by water or gases, unlike the situation of coarse rocks/soils, where the pore space is large enough to accommodate the soil and the smaller rock fragments. The presence of these fragments and smaller particles will result in decreasing resistivity.

Water saturation will eventually imply low conductivity since it is ranked among the least conducting materials and is considered as a bad current conductor, unless it contains electrolytes. Therefore, as the saturation of rock or soil with water increases, the degree of rock/soil porosity decreases and so, the conductivity, whereas the resistivity increases.

Saline water and mineralized clay are good conductors for the current, such that high conductance implies low resistivity. Therefore, in the situation of water salinity and clay mineralization, resistivity records tend to be low. Clay mineralization, which means the presence of minerals in the clay, means also, current can be generated. Salt-water intrusion provides more ions for conduction and therefore reduces resistivity. Moreover, with the increase of salinity, the dissolved salt concentrations will increase, which leads to decrease in porosity, and as a result, resistivity will increase.

Resistivity values varies by seasons such that, during rainfall seasons and snow melt there is abundance of water, while in snow season and summer, water is scarce, hence there is less dissolved rock and soil material, and accordingly the recorded

resistivity values are high. When the pore water freezes, there is an increase in resistivity, perhaps by a factor of 10^4 or 10^5, depending on the salinity.

6.3. METHODOLOGY

The principle of the electrical resistivity survey is described by the distribution of electrical potential in the inhomogeneous surface ground, around a current carrying electrode, which depends on the resistivities and distribution of the surrounding soils and rocks. Practically a direct current is applied between the electrodes that are implanted in the ground to measure the difference of potential between other additional electrodes that do not carry current. The relationship between the distributed potentials and the ground resistivities and their distributions is the basic factor in interpretation the resistivity distributions. The resistivity of soils and rocks is governed primarily by the amount of pore water, its resistivity, and the arrangement of the pores. For this reason, there are wide ranges in resistivity values for any soil or rock type, and resistivity values cannot be directly interpreted in terms of soil type or lithology, but, instead, zones of distinctive resistivity can be associated with specific soil or rock units based on local field or drill hole information.

6.3.1. Electrode Array Configurations. The principle problem of resistivity surveying is the use of apparent resistivity values from field observations at various locations and with various electrode configurations to estimate the true resistivities of the various earth materials of the study site and to spatially locate the boundaries below the surface.

An electrode array with constant spacing is used to investigate the lateral changes in apparent resistivity values, thus, depicting the lateral geologic variability or localized anomalous features. The apparent resistivity depends on the geometry of the electrodes array. The types of electrode arrays that are most commonly used in practice are Wenner, Schlumberger, and the dipole-dipole (Figure 6.4).

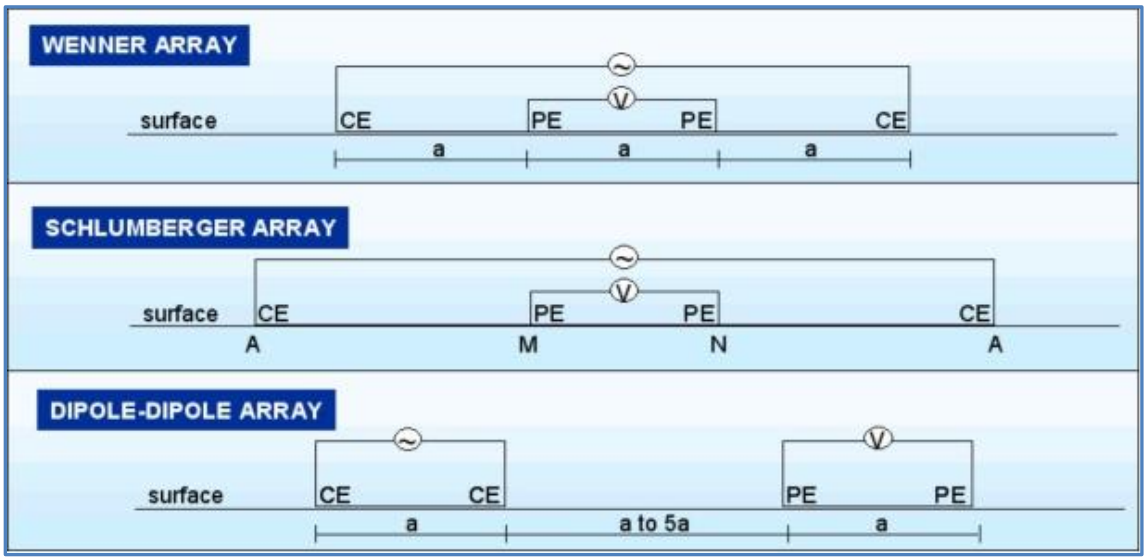

Figure 6.4: The most common array types generally employed in electrical resistivity surveys (Source: http://old.acogok.org/geophysical-tutorial).

The choice of the "best" array for a field survey depends on the type of structure to be mapped, the sensitivity of the resistivity meter and the background noise level. The characteristics of an array that should be considered are (i) the depth of investigation, (ii) the sensitivity of the array to vertical and horizontal changes in the subsurface resistivity, (iii) the horizontal data coverage, and (iv), the signal strength (Loke, 2016).

6.3.1.1. Wenner array. The array (Figure 6.5), utilizes four equally spaced and aligned electrodes. This was considered an advantage for Schlumberger array and disadvantage for Wenner, since it is faster in the field to move the two current electrodes

of Schlumberger than to move the four electrodes of the Wenner array between the successive observations, in addition to that Schlumberger array is considered more robust in distinguishing lateral from vertical variations in resistivity.

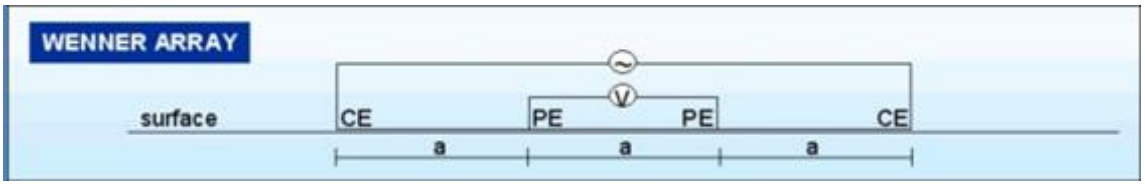

Figure 6.5: Wenner array configuration (Source: http://old.acogok.org).

A major advantage of Wenner array is that it allows for data minimization and requires less attention to equipment sensitivity. In general, the Wenner array is good in resolving vertical changes (i.e. horizontal structures), but relatively poor in detecting horizontal changes (i.e. narrow vertical structures), because it is sensitive to vertical changes in the subsurface resistivity below the center of the array. The median depth of investigation for the Wenner Alpha array is approximately 0.5 times the "*a*" spacing used. Compared to other arrays, the Wenner Alpha array has a moderate depth of investigation. The signal strength is inversely proportional to the geometric factor used to calculate the apparent resistivity value for the array. The apparent resistivity is given by the equation:

$$\rho_a = 2\pi aV/I = k\ V/I \qquad (13)$$

where,

a = electrode spacing

k = the geometric factor for the Wenner array, and itis given by the equation:

k = 2πa

The geometric factor for the Wenner array is smaller than the geometric factor for other arrays. Among the common arrays, the Wenner array has the strongest signal strength. This can be an important factor if the survey is carried in areas with high background noise. One disadvantage of this array for 2-D surveys is the relatively poor horizontal coverage as the electrode spacing is increased. (Loke, 2016).

6.3.1.2. Schlumberger array. Schlumberger is another array that operates with four aligned electrodes (Figure 6.6); the outer two of them are current source providers while the inner two electrodes are potential receivers. The potential electrodes are slightly separated (< 1/5 of current electrodes spacing) and are kept in fixed position at the center of the array, while the current electrodes are mobilized to greater separation during the survey to obtain the minimum observed voltage.

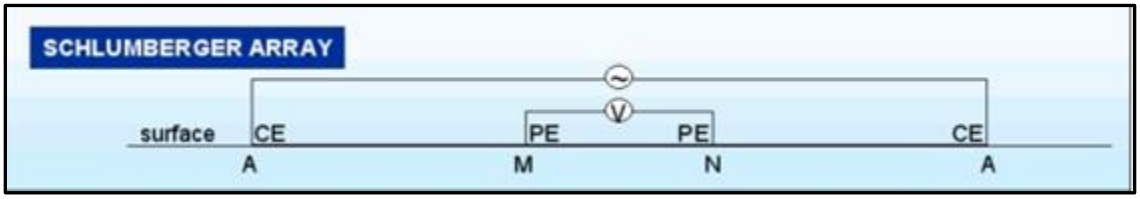

Figure 6.6: Schlumberger array configuration (Source: http://old.acogok.org/ geophysical-tutorial).

The potential electrodes spacing could be adjusted with constant current electrodes spacing to detect the proximal heterogeneities or lateral resistivity changes around the potential electrodes. The apparent resistivity for the Schlumberger array is given by the equation:

$$\rho_a = \pi/a\,[(L/2)^2 - (a/2)^2]V/I = k\,V/I \qquad (14)$$

where,

a = electrode spacing

L = is the distance between the current electrode and the mid-point of the potential electrodes.

k = the geometric factor for the Schlumberger array and it is given by the equation:

$$k = \pi/a\,[(L/2)^2 - (a/2)^2] \quad (15)$$

6.3.1.3. Dipole-dipole array. The was used for this study owing to its high sensitivity to lateral changes in resistivity, despite that it is relatively insensitive to vertical changes in the resistivity. The array uses equally spaced electrode pairs (The spacing between the current electrodes is the same as the spacing between the potential electrodes and equals to a) to measure the curvature of the potential field, which means it is good in mapping vertical structures, such as dykes and cavities, but relatively poor in mapping horizontal structures such as sills or sedimentary layers (Figure 6.7).

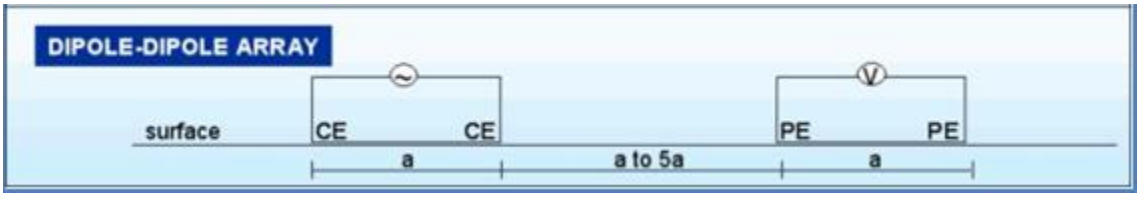

Figure 6.7: The dipole-diploe array configuration (Source: http://old.acogok.org/ geophysical-tutorial).

The apparent resistivity for the dipole-dipole array is given by the equation:

$$\rho_a = \pi an(n+1)(n+2)V/I = k\ V/I \qquad (16)$$

where

a = electrode spacing

n = the ratio of the distance between the C1 and P1 electrodes to the C2-C1 or (P1-P2)

k = the geometric factor for the dipole- dipole array, and it is given by the equation:

$$k = \pi n(n+1)(n+2)a \qquad (17)$$

Dipole-dipole was preferred in karst terrain over the Schlumberger and Wenner for its overall advantage of the high sensitivity to lateral changes in resistivity and of mapping the vertical structures which are considered significant factors in imaging the karst terrain.

6.3.2. Depth of Investigation. To investigate the change in resistivity at greater depths, the spacing's between electrodes are increased to allow more current to flow deeper, and the apparent resistivity becomes increasingly similar to the average resistivity of the earth over a greater range of depths. This relationship is plotted as apparent resistivity versus electrode spacing to indicate vertical variations in resistivity. The smaller the spacing's between electrodes, the closer the apparent resistivity values to the surface material and the larger spacing's between electrodes, the more resemblance of the apparent resistivity to the bedrock.

The relationship between the electrode spacing and the apparent resistivity of layers (1, 2 and 3) is illustrated by Figure (6.8), such that, most of the current induced by array (1) is close to the resistivity of layer (1). Similarly, the bulk of the current induced

by array (2) resembles an average apparent resistivity for layers (1 and 2), whereas a high percentage of the induced current of array (3) defines an apparent resistivity average for the three layers.

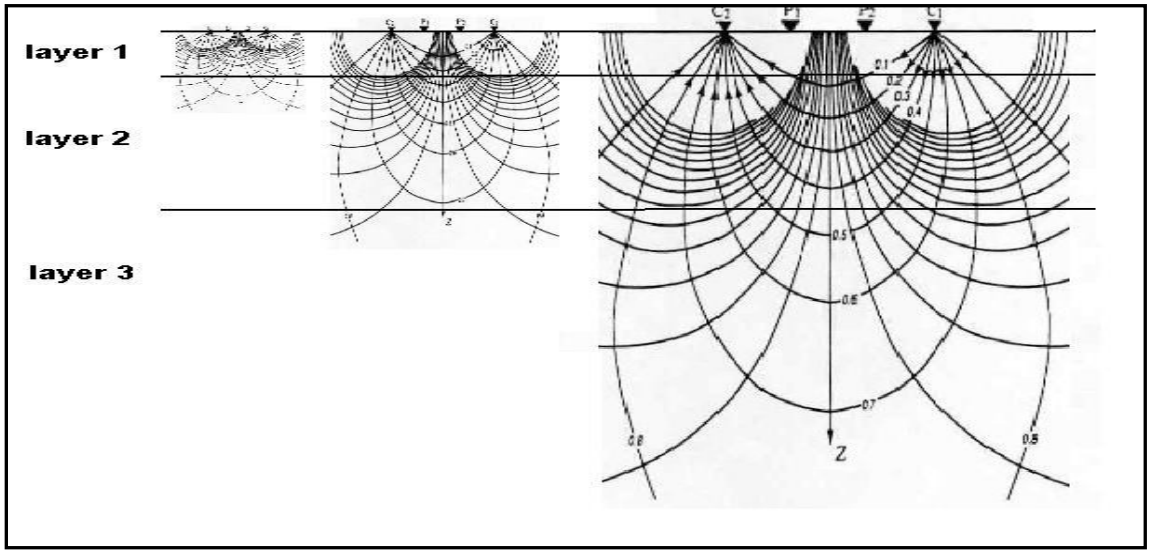

Figure 6.8: The relationship between depth and electrode spacing (Source: Wightman, W., F. Jalinoos, et al. (2004)).

For small electrode spacing's, the apparent resistivity is close to the surface layer resistivity, whereas at large electrode spacing's, the resistivity approaches the resistivity of the basement layer.

6.4. DATA ACQUISITION

Two-dimensional electrical imaging/tomography surveys are usually carried out using many electrodes, and a resistivity meter system with multi-core cables and electronic switching unit. In this work SuperSting R8 system was used to acquire the data to generate 2-D and 3-D electrical resistivity images of the subsurface (Figure 6.9).

The system control unit can be interconnected to many electrodes, with only four electrodes that are active at a time. The dipole-dipole array configuration was used for data acquisition. For a dipole-dipole data collection, the system is set to use two electrodes as current electrodes injecting the current into the ground and the two others as voltmeter electrodes measuring the resulting voltage, whereas the electrode pairs are separated by a pre-determined distance (Figure 6.10). The depth of investigation depends on the type and the length of the electrode array.

Figure 6.9: SuperSting R8 system (Source: http://www.belirti.com/resistivity_%20instrumentation.html).

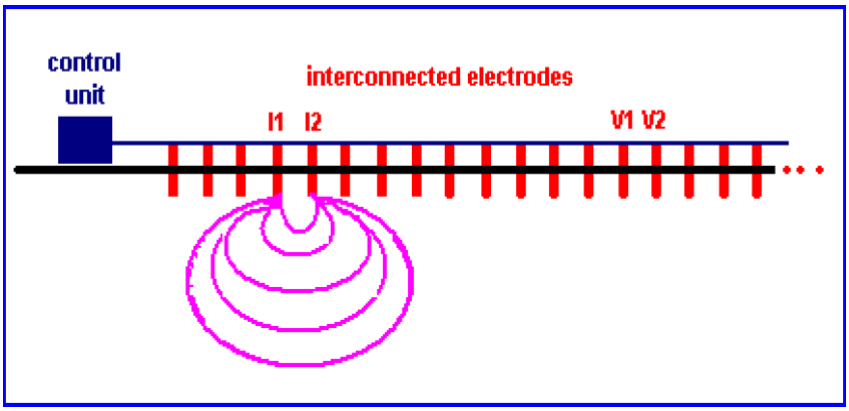

Figure 6.10: Dipole-dipole interconnected electrodes (Source: Anderson, 2015).

To obtain high quality ERT data, some pre-arrangements and settings were found to be appropriate, which include:

- The choice of a spot on the study site where the deepest measurement is anticipated (the mid-point)
- The equipment's are placed in the mid-point and the cables are spread out away on both sides (depth of penetration of the ERT depends on the type and length of the electrode array).
- The electrodes are installed into the ground at each contact on the cable and jumper cables are used to join the cable connections to the electrodes.

Figure (6.10) shows the typical setup for a 2-D survey with several electrodes along a straight line attached to a multi-core cable. Normally a 1.5 m (5 feet) constant spacing between adjacent electrodes is used. The multi-core cable is attached to an integrated resistivity meter system that includes an electronic switching unit. The sequence of measurements to take, the type of array used and other survey parameters (such the current to use) is normally transferred to an internal microprocessor system within the resistivity meter from a personal computer. After reading the control file, the control program then automatically selects the appropriate electrodes for each measurement.

In a typical survey, most of the fieldwork is in laying out the cable and electrodes. After that, the measurements are taken automatically and stored in the resistivity meter system. Most of the survey time is spent waiting for the resistivity meter to complete the set of measurements. (Loke, 2016).

A known current is transmitted by the SuperSting control unit into the subsurface, while the unit also records the corresponding potential difference Figure. The apparent resistivity will then be calculated for the pre-determined distance (a). The apparent

resistivity (ρ_a) for all separations between electrodes is then calculated and a profile for the apparent resistivity is plotted as a function of the midpoint and the number of electrodes. (Figure 6.11).

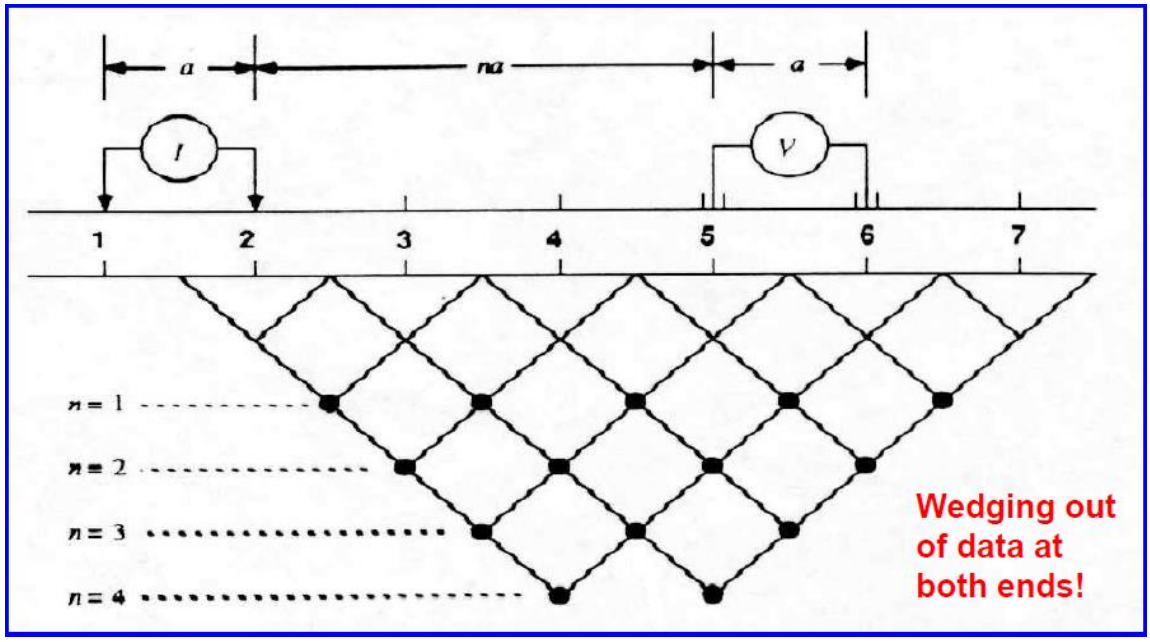

Figure 6.11: Profile plotted from data acquired using (n) number of electrodes at pre-determined distance of (ρ_a) (Source: Anderson, 2015).

To get the best results, the measurements in a field survey should be carried out in a systematic manner so that, as far as possible, all the possible measurements are made. This will affect the quality of the interpretation model obtained from the inversion of the apparent resistivity measurements (Dahlin and Loke, 1998).

6.5. DATA PROCESSING

Electrical Resistivity Tomography [ERT] data is processed using RES2DINV software that transforms the ERT data acquired along traverses into two and three dimensional (2D and 3D) electrical resistivity images of the subsurface. RES2DINV

inverts the actual pseudo-section data using a tomographic approach and transforms it into a 2D or 3D resistivity image of the subsurface.

The inversion theory is based on finding a mode*l* that gives a response that is similar to the actual measured values. The model is an idealized mathematical representation of a section of the earth. The model has a set of model parameters that are the physical quantities we want to estimate from the observed data. The model response is the synthetic data that can be calculated from the mathematical relationships defining the model for a given set of model parameters. All inversion methods essentially try to determine a model for the subsurface whose response agrees with the measured data subject to certain restrictions and within acceptable limits. (Loke, 2016).

The RES2DINV program uses the cell-based method, where the model parameters are the resistivity values of the model cells, while the data is the measured apparent resistivity values (Loke, 2016).

6.6. DATA INTERPRETATION

The aim of the interpretation is to determine the resistivity and thickness of sub surface layers based on observed resistivity. The interpreter seeks to map the variations in the elevations of top of rock, and to determine the moisture content of soil, rock and the fly ash, and as well, to detect any probable groundwater flow or seepage pathways and potential karst features.

The interpretation is done usually for the processed resistivity data using RES2DINV software that produces a plot of resistivity against depth. Data interpretation is considered a complicated process, since it relates to the skillfulness of the interpreter, the data and the environmental factors related to the location, time, geology and the weather at

the site under investigation. The geophysicist should select the model that agrees best with the known geological and hydrogeological structures of the ground (Loke, 2016).

The major factor in the data interpretation process is the contrast in resistivity. An example of that is the case of cavities and host rocks. Air-filled cavities will have higher resistivity than the host rock; however, if the cavity is filled with water, its resistivity might become similar to that of the host rock. In another scenario, if the host rock is resistive or that, the water in the cavity is saline (i.e. has a low resistivity), the cavity might become low-resistivity target.

It is most often that the moisture contents of fly ash and soils are greater than underlying rock because of the increased porosity of soil and fly ash, thus, their resistivities are lower. On the other hand, the fractured, moisty weathered rock with clay infill could have low resistivities, similar to the electrical resistivity of soils and fly ash.

Anderson N. (2016), considers that It is generally difficult to differentiate fly ash and soil on ERT data because both materials are porous and permeable. It can be difficult to map the contact between soil and rock where both materials are either very moist or very dry, and the presence of clay in soil or rock increases the conductivity of that soil or rock. Hence, clay-bearing soil and rock is generally less resistive than non-clay-bearing soil or rock (moisture content remaining the same).

A general geologic interpretation of a 2-D ERT image (Figure 6.12), reveals that the units with resistivities greater than 405 ohm-m were mapped as limestone, and that the units with resistivities less than 105 ohm-m are moist soil or clay, whereas the units with resistivities greater than 105 ohm-m and less than 405 ohm-m, were variously mapped as either dry soil or moderately to intensely fractured/weathered limestone, with clay in-fill.

The bedrock is overlain by soil or clay and a relatively continuous limestone lenses and intervening clay in some places.

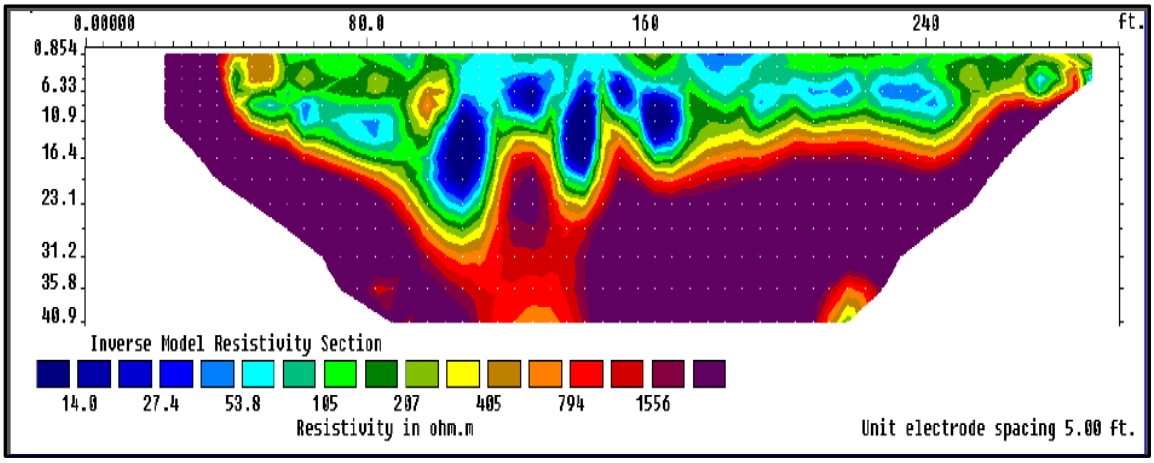

Figure 6.12: 2-D electrical resistivity tomography image showing the interpretation of the geology of a study area (Source: Anderson, 2015).

Figure (6.13) provides a typical 2-D ERT profile (454) of a fly ash landfill. The resistivity values less than 125 ohm-m were interpreted as moist soils, whereas the values greater than 125 ohm-m, were considered as dry soil.

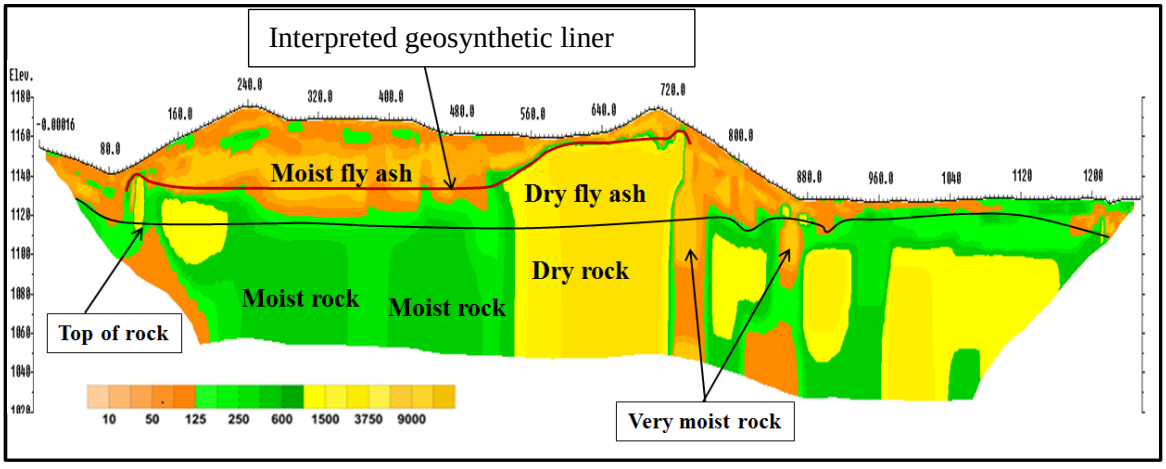

Figure 6.13: 2-D interpreted ERT profile (454) of a fly ash landfill.

The intact rock has resistivity values greater than 600 ohm-m, while the moist weathered rock has resistivity values less than 600 ohm-m. The black line in Figure (6.13) represents the depth to the top of rock, which varies between 6 m to 12 m (20 to 40 feet). The interpretation of the ERT profile of a fly ash landfill of Figure (6.13) shows the geosynthetic liner and the top of rock, and the suggested seepage pathways.

7. MULTICHANNEL ANALYSIS OF SURFACE WAVES (MASW)

7.1. THEORITICAL PRINCIPLES

MASW is a non-invasive geophysical method designed to measure the spatial variations of the average shear-wave velocity of subsurface earth materials.

The shear-wave velocity is a function of the earth materials rigidity, such that, the less rigid the material, the lower the shear-wave velocity, and the more rigid the material, the higher the shear wave velocity.

MASW uses the dispersive nature of surface waves to measure the spatial variations in the average shear wave velocities (Vs) of the subsurface that was generated by an impulsive source. When the source is fired, the short-duration pulse creates a packet of seismic waves that travel in all directions through the body and along the surface in a form of a compressional waves (P-waves), shear waves (S-waves) and surface waves (Rayleigh waves), (Figure 7.1).

The two fundamental types of multichannel analysis of surface waves data (MASW) are the active and the passive (MASW). The active MASW data are the most commonly acquired type of data, and is usually acquired using the sledge hammer as proximal acoustic source.

When the source is fired the short-duration pulse creates a packet of seismic waves that travel through the body and along the surface. The shear wave velocity of the subsurface could then be utilized to determine the geological properties of the subsurface using the MASW software for the transformation and inversion of the surface wave velocity to shear wave velocity. On the other hand, the passive MASW data are acquired

from the background acoustic energy generated by natural and anthropogenic sources, such as the distal earthquakes and traffic (Figure 7.2).

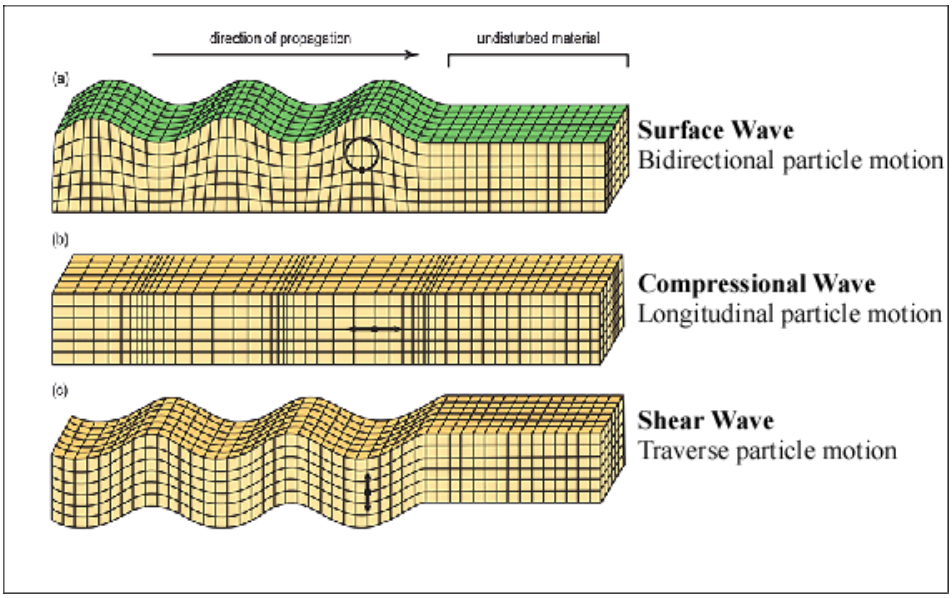

Figure 7.1: Kinds of seismic waves generated by seismic waves source (Source: http://www.parkseismic.com).

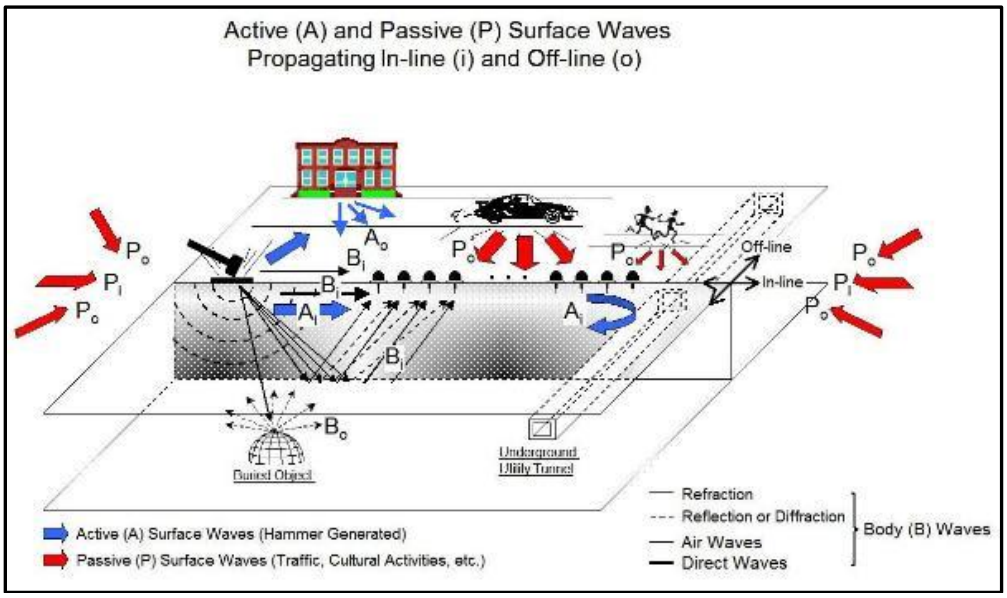

Figure 7.2: Illustration of active and passive MASW sources (Source: http://masw.com/Whatisseismicsurvey.html).

7.2. METHODOLOGY

A large sledgehammer was used to generate surface waves that are recorded by a linear array of equally spaced geophones, aligned along pre-determined locations. A dispersion curve relates the phase velocity and the frequency is generated from the recorded data, which are then modeled to a profile of shear wave velocity values (Vs) to give information in either 1D (depth) or 2D (depth and surface location) format.

7.3. DATA ACQUISITION

The actual field configuration of MASW is illustrated in (Figure 7.3), which is composed of a 24-channel Seistronix engineering seismograph, GPS sensor, and 24 interchangeable low-frequency geophones (4.5 Hz) spaced at 1.5 m (5feet) and 0.762 m (2.5 feet) intervals, a laptop computer, and fully-automated interpretation software, and sledge hammer, and an impact plate (base plate) to concentrate the source energy and direct it horizontally or vertically and prevent the source impact point intrusion into soil (Figure 7.4).

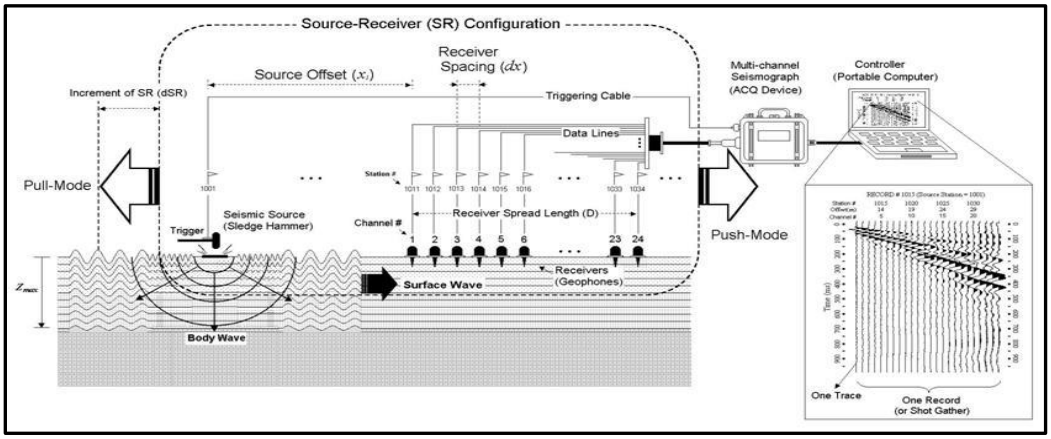

Figure 7.3: Active MASW field survey (Source: http://www.masw.com/ DataAcquisition.html).

Figure 7.4: Acquisition of MASW data in the field.

The geophones are placed at intervals of 5 or 2.5 ft. in relation to the value of the shortest wavelength, which is determined by the desired depth of investigation. However, the length of the receiver spread is directly related to the longest wavelength that can be analyzed to determine the maximum depth of investigation. The depth of investigation often varies between 9 m (30 feet) and 30.49 m (1,00feet), and is affected by the site conditions and the type of active source utilized.

The source offset (x_1) and the receiver spacing (dx) are considered the most two important parameters in the MASW data acquisition (Figure 7.5). The source offset is set at a predetermined distance (e.g. 5, 10, 30 ft.) from the nearest geophone that is selected in conjunction with the geophone spacing's and the desired depth of investigation to obtain the best dispersion curve, from which the 1-D the time-depth model is extracted.

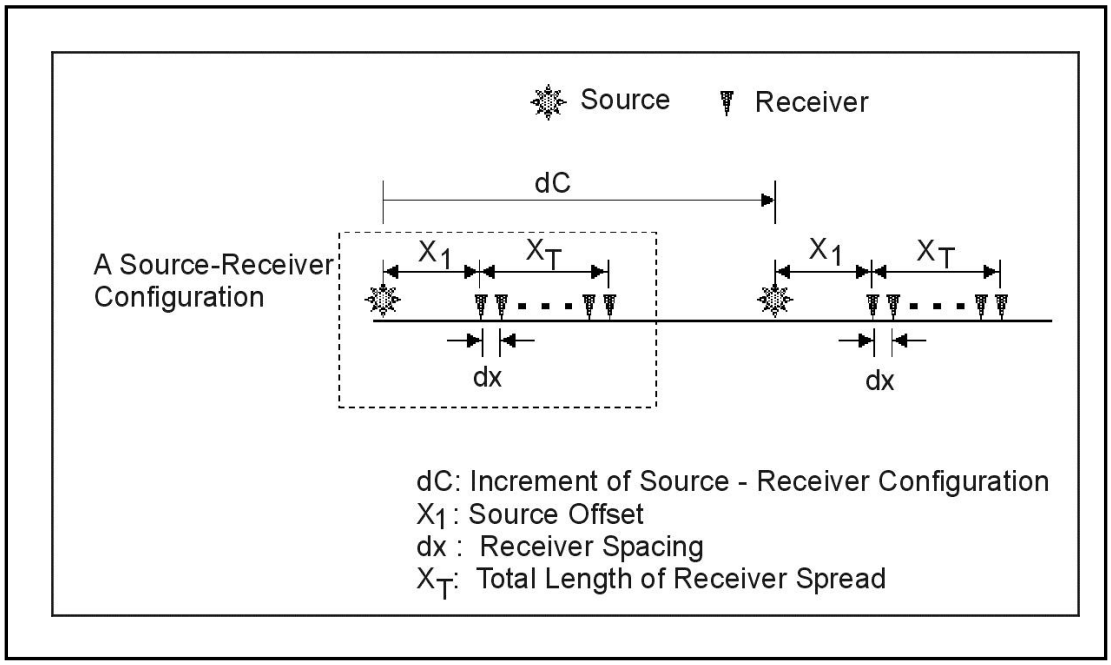

Figure 7.5: Definition of a source-receiver configuration and increment of the configuration (Source: Anderson, 2015).

For this study, the MASW data were acquired at different locations in a west-east orientation, along traverses of about 61 m (200 feet) intervals, parallel to the ERT traverses. The geophones spacing's used were 1.5 m (5 feet) and were 0.762 m (2.5 feet) in some instances. Where these MASW traverses acquired, their locations were re-adjusted to avoid the obstacles that obstruct the data acquisitions, and these included, water bodies, steep slopes and roadways.

7.4. DATA PROCESSING

The acquired MASW data are processed using the Kansas Geologic Survey (KGS) software package SURFSEIS that transform the raw seismic data into1-D shear velocity profile, by extracting the fundamental-mode dispersion curves (velocity vs frequency), then apply an inversion process to the curves to calculate 1D shear-wave velocity profiles (Figure 7.6).

The second processing stage involves the generation of a frequency vs. phase velocity dispersion curve of the acquired Rayleigh wave field data, using the wave-field transformation and the modified wave-field transform.

The resulting curve is transformed into a 1D depth vs shear wave velocity profile, from which the elastic properties, rigidity, density, and thickness of layers of the subsurface are attained.

To create 2D shear wave velocity geologic model, the MASW data sets are collected at close distances and constrained with external data (Park 1999). To acquire a 2-D MASW data, multiple 1-D Vs profiles acquired at adjacent locations along a traverse are compiled (Figure 7.7).

The data are acquired by simply moving the entire array (active or passive) along the traverse. 2D velocity profiles can be generated following these steps: (i) acquiring multiple MASW field records by moving source-receiver array along traverse (ii) preparing multiple 1-D shear wave velocity curves, each array will have one curve (iii) constructing 2-D shear wave velocity profile.

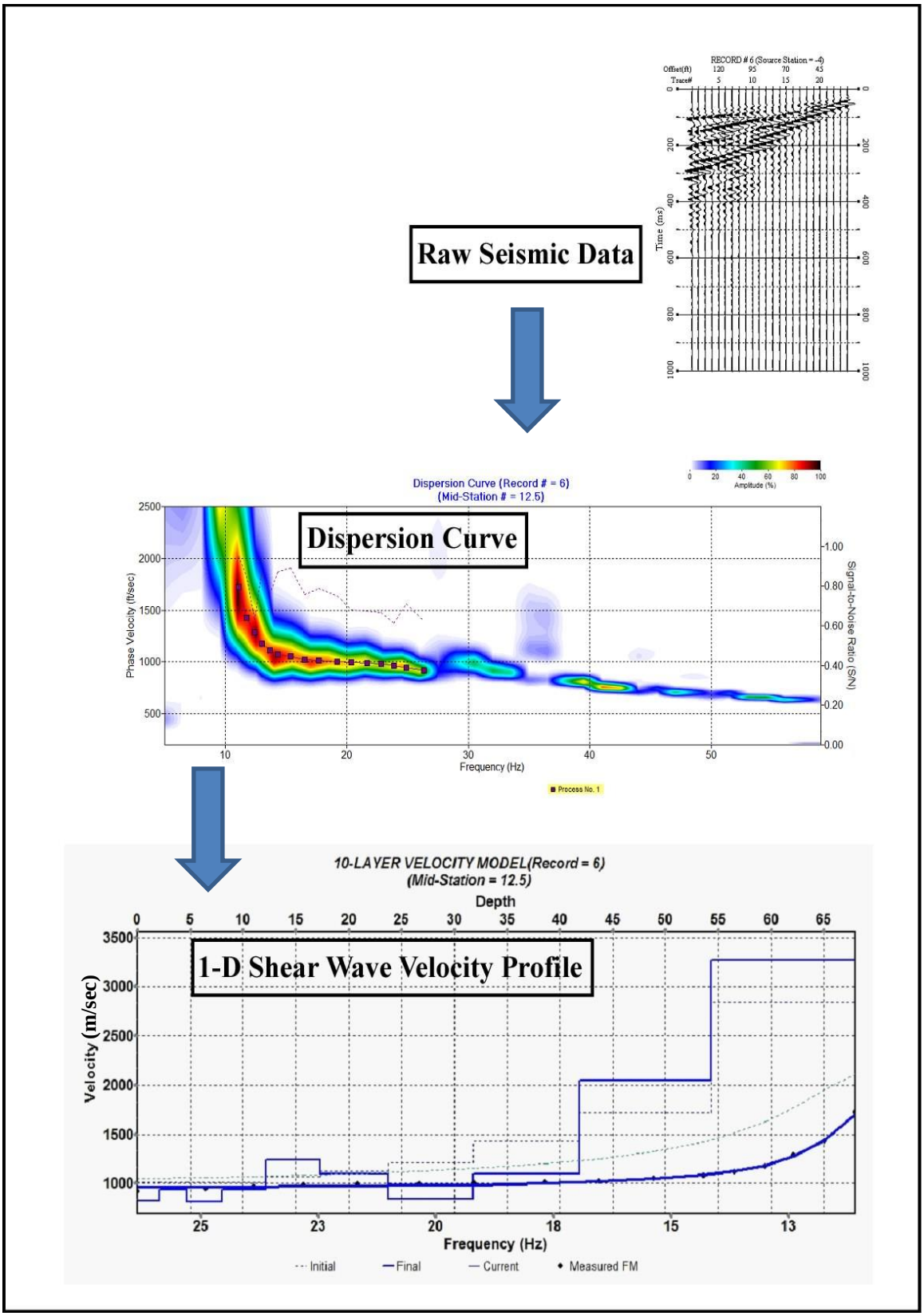

Figure 7.6: MASW surface wave data set transformed into a 1-D shear-wave velocity profile of the subsurface (Source: Anderson, 2015).

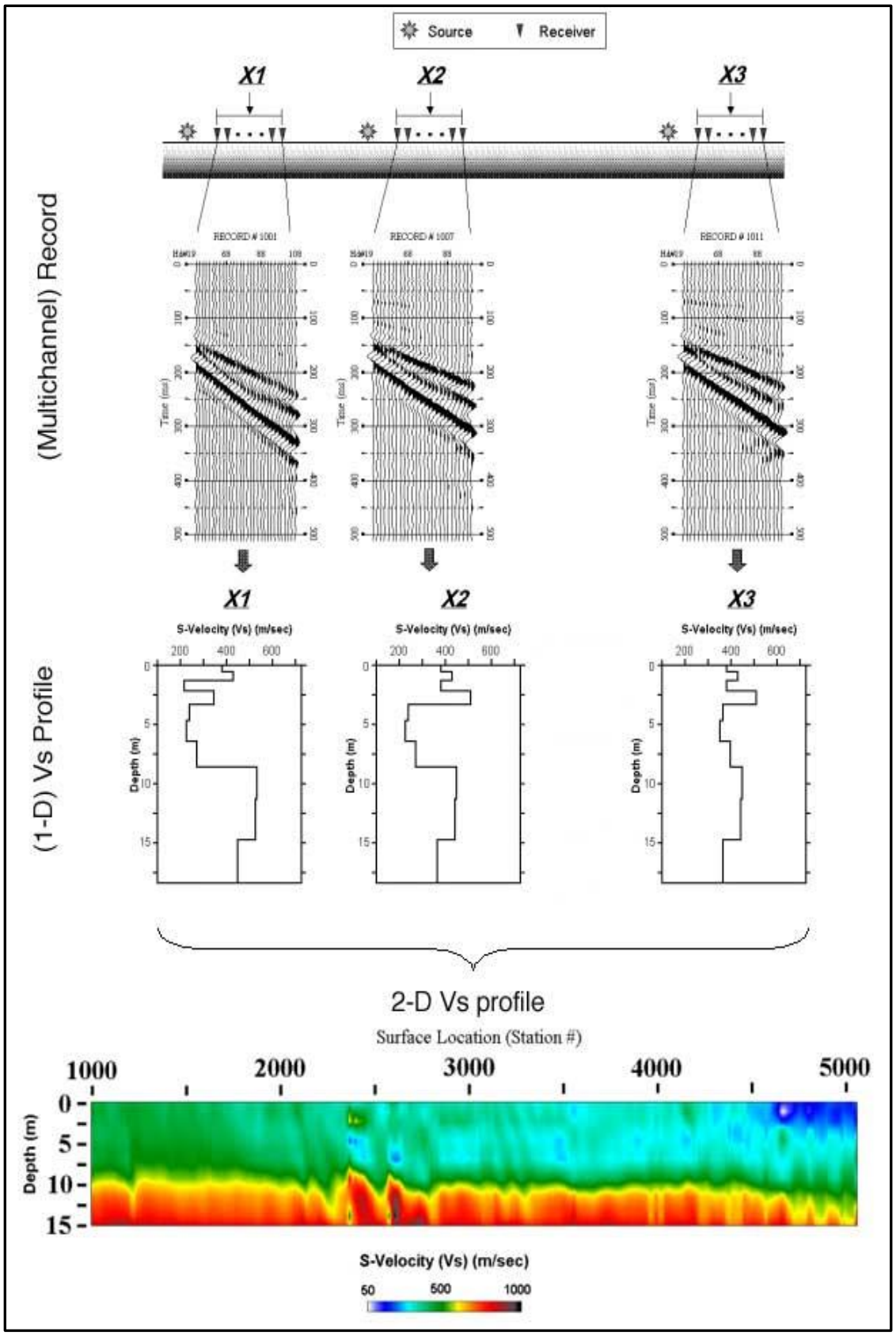

Figure 7.7: 1-D & 2-D shear velocity profiles (Source: https://expservices.ku.edu).

7.5. DATA INTERPRETATION

The multi-channel analysis of surface waves method (MASW) was primarily developed to measure the spatial variations in the shear wave velocity of subsurface materials like soil, rock, and fly ash. The shear wave velocity is a function of the rigidity of the material. The higher the shear-wave velocity, the more rigid the material. Rock is more rigid and has higher shear wave velocity than soil and fly ash, which have lower shear wave velocity (Figure 7.8).

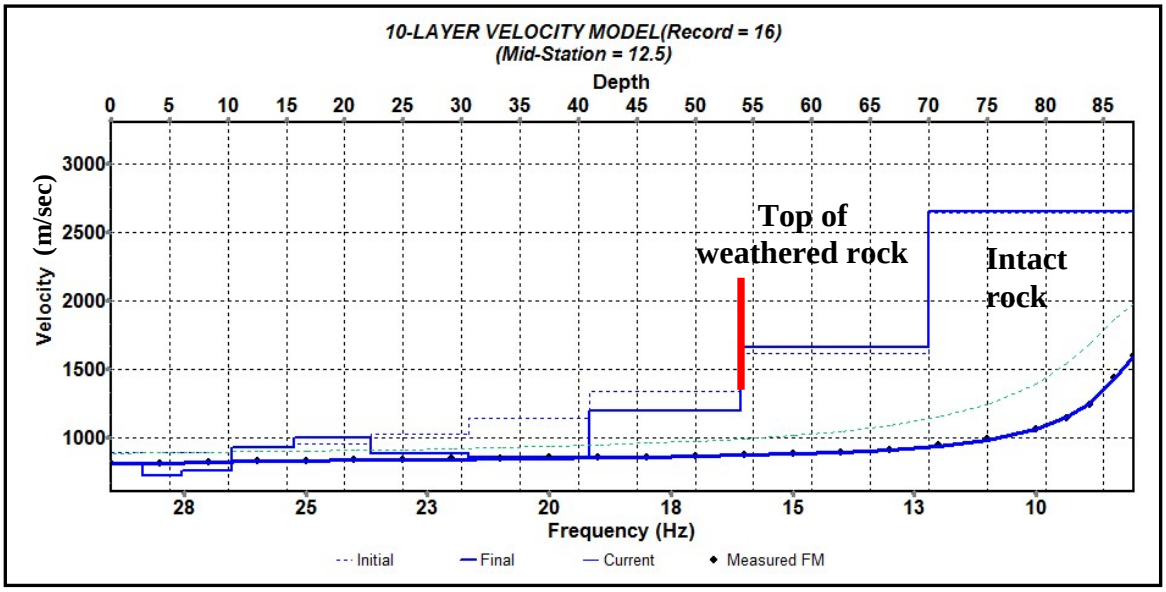

Figure 7.8: 1-D shear-wave velocity profile generated from the fly ash landfill site. The red line indicates that the depth to the top of rock is about 16 m (53 feet).

The NEHRP National Earthquake Hazard Reduction Program (NEHRP) classified the subsurface materials depending on their shear-wave velocity values, given in Table (7.1). (Bauer, R.A., 2004).

Table 7.1: NEHRP soil classification by shear wave velocity and material properties.

Soil type	**Soil name**	**Average Soil Properties for Top 100 feet**		
		Shear-wave velocity, V_s (ft/s)	**Standard penetration test, N (blows/foot)**	**Undrained shear strength $S_{u\ (kPa)}$**
S_A	Hard rock	> 4,921	-	-
S_B	Rock	2,493 to 4,921		
S_C	Very dense soil and soft rock	1,181 to 2,493	>50	>100
S_D	Stiff soil	590.6 to 1,181	15 to 50	50 to 100
S_E	Soft soil	<590.6	<15	<50
S_F	Soil requiring site-specific evaluation			

8. RESULTS AND INTERPRETATION

The (ERT) data were acquired to aid in interpreting the subsurface conditions beneath an existing fly ash landfill to a depth of ~ 30 m (100 feet). Dipole-dipole arrays consisting of 168 electrodes were used on each traverse. 1.5 m (5 feet) electrode spacing was used in a west-to-east orientation, normal to the dominant north-to-south trend of joints.

Figure 8.1 represents an illustration of the fly ash landfill, with 31 ERT traverses on the northern part of the landfill under study. The new fly ash landfill was established on a former fly ash landfill that consisted of a clay liner. A new geosynthetic liner was placed, on the remnants of the former fly ash landfill.

The ERT traverses covering the northern part of the landfill are the subject of this study, running from west to east, whereas the general orientation of structures is in a north-south direction that includes faults and drainage systems.

The fly ash landfill is thinning-out to the north and the study area, in general is slightly dipping to the south. Clay embankments surround the fly ash landfill, and are separated by drainage system that removes the excess surface water to the natural drainage system.

The run off from the inner flanks of the fly ash landfill will be collected in the retention pond, and then this water can be removed to the detention pond for further treatments. The rain water from the outer flanks of the landfill can be collected directly to the detention pond.

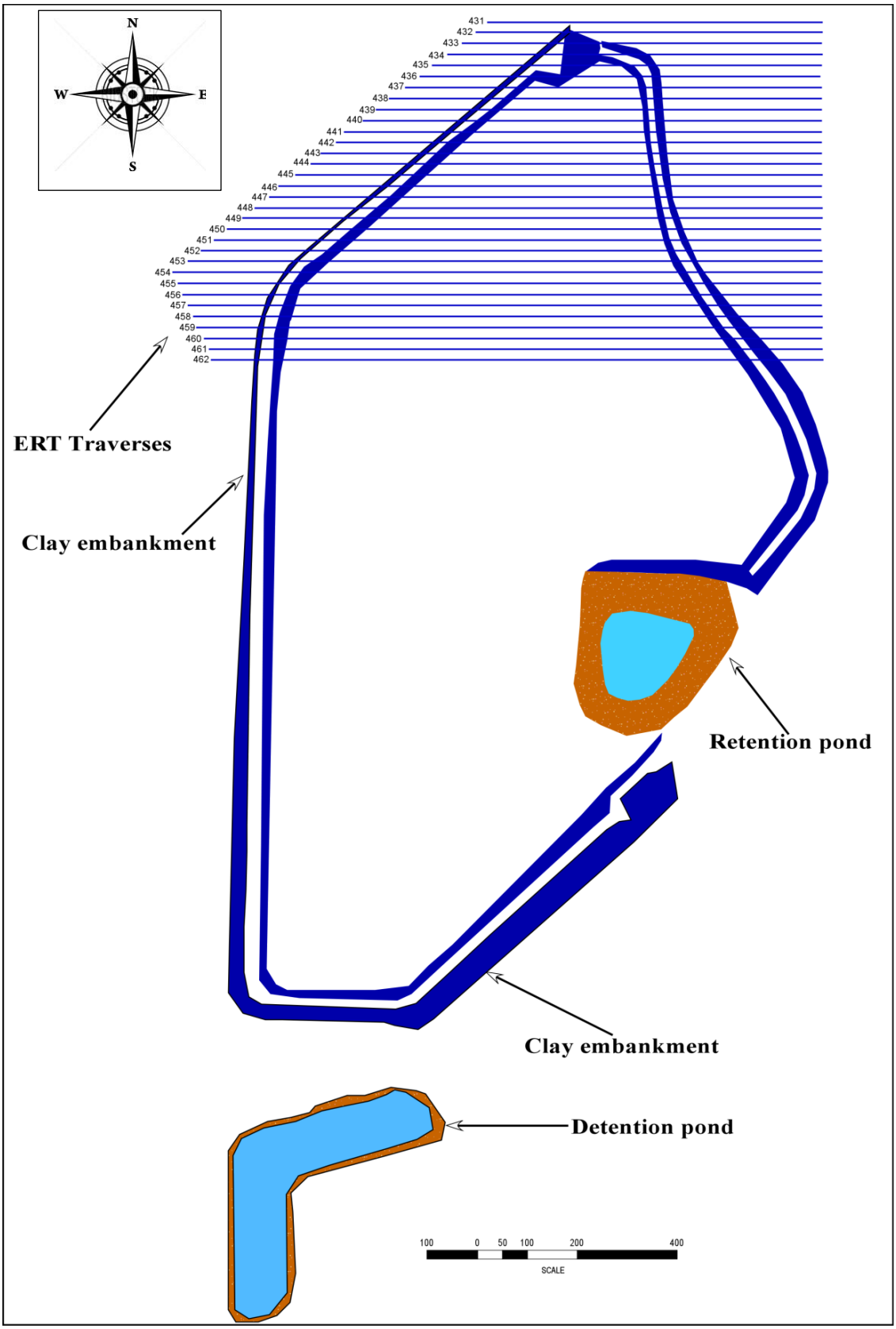

Figure 8.1: Illustrative figure for a fly ash landfill, with ERT traverses 431 to 462.

In the process of establishing new channels, streams and rivers leave behind flood plains, drainage ditches and stream-cut terraces, such as in the case of the study area, where an existing upper terrace and a lower terrace indicates two consecutive shifts of the stream in the study area, added to that, the man-made ditches that are constructed to drain the water run-off along roads and around the fly ash landfill. The existing condition resulted in multiple sources of water that could ultimately affect the fly ash landfill moisture content, following different pathways. These sources include the direct rain-water from the northwest of the study area and the water flowing off the flanks to the toe of the landfill. The run-off over-flow and by-pass the terrace at the toe of the landfill, to seep into the soil and underlying rock, while also seeps through the natural and man-made ditches that are established to divert water away from the landfill (Figure 8.2 and Figure 8.3).

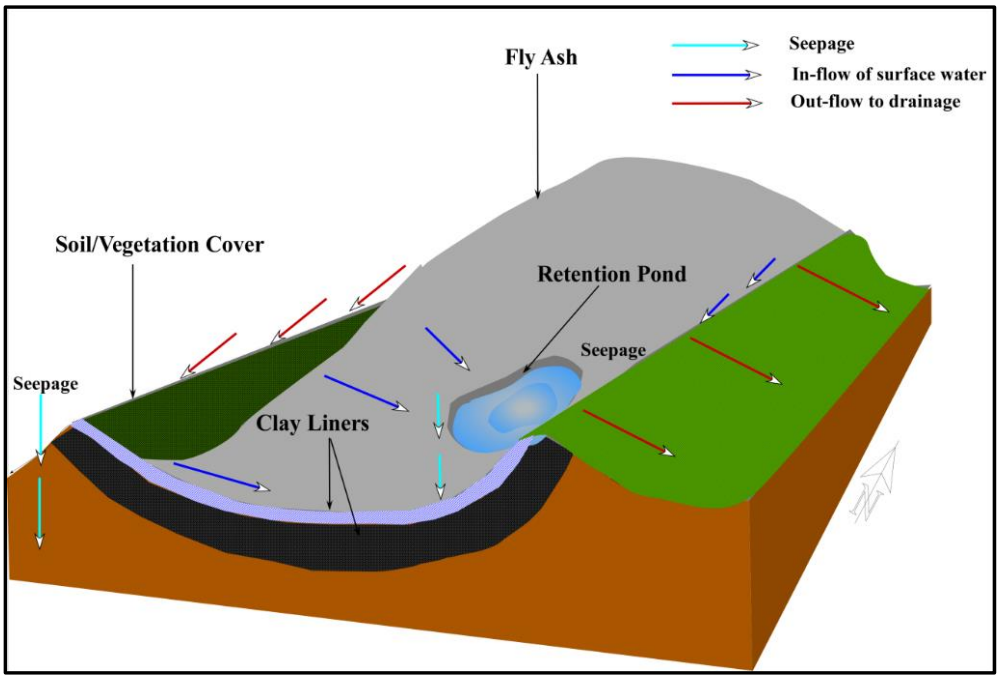

Figure 8.2: Flow directions of drainage in a fly ash landfill.

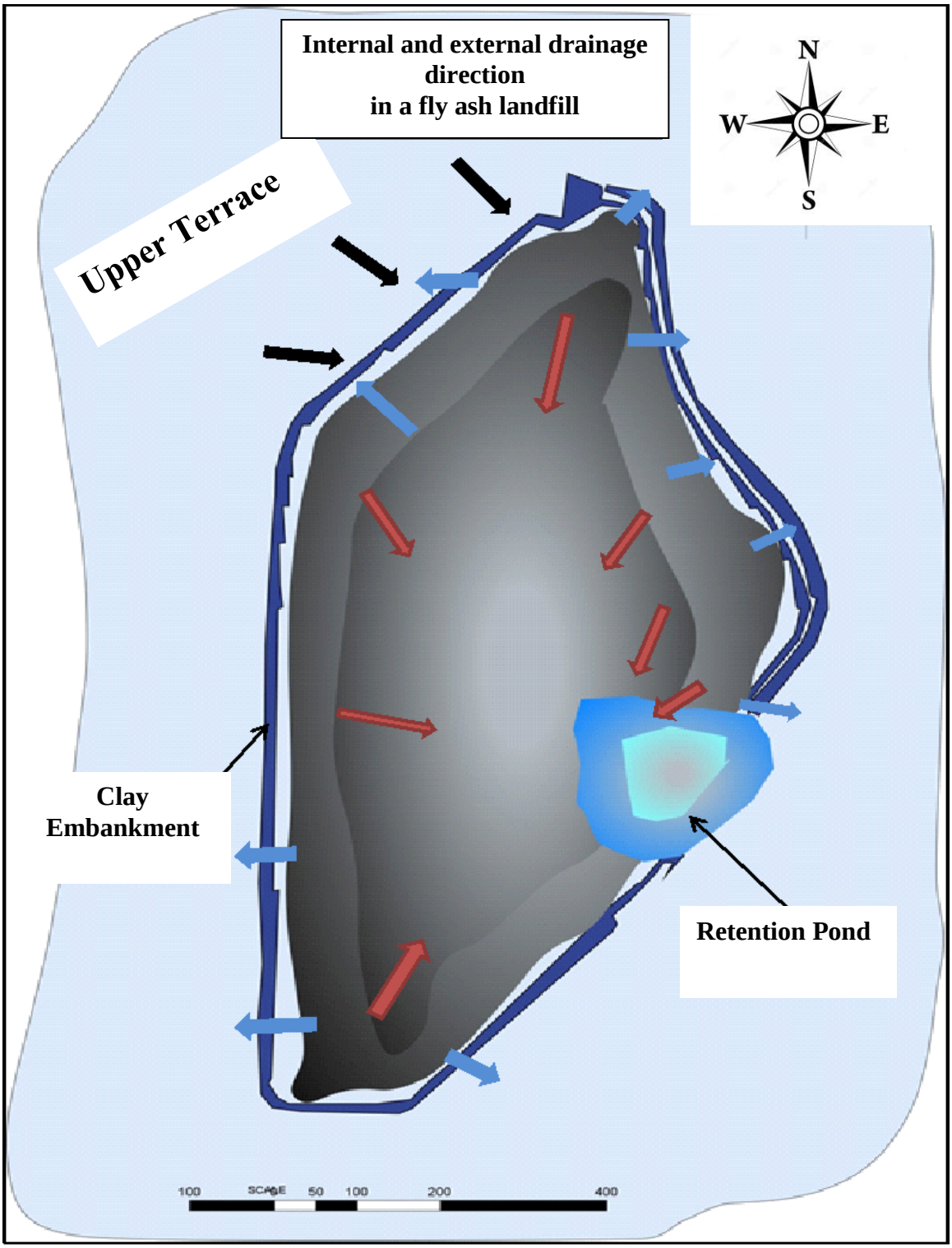

Figure 8.3: Drainage directions and pathways of moisture in the fly ash landfill.

To explain the ways by which moisture accumulate beneath the landfill, the soil and rock, Figure (8.4) displays two pathways (1) and (2), that are controlled by the topography at the proximity of the landfill. Figure (8.4) displays a 3-D ERT profile that images the upper terrace, the lower terrace (where the fly ash landfill is placed) and a stream-cut terrace west of the fly ash landfill. Two seepage pathways were identified from the imaging, as indicated in Figure (8.4) as pathway (1) and pathway (2).

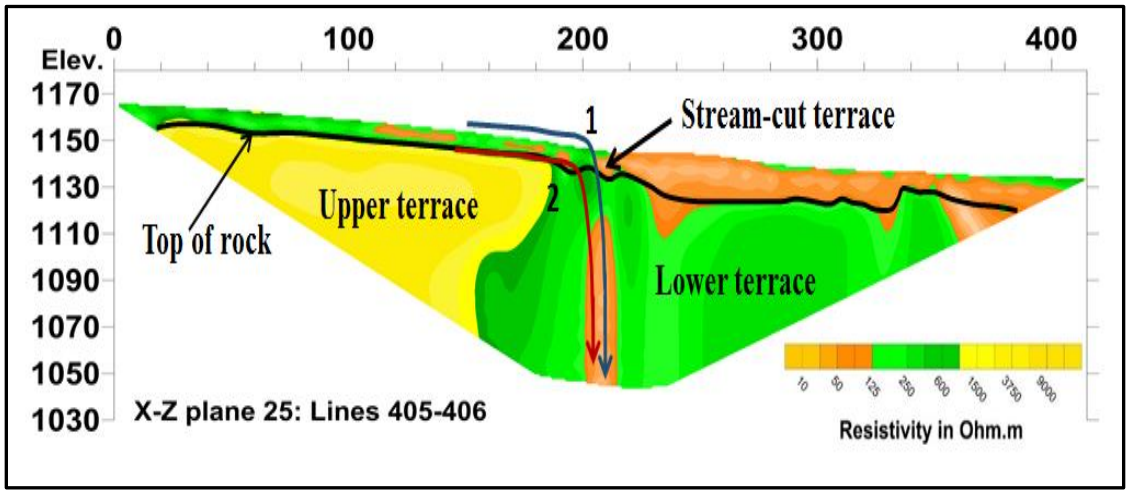

Figure 8.4: 3-D electrical resistivity image of the subsurface mid-way between ERT traverses 405 and 406 to the north of the fly ash landfill site. Interpreted top-of-rock is highlighted in black. Seepage pathway #1 is highlighted in blue and seepage pathway #2 is highlighted in red.

Pathway (1) indicates a run-off flowing down dip along the upper terrace from the west to the east and seeping into the subsurface along or in proximity of the stream-cut terrace. This run-off would flow into the western drainage at the proximity of the landfill, where some of its water seeps vertically in into soil and underlying rocks, leading to increase in the moisture of the top of rock beneath the fly ash. Figure (8.4) suggests that some water also flows toward the stream (N-S direction) as well.

In pathway 2, Figure (8.4), the subsurface flow along the bedrock surface down-dip from the west to the east along the upper terrace and seep vertically to the underlying soil and rock.

The 3-D ERT profile (432–433) presents one of the subsurface electrical resistivity profiles along a traverse located mid-way between traverse lines 432 and 433 (Figure 8.5).

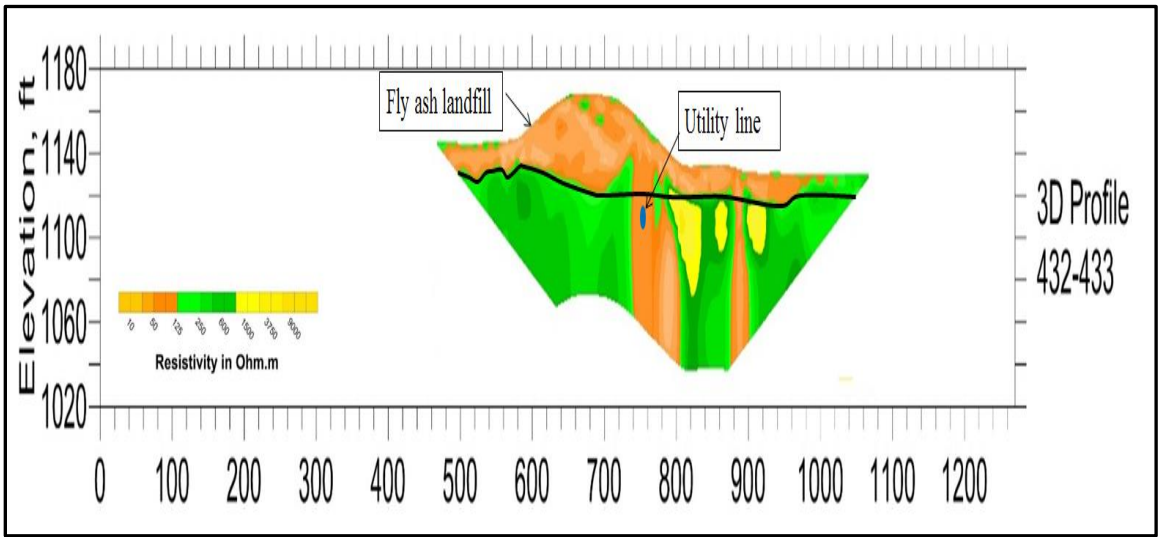

Figure 8.5: 3-D electrical resistivity image of the subsurface along a "traverse" mid-way between ERT traverses 432 and 433, as shown in Figure 8.1.

The upper boundary is coincident the ground surface, while the black line denotes the interpreted top-of-rock. This estimate correlates well with the 125 ohm-m resistivity value; as verified by the MASW results, except in a few locations exhibiting increased moisture contents, where the interpreted ERT values fall below the 125 ohm-m limit. In the absence of the geosynthetic liner, the moisture content of the fly ash is usually assumed to be relatively uniform except in the places that have seepage pathways with low resistivity values.

The 3-D ERT profile (433–434) presents one of the subsurface electrical resistivity profiles along the traverse located mid-way between traverse lines 433 and 434 (Figure 8.6). The upper boundary is coincident the ground surface, while the black line denotes the interpreted top-of-rock. This estimate correlates well with the 125 ohm-m resistivity value; as confirmed by the MASW interpreted results.

Figure (8.6) represent a different condition, in which, the upper fly ash is drier than the fly ash at the bottom of the landfill, which indicates that the moisture content of the fly ash increases with the depth of burial. The interpretation of Figure (8.6) is that, some rain-water has seeped through the upper cap of landfill, and reached down to the clay liner flowing almost vertically along pathway 3. The high resistivity patches shown in green in the upper part of the fly ash indicates high porosity of the fly ash that facilitated the escape of moisture to the bottom of the landfill.

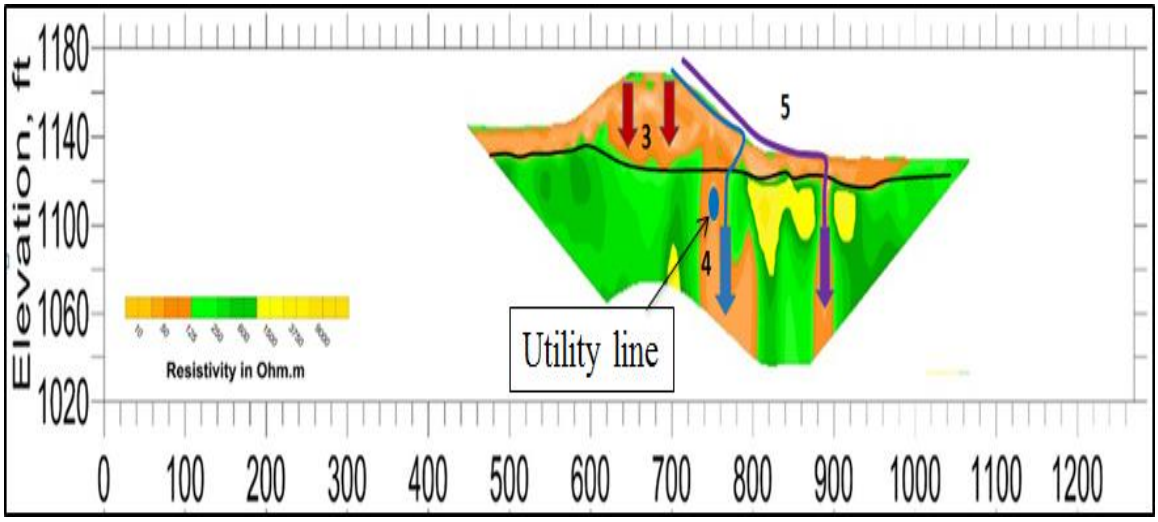

Figure 8.6: 3-D electrical resistivity image of the subsurface along a "traverse" mid-way between ERT traverses 433 and 434, as shown in Figure 8.1. Possible seepage pathways highlighted in red, blue and purple.

This interpreted profile in Figure (8.6) also suggests some of the run-off from the flanks of the fly ash landfill is intercepted at the toe of the landfill and it seeped into soil and rock near the toe of the landfill along pathway (4). This seeping moisture goes into the vertical joints of the rock almost vertically, which yield resistivities less than 125 ohm-m, generally indicative of very moist weathered and/or fractured rock, or for moist residual soil. Above the interpreted top of rock (black line), the interpreted profile suggests moisture retention by the fly ash. The size of the joint in Figure (8.6) indicates that the amount of moisture at the toe of the landfill is greater and it decreases away from the landfill. The size of the interpreted area exhibiting low resistivity is denoted by flow/seepage pathway (4) in Figure (8.6). This potential flow path appears continuous to the maximum depth of the profile. It is suggestive of radial drainage, presumably natural precipitation that percolates vertically into the residual soil profile at the toe of the landfill.

This interpreted profile of Figure (8.6) also suggests that the run-off from the flanks that continue to flow away from the landfill carries a lesser amount of water as it is distance from the toe of the landfill increase as shown by pathway (5). Some of this water seeps into soil and underlying rock in almost vertical as shown in Figure (8.6), and the relatively moderate joint indicates the lesser amount of water.

In Figure 8.7, 3-D ERT profile 439-440, the data acquired at some locations where there exist a geosynthetic liner beneath the fly ash embankment(denoted by the red line), and the interpreted top of rock is demarcated by a solid black line that is conformable with the 125 ohm-m resistivity value. In the Figure (8.7) below, the inconsistency of the low moisture content of the shallow rock beneath the landfill

geosynthetic liner makes it more difficult to discern the top-of-rock. The underlying soil and rock appear to be moistened by seepage along or near the top-of-rock an expected permeability contrast. The fly ash placed before the geosynthetic liner is characterized by resistivity values above 125 ohm-m in areas where the fly ash and underlying soils are considerably drier.

In Figure 8.7, the moisture that seeps from different sources into the fly ash, reaches the clay liner and drains to the retention pond or the leachate collection system. The moisture that flows down dip along the top of the geosynthetic liner to the outer edges of the geosynthetic liner and the moisture flows off the edges of the geosynthetic liner seeps vertically into underlying soil and rock (seepage pathway 6).

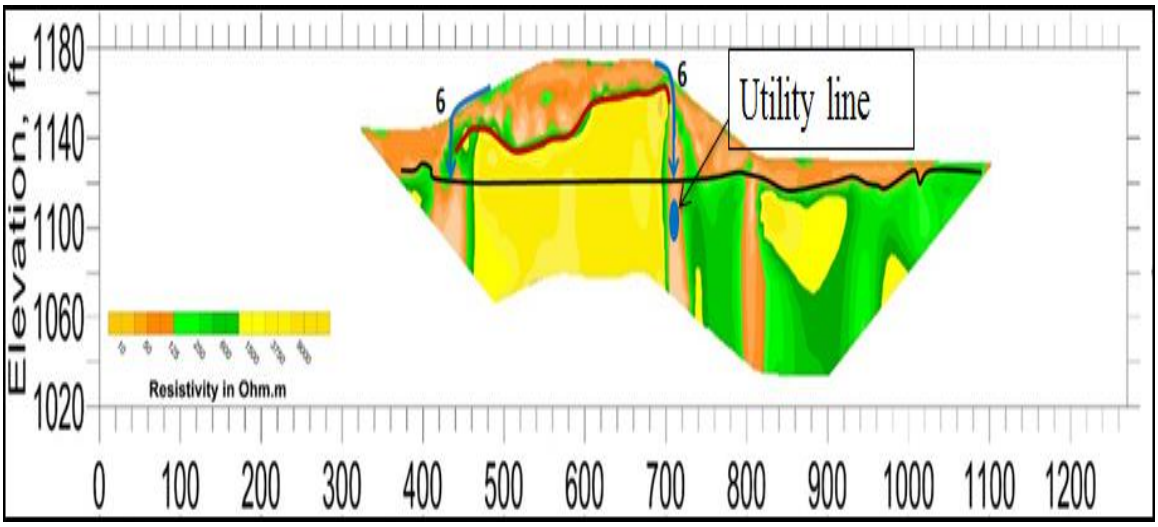

Figure 8.7: 3-D electrical resistivity image of the subsurface along a "traverse" mid-way between ERT traverses 439 and 440, as shown in Figure 8.1. Possible seepage pathways highlighted in blue. The approximate geosynthetic liner location is highlighted in red.

Figures 8.8 to 8.10 present examples of the acquired 3-D ERT data for an existing fly ash landfill which incorporates a geosynthetic liner (shown in red). Based on the visual interpretation of the resistivity values, these profiles exhibit a much higher

variability and inconsistency in the moisture contents of fly ash, residual soils and weathered rock interfaces. For example, in Figure (8.8), the shallow rock appears to retain much less moisture in some places than others, beneath the geosynthetic liner. The fly ash beneath the geosynthetic liner is characterized by resistivity values lower than 125 ohm-m in some locations, while in other locations, moisture appears to be seeping along preferred percolation pathways within the shallow bedrock, which may be structurally controlled by jointing, shears, or joint clusters. On the other hand, resistivity values greater than 125 ohm-m were measured in areas of dry fly ash and soils lying beneath the geosynthetic liner. One of the ERT application limitations is the identification of the contact between soil and rock, in which situation both the residual soils and weathered rock are either very dry or are both moist.

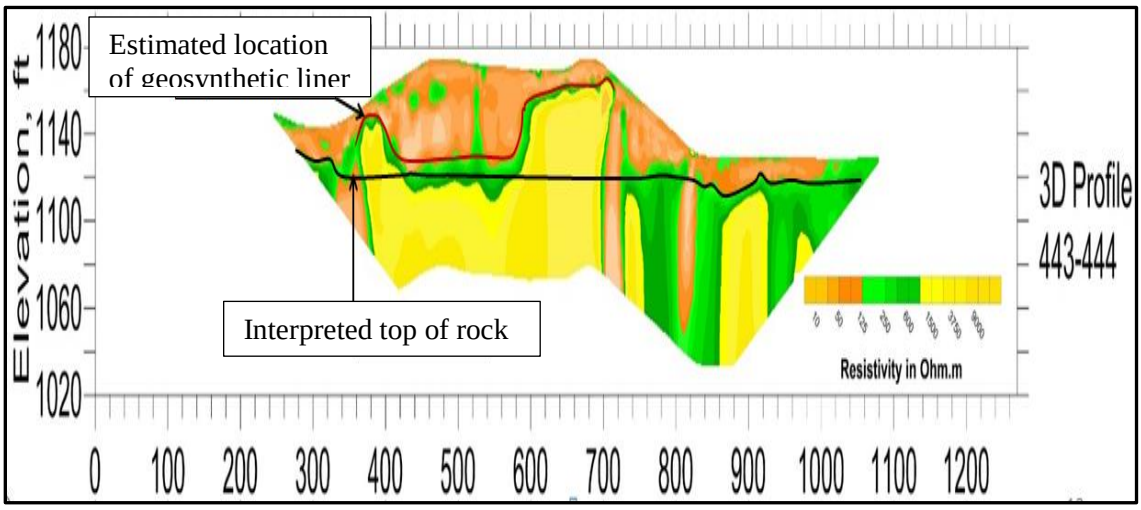

Figure 8.8: 3-D electrical resistivity image of the subsurface along a "traverse" mid-way between ERT traverses 443 and 444, as shown in Figure 8.1. The approximate geosynthetic liner location is highlighted in red.

The 3-D ERT profile 449-450 (Figure 8.9) and profile 453-454 (Figure 8.10) indicate that some of the moisture that follow the seepage pathways 1, 2, 4 and 6, flows

along or near the top of the pervasively fractured shallow rock beneath the landfill geosynthetic liner and above the clay liner (shown in Figure 8.9). The increased moisture coupled with the shallowness in depth, appears to create no contrast in the resistivity that could allow for successful imaging of the interface between the soil, rock and fly ash, using the ERT method.

All kinds of liner systems (clay or geosynthetic liners) exhibit some degree of permeability that allows some amount of moisture to pass through. Thus, the interpretation of Figure 8.9 and Figure 8.10 suggests that the geosynthetic liner permeability has allowed the passage of some moisture, which eventually created minor resistivity difference above and below the geosynthetic liner and allowed the imaging of moisture using the ERT. A utility line is shown in Figure(8.9).

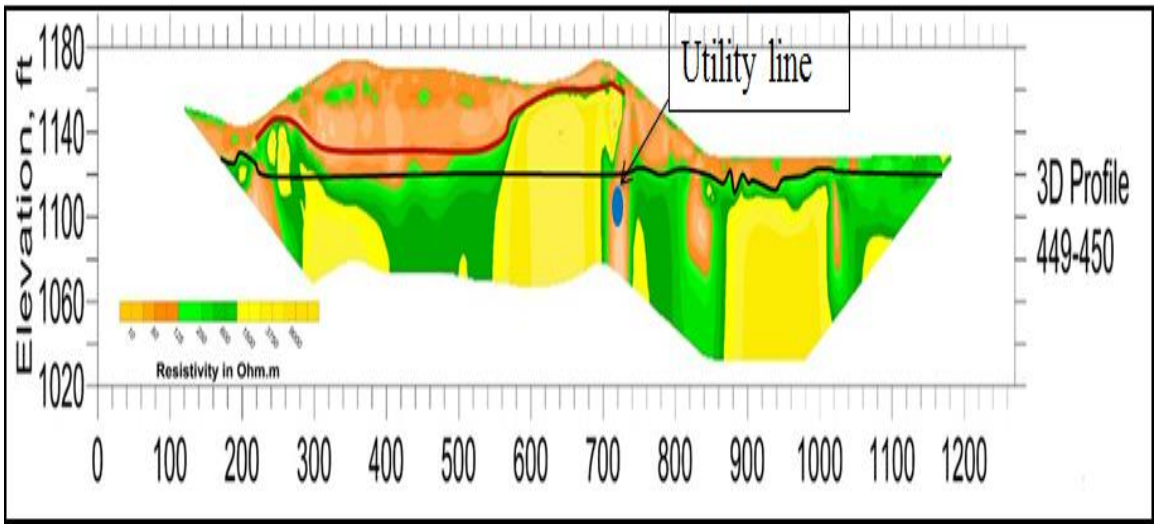

Figure 8.9: 3-D electrical resistivity image of the subsurface along a "traverse" mid-way between ERT traverses 449 and 450, as shown in Figure 8.1. The approximate geosynthetic liner location is highlighted in red.

Figure (8.10) also shows a utility line, where the original soil has been replaced after the excavation and placing the utility line, as a result the soil will allow the moisture to seep to the underlying rocks.

Fine-ground materials, like silt clay, or fly ash, will tend to absorb any free moisture through capillary attraction. The wet fly ash fill beneath the geosynthetic liner may have been at field capacity (near saturation) before the liner was placed, or moisture may have migrated downward through tears or seams in the geosynthetic membrane, under increased hydrostatic pressure affected by the greater height/depth of fly ash fill.

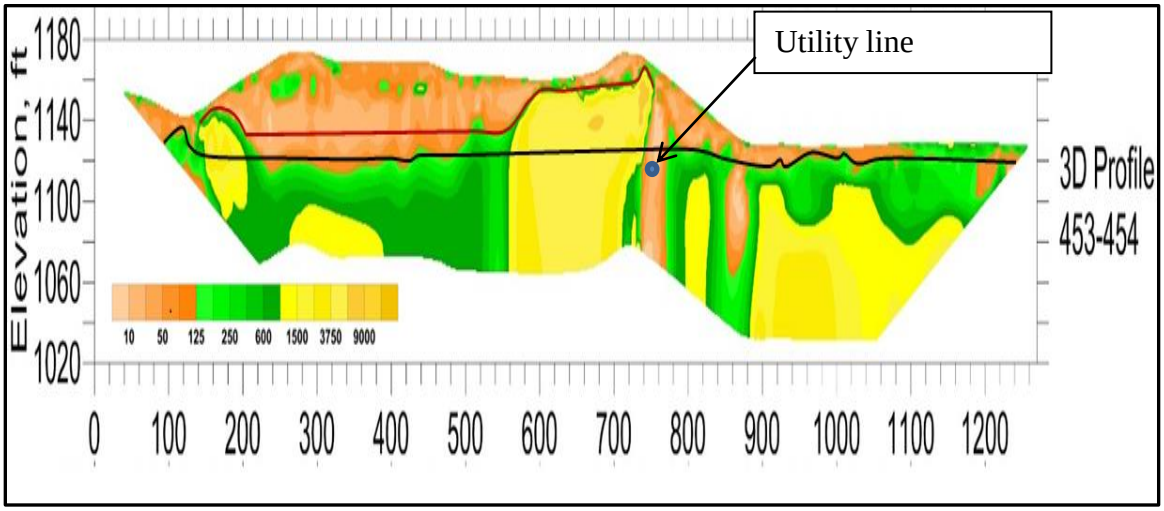

Figure 8.10: 3-D electrical resistivity image of the subsurface along a “traverse” mid-way between ERT traverses 453 and 454, as shown in Figure 8.1. The approximate geosynthetic liner location is highlighted in red.

Based on the interpretation of the results of Figure (8.9), Figure (8.10), and the illustration of Figure (8.11), the primary source of moisture is the seepage from the sides of the landfill, where the run-off from the surface water or the flanks of the landfill seeped through the toe of the landfill and the natural and man-made ditches around and at the vicinity of the landfill to the clay liner.

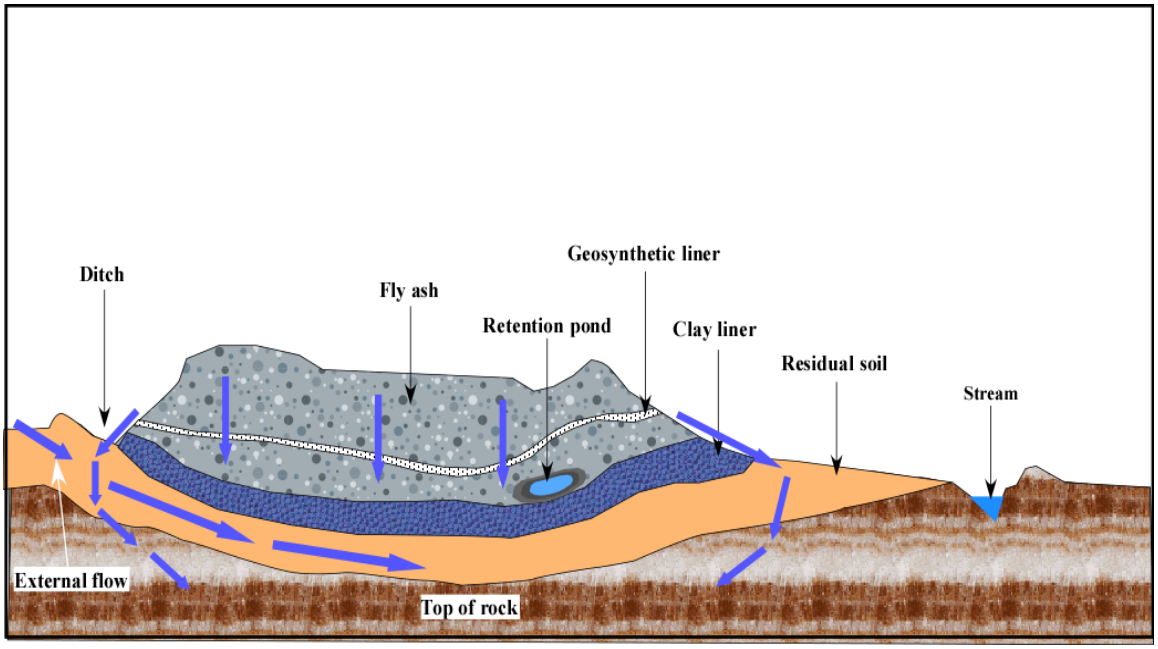

Figure 8.11: Illustrative diagram for the direction of flow of moisture onto and beneath the fly ash landfill layers.

Figure (8.12) shows the dispersion curve and the related 1-D shear wave velocity profile generated for the MASW field record. This suggests that the estimated top-of-rock is 16 m (53 feet) at specific chosen location. The ERT derived top-of-rock for the same location was about 14 m (48 feet) (Figure 8.9). The difference between the MASW and the ERT measures could be referred to many factors that are related mainly to measuring instruments, the properties of the earth material and the field setting during data acquisition.

The resolution of the ERT data is higher compared to the MASW data, and is influenced by the spacing between adjacent electrodes. However, Figure 8.12 show that the shear velocity is increasing with depth from 152 m/s (500 ft/s) to 365 m/s (1200 ft/s) for the compacted fly ash and soil, while the shear wave velocity for the fractured rock

reached values of approximately 518 m/s (1700 ft/s). The shear wave velocity of intact rock in Figure 8.12 exceeded the 762 m/s (2500 ft/s).

The obtained ERT value of the top of rock is based on the contrast between the rock and soil resistivities, whereas for the MASW, the value of the top of rock is obtained based on the contrast between the rock and soil acoustic properties.

The average depth to the top of rock using the MASW is influenced by the length of the array, therefore, different averages will be produced using different arrays lengths, while the spacing between adjacent electrodes will produce different levels of details.

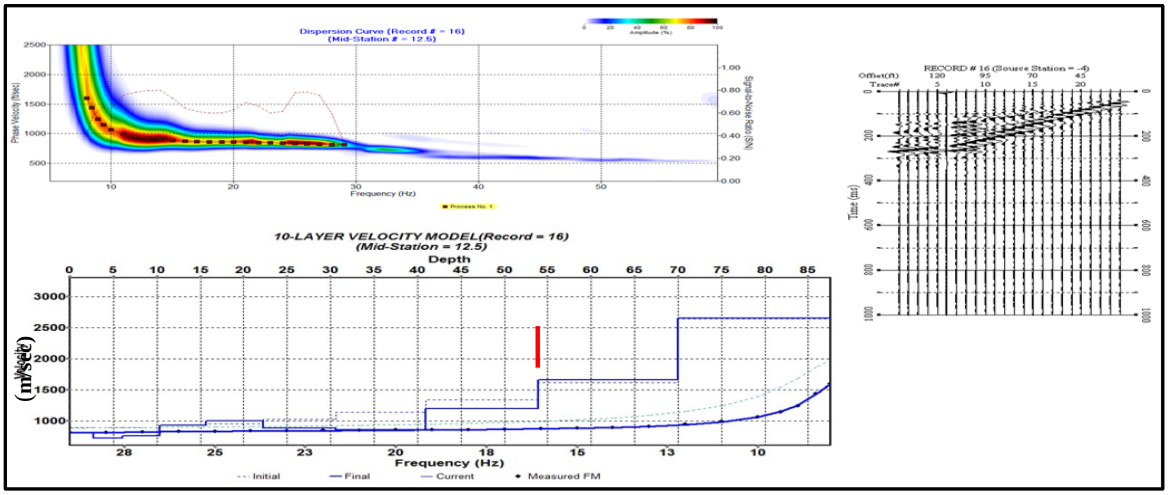

Figure 8.12: Dispersion curve and its related 1-D shear – wave velocity profile generated for the MASW field record acquired on 3-D ERT profile 449-450.

9. CONCLUSIONS

The integrated use of electrical resistivity tomography (ERT) and multi-channel analysis of surface waves (MASW) are complimentary techniques that, when applied together, can provide one of the cost effective means of non-intrusive geophysical profiling to detect anomalies in foundations up to 30 m (100 feet) beneath the ground surface. These are useful techniques to map foundation conditions beneath an existing landfill site founded on karst terrain areas.

In this study, the ERT geophysical method succeeded in locating the geosynthetic liner of a fly ash landfill. The visual interpretation of the ERT data was very useful in terms of discerning variations in the moisture content of the fly ash above and below the geosynthetic liner. The moisture below the geosynthetic liner was due mostly to seepage from the flanks of the landfill.

The study identified seepage pathways through the existing fly ash landfill (but above the basal clay liner) and seepage pathways below the base of the landfill. These seepage pathways were typically characterized by low resistivity values (less than 125 ohm-m) because moisture content was relatively high. Based on the interpretation of ERT data there is no evidence of any prominent karst features beneath the fly ash deposit, which could adversely affect the landfill's structural stability.

Mapping of the contact between soil and rock proved difficult where the resistivity values of the rock and the overlying soil was similar. Furthermore, variations in moisture content of the soil, rock and the fly ash could be mapped on the ERT data. The moisture content of the fly ash above the geosynthetic liner was found to exhibit a

uniform trend (which would be expected if the liner is functioning as intended), opposite to the trend observed below the geosynthetic liner, where moisture content appeared to be more variable.

Interpretation of the acquired ERT data appears to correlate well with the MASW data and borehole control in estimating the depth to the top-of-rock. The MASW data provides verification of the ERT data interpretations.

The interpretation of the ERT and MASW results indicates that the subsurface beneath the landfill is intact, showing no karst features that might adversely affect the stability of the landfill. Also, detected seepage pathways are diverting the non-contaminated storm water and the channeled water flow into the groundwater. Therefore, the groundwater appears to be secured from leachate pollution.

BIBLIOGRAPHY

Adamski, James C., James C. Petersen, David A. Freiwald, and Jerri V. Davis. "Environmental and hydrologic setting of the Ozark Plateaus study unit, Arkansas, Kansas, Missouri and Oklahoma." Wrir94-4022. N.p., 1995. Web. 11 Feb. 2017. <https://pubs.usgs.gov/wri/wri944022/>.

Ahmed, A. M. and W. N. Sulaiman (2001). "Evaluation of groundwater and soil pollution in a landfill area using electrical resistivity imaging survey." Environmental management 28(5): 655-663.

Almes, W. S. and J. J. Bowders (1991). Stabilized fly ash cover for a municipal waste landfill. The ASCE Energy Division Specialty Conference on Energy, Pittsburgh, PA, USA, 03/10-13/91.

Alpha, Tau Rh, John P. Galloway, and John C. Tensley, III. "Karst Topography Paper Model." National Parks Service. U.S. Department of the Interior, n.d. Web. 11 Feb. 2017. <https://www.nature.nps.gov/geology/usgsnps/cave/karst.html>.

Andrabi, Syed Javid, Avinash Chandra, Mohd Aslam, and Hassan I. A. "Influence of Chemical Composition on the El Ectrical Resistivity of Fly Ash Generated from Indian Coal Based Thermal Power Plants." Journal of Applied Sciences, Engineering and Technology 5.6 (2013): 2284-289. Print.

Ansari, F., A. Gupta, et al. (2010). "Fly-ash from coal-fed thermal power plants: Bulk utilization in horticulture–a long-term risk management option." International Journal of Environmental Research 5(1): 101-108.

Bergado, D., G. Ramana, et al. (2006). "Evaluation of interface shear strength of composite liner system and stability analysis for a landfill lining system in Thailand." Geotextiles and Geomembranes 24(6): 371-393.

Carey, P. and G. Carty (2000). Landfill manuals: landfill site design, EPA.

Chambers, J. E., O. Kuras, et al. (2006). "Electrical resistivity tomography applied to geologic, hydrogeologic, and engineering investigations at a former waste-disposal site." Geophysics 71(6): B231-B239.

Cherkauer, D. S. (1980). "The Effect of Flyash Disposal on a Shallow Ground- Water System." Ground Water 18(6): 544-550.

Chugh, Y. P. (2001). Coal combustion by-products-based lightweight structural materials and processes for making them, Google Patents.

Dixon, N., D. R. V. Jones, et al. (2006). "Interface shear strength variability and its use in reliability-based landfill stability analysis."

Edil, T., P. Berthouex, et al. (1987). "Fly ash as a potential waste liner." IN: Geotechnical Special Publication (13).

El-Mogazi, D., D. J. Lisk, et al. (1988). "A review of physical, chemical, and biological properties of fly ash and effects on agricultural ecosystems." Science of the Total Environment 74: 1-37.

Eriksen, P. B. and B. Donslund (1990). Impacts on groundwater and surface water from landfills of residues produced by coal fired power plants. 1990 International Joint Power Generation Conference, Boston, MA, USA, 10/21-25/90.

Fehdi, C., F. Baali, et al. (2011). "Detection of sinkholes using 2D electrical resistivity imaging in the Cheria Basin (north–east of Algeria)." Arabian Journal of Geosciences 4(1-2): 181-187.

Foreman, A. T. (2014). Climate Change Influence on Historical Flood Variability in Ozark Highland Rivers, Missouri State University.

Frid, V., G. Liskevich, et al. (2008). "Evaluation of landfill disposal boundary by means of electrical resistivity imaging." Environmental geology 53(7): 1503-1508.

Gilbert and Meek. "ITIS Standard Report Page: Percina Cymatotaenia." ITIS Standard Report Page: Percina Cymatotaenia. N.p., n.d. Web. 11 Feb. 2017. <https://www.itis.gov/servlet/SingleRpt/SingleRpt?search_topic=TSN&search_value=168482#null>.

Genelle, F., C. Sirieix, et al. (2011). Automatic Resistivity Profiling and Electrical Resistivity Tomography for Landfill Cover Surveying. Near Surface 2011-17th EAGE European Meeting of Environmental and Engineering Geophysics.

Gong, Y. and D. Kirk (1994). "Behaviour of municipal solid waste incinerator flyash: I: General leaching study." Journal of hazardous materials 36(3): 249-264.

Kruse, S., M. Grasmueck, et al. (2006). "Sinkhole structure imaging in covered Karst terrain." Geophysical Research Letters 33(16).

Landva, A. and G. D. Knowles (1990). Geotechnics of waste fills: theory and practice, ASTM International.

Le Seur Spencer, L. and L. D. Drake (1987). "Hydrogeology of an alkaline fly ash landfill in eastern Iowa." Ground Water 25(5): 519-526.

Loke, M. H. "Tutorial: 2-D and 3-D Electrical Imaging Surveys." Geotomo Software - Home. N.p., 2016. Web. 11 Feb. 2017. <http://www.geotomosoft.com/>.

McCarthy, J. F. and J. M. Zachara (1989). "Subsurface transport of contaminants." Environmental science & technology 23(5): 496-502.

Michaud, D. T. and L. Sohns (1985). Stabilized flyash as artificial reef construction material. Proceedings of the American Power Conference, Illinois Institute of Technology.

Morelli, G., G. Corsini, et al. (1997). Integrating electrical resistivity tomography and soil sampling methods to characterize a solid waste landfill area. 3rd EEGS Meeting.

Muchingami, I., J. Nel, et al. (2013). "On the use of electrical resistivity methods in monitoring infiltration of salt fluxes in dry coal ash dumps in Mpumalanga, South Africa." Water SA 39(4): 00-00.

Muchingami, I. I. (2013). "Non-invasive characterization of unsaturated zone transport in dry coal ash dumps: A case study of Tutuka, South Africa."

Muralidhar Yadav, S., D. Reddythota, et al. (2014). "Application of leachate pollution indices for assessment of leachate pollution potential of landfills (a case study of an unlined landfill with lime sludge and fly ash)." International Journal of Environment and Waste Management 13(2): 146-159.
Nhan, C., J. Graydon, et al. (1996). "Utilizing coal fly ash as a landfill barrier material." Waste Management 16(7): 587-595.

Nhan, C., J. Graydon, et al. (1996). "Utilizing coal fly ash as a landfill barrier material." Waste Management 16(7): 587-595.

Ogilvy, R., P. Meldrum, et al. (2002). "The use of 3D electrical resistivity tomography to characterise waste and leachate distribution within a closed landfill, Thriplow, UK." Journal of Environmental & Engineering Geophysics 7(1): 11-18.

Percina Cymatotaenia. N.p., n.d. Web. 11 Feb. 2017. <https://www.itis.gov/servlet/SingleRpt/SingleRpt?search_topic=TSN&search_value=168482#null>.

Rafferty, Milton D., and Edwin J. Westermann. Https://www.britannica.com/place/Missouri-state. N.p., 23 Aug. 2016. Web. 11 Feb. 2017. <https://www.britannica.com/place/Missouri-state>.

Ripp, J. and J. Villaume (1985). Monitoring the Hydrology and Chemistry of a Dry Fly Ash Landfill. Toxic and Hazardous Wastes: Proceedings of the Seventh Mid-Atlantic Industrial Waste Conference June 23-25, 1985. Technomic Publishing Co., Lancaster, PA. 1985. p 292-304, 3 fig, 3 tab, 2 ref.

Sajwan, K. S., A. K. Alva, et al. (2000). Biogeochemistry of trace elements in coal and coal combustion byproducts, Springer Science & Business Media.

"Salem Plateau." Ozarknationalpark. N.p., 28 Jan. 2012. Web. 11 Feb. 2017. <https://ozarknationalpark.wordpress.com/2012/01/28/salem-plateau/>.
"ITIS Standard Report Page: Percina Cymatotaenia." ITIS Standard Report Page

Scapozza, C. and L. Laigre (2014). "The contribution of Electrical Resistivity Tomography (ERT) in Alpine dynamics geomorphology: case studies from the Swiss Alps." Géomorphologie: relief, processus, environnement 20(1): 27-42.

Seed, R. B., J. K. Mitchell, et al. (1990). "Kettleman hills waste landfill slope failure. II: stability analyses." Journal of Geotechnical Engineering 116(4): 669-690.

Singh, D. N., P. K. Kolay, et al. (2002). "New approach to study leaching of fly ash from landfills." Journal of solid waste technoligy and management 28(3): 138-144.

Strauss, S. (1984). "Disposing of power plant fly ash can be effected in an environmentally safe manner." Power ;(United States) 128(2).

Thom, R. H. and J. H. Wilson (1980). "The natural divisions of Missouri." Transactions of the Missouri Academy of Science 14: 9-23.

Van Schoor, M. (2002). "Detection of sinkholes using 2D electrical resistivity imaging." Journal of Applied Geophysics 50(4): 393-399.

Wightman, W., F. Jalinoos, et al. (2004). Application of geophysical methods to highway related problems.

Yeheyis, M. B., J. Q. Shang, et al. (2009). Chemical and mineralogical transformations of coal fly ash after landfilling. World of Coal Ash Conference, Lexington, Kentucky.

Youssef, A. M., H. El-Kaliouby, et al. (2012). "Sinkhole detection using electrical resistivity tomography in Saudi Arabia." Journal of Geophysics and Engineering 9(6): 655.

Zhou, W., B. F. Beck, et al. (2002). "Effective electrode array in mapping karst hazards in electrical resistivity tomography." Environmental geology 42(8): 922-928.

VITA

Atiat Shaban Alsaaideh born and grew up in Ma'an, Jordan. She received her Bachelor's degree in Medical Physics from Zarqa University, Jordan in January of 2001. Atiat attended Al Hussain Bin Talal University as laboratory assistant in the physics department till 2006. She received her Master's degree in Physics from Mutah University in May 2006.

Atiat enrolled in a Masters/PhD degree program at Missouri University of Science and Technology in 2011, and she received Master's degree in Physics from Missouri University of Science and Technology in May 2014, and she received her PhD degree in Geological Engineering from Missouri University of Science and Technology in May 2017.